REPORT DOCUMENTATION PAGE

Form Approved
OMB No. 0704-0188

1. AGENCY USE ONLY (Leave blank)	2. REPORT DATE	3. REPORT TYPE AND DATES COVERED
	20/August/1996	Final Technical 1/Jun/93-31/May/96

4. TITLE AND SUBTITLE
Swirl Effects on Coaxial Injector Atomization

5. FUNDING NUMBERS
PE - 61103D
PR - 3484
SA - WS
G - F49620-93-I-0365

6. AUTHOR(S)
Robert J. Santoro

7. PERFORMING ORGANIZATION NAME(S) AND ADDRESS(ES)
The Pennsylvania State University
Dept. of Mech. Engr./PERC
240 Research Bldg. East
University Park, PA 16802

AFOSR-TR-96

0457

9. SPONSORING/MONITORING AGENCY NAME(S) AND ADDRESS(ES)
AFOSR/NA
110 Duncan Avenue, Suite B115
Bolling AFB, DC 02332-0001

NA

10. SPONSORING/MONITORING AGENCY REPORT NUMBER
93-1-0365

11. SUPPLEMENTARY NOTES

12a. DISTRIBUTION/AVAILABILITY STATEMENT
Approved for public release; distribution is unlimited.

12b. DISTRIBUTION CODE

13. ABSTRACT *(Maximum 200 words)*

The focus of this AASERT grant was the investigation of atomization processes for swirl coaxial gas/liquid spray injection for rocket combustor applications. The work has included review and analysis of atomization literature for swirled and non-swirled gas/liquid sprays, design and fabrication of a rocket-scale swirl coaxial injector for research, and cold-flow and hot-fire characterizations of atomization and combustion with the designed injector. Two significant findings have emerged from the present studies; (1) our experiments in a windowed research combustor were the first to demonstrate that swirl coaxial injection allows for highly efficient propellant combustion (liquid oxygen/gaseous hydrogen) over a wide range of oxidizer-to-fuel ratios from 3 to 175. The result was of interest to industry in conceptual design of a novel rocket-engine cycle, for RLV application, relying upon very high oxidizer-to-fuel ratio combustion in a liquid oxygen preburner, and (2) optical diagnostics were applied to demonstrate a methodology for scaling spray drop size/velocity results based on liquid Weber number. This is of intrinsic value to the spray community, and of direct impact within the rocket-injector design community, where the scaling approach can be incorporated into injector sizing activities.

14. SUBJECT TERMS	15. NUMBER OF PAGES
Rocket injectors, swirl atomizers, sprays, atomization	93
	16. PRICE CODE

17. SECURITY CLASSIFICATION OF REPORT	18. SECURITY CLASSIFICATION OF THIS PAGE	19. SECURITY CLASSIFICATION OF ABSTRACT	20. LIMITATION OF ABSTRACT
UNCLASSIFIED	UNCLASSIFIED	UNCLASSIFIED	UL

GENERAL INSTRUCTIONS FOR COMPLETING SF 298

The Report Documentation Page (RDP) is used in announcing and cataloging reports. It is important that this information be consistent with the rest of the report, particularly the cover and title page. Instructions for filling in each block of the form follow. It is important to ***stay within the lines*** to meet ***optical scanning requirements***.

Block 1. Agency Use Only *(Leave blank)*.

Block 2. Report Date. Full publication date including day, month, and year, if available (e.g. 1 Jan 88). Must cite at least the year.

Block 3. Type of Report and Dates Covered. State whether report is interim, final, etc. If applicable, enter inclusive report dates (e.g. 10 Jun 87 - 30 Jun 88).

Block 4. Title and Subtitle. A title is taken from the part of the report that provides the most meaningful and complete information. When a report is prepared in more than one volume, repeat the primary title, add volume number, and include subtitle for the specific volume. On classified documents enter the title classification in parentheses.

Block 5. Funding Numbers. To include contract and grant numbers; may include program element number(s), project number(s), task number(s), and work unit number(s). Use the following labels:

C	- Contract	**PR**	- Project
G	- Grant	**TA**	- Task
PE	- Program Element	**WU**	- Work Unit Accession No.

Block 6. Author(s). Name(s) of person(s) responsible for writing the report, performing the research, or credited with the content of the report. If editor or compiler, this should follow the name(s).

Block 7. Performing Organization Name(s) and Address(es). Self-explanatory.

Block 8. Performing Organization Report Number. Enter the unique alphanumeric report number(s) assigned by the organization performing the report.

Block 9. Sponsoring/Monitoring Agency Name(s) and Address(es). Self-explanatory.

Block 10. Sponsoring/Monitoring Agency Report Number. *(If known)*

Block 11. Supplementary Notes. Enter information not included elsewhere such as: Prepared in cooperation with...; Trans. of...; To be published in.... When a report is revised, include a statement whether the new report supersedes or supplements the older report.

Block 12a. Distribution/Availability Statement. Denotes public availability or limitations. Cite any availability to the public. Enter additional limitations or special markings in all capitals (e.g. NOFORN, REL, ITAR).

- **DOD** - See DoDD 5230.24, "Distribution Statements on Technical Documents."
- **DOE** - See authorities.
- **NASA** - See Handbook NHB 2200.2.
- **NTIS** - Leave blank.

Block 12b. Distribution Code.

- **DOD** - Leave blank.
- **DOE** - Enter DOE distribution categories from the Standard Distribution for Unclassified Scientific and Technical Reports.
- **NASA** - Leave blank.
- **NTIS** - Leave blank.

Block 13. Abstract. Include a brief *(Maximum 200 words)* factual summary of the most significant information contained in the report.

Block 14. Subject Terms. Keywords or phrases identifying major subjects in the report.

Block 15. Number of Pages. Enter the total number of pages.

Block 16. Price Code. Enter appropriate price code *(NTIS only)*.

Blocks 17. - 19. Security Classifications. Self-explanatory. Enter U.S. Security Classification in accordance with U.S. Security Regulations (i.e., UNCLASSIFIED). If form contains classified information, stamp classification on the top and bottom of the page.

Block 20. Limitation of Abstract. This block must be completed to assign a limitation to the abstract. Enter either UL (unlimited) or SAR (same as report). An entry in this block is necessary if the abstract is to be limited. If blank, the abstract is assumed to be unlimited.

DISCLAIMER NOTICE

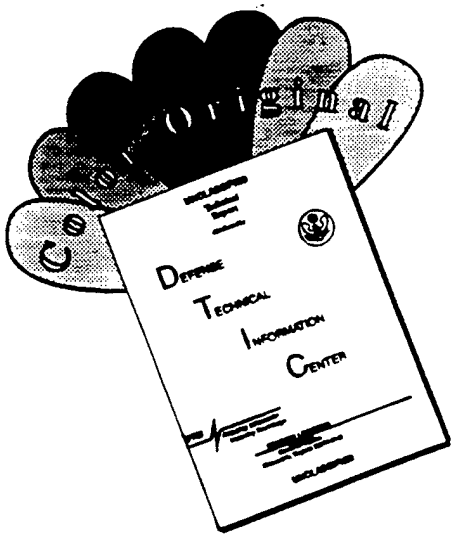

THIS DOCUMENT IS BEST QUALITY AVAILABLE. THE COPY FURNISHED TO DTIC CONTAINED A SIGNIFICANT NUMBER OF COLOR PAGES WHICH DO NOT REPRODUCE LEGIBLY ON BLACK AND WHITE MICROFICHE.

Final Technical Report

on

Swirl Effects on Coaxial Injector Atomization

(AFOSR Grant F49620-93-1-0365)

For the Period June 1, 1993 through May 31, 1996

Prepared by

Robert J. Santoro
Department of Mechanical Engineering
The Pennsylvania State University
University Park, PA 16802

Submitted to

Air Force Office of Scientific Research
Bolling Air Force Base
Washington, DC

August 1996

Table of Contents

Summary

1.0 Introduction 1

2.0 Research Objectives 1

3.0 Research Accomplishments 3

3.1 Review of Coaxial Gas/Liquid Spray Literature

3.2 Swirl Coaxial Injector Combustion Studies

3.3 Scaling Methodology for Swirl Coaxial Atomization

4.0 Conclusion 5

5.0 References 6

6.0 Publications 6

7.0 Interactions 6

8.0 Attachments

A. A review of coaxial gas/liquid spray experiments and correlations

B. Swirl coaxial atomization: cold-flow and hot-fire experiments

C. Coaxial swirl injector studies at high O/F ratios

D. Similitude in pressure-swirl atomizer sprays

Summary

The focus of this AASERT grant was the investigation of atomization processes for swirl coaxial gas/liquid spray injection for rocket combustor applications. The work has included review and analysis of atomization literature for swirled and non-swirled gas/liquid sprays, design and fabrication of a rocket-scale swirl coaxial injector for research, and finally, cold-flow and hot-fire characterizations of atomization and combustion with the designed injector. Two significant findings have emerged from the present studies. First, our experiments in a windowed research combustor were the first to demonstrate that swirl coaxial injection allows for highly efficient propellant combustion (liquid oxygen/gaseous hydrogen) over a wide range of oxidizer to fuel ratios from 3 to 175. The result was of interest to industry in conceptual design of a novel rocket-engine cycle, for Reusable Launch Vehicle application, relying upon very high oxidizer to fuel ratio combustion in a liquid oxygen preburner. Second, optical diagnostics were applied to demonstrate a methodology for scaling spray drop size/velocity results based upon liquid Weber number. This is of intrinsic value to the spray community, and of direct impact within the rocket-injector design community where the scaling approach can be incorporated into injector sizing activities.

1.0 Introduction

The following report describes the progress made on the Augmentation Awards for Science and Engineering Research Training (AASERT) Program of Mr. Shamim Rahman. Mr. Rahman's project is entitled "Swirl Effects on Coaxial Injector Atomization" and is associated with the parent grant entitled "Combustion Instability Phenomena of Importance to Liquid Propellant Engines," AFOSR-91-0336. In the material which follows the research objectives and accomplishments for the three-year program are reviewed. Significant results are highlighted and specific impacts to the rocket-combustor design community are noted.

2.0 Research Objectives

Coaxial injectors are currently the most common injector configuration used in hydrogen/oxygen propelled rocket engines. These injectors are at a mature stage of development and feature good performance and stability. However, in order to achieve these characteristics, high pressure drops across the injector are required to ensure adequate liquid atomization and propellant mixing, and considerable effort is expended in designing baffles and acoustic cavities for the combustion chamber to prevent potential instabilities, as in the case of the Space Shuttle Main Engine. Swirl coaxial injectors have been proposed as a means to alleviate these difficulties.

The conventional coaxial injector achieves atomization through the shear interactions between the high speed gaseous hydrogen jet which surrounds the liquid oxygen core flow at the point of injection. For sufficiently high gas velocity to liquid velocity ratios, typically 8 to 1, rapid atomization of the core can be achieved. Achieving the necessary high gas injection velocities requires high pressure differences across the injector and consequently, the components upstream of the injector element are also subjected to high pressure levels.

In contrast, for swirl coaxial injectors, a swirling motion is imparted to the liquid. This enhances the atomization and mixing processes resulting in lower injector pressure drop for equivalent injector performance. The results of a limited number of studies also indicate that swirl

coaxial injectors provide operating stability over a wider range of fuel to oxidizer velocity ratio. Swirl coaxial injectors were shown to be stable at gas to liquid velocity ratios of 3.5 and greater, whereas conventional coaxial injectors required a velocity ratio of at least 6.5 or higher. The ability to utilize lower gas injection velocity results in lower injection pressure requirements, and thus offers hardware design and cost benefits.

In order to make rocket injector design choices for swirl coaxial elements, a better understanding of their atomization and mixing characteristics is required. A review of the literature reveals that very little fundamental information, either cold-flow or hot-fire, is available for this type of rocket injector. Therefore, the present study augments knowledge of the swirl coaxial injector by considering the following aspects of this problem:

1. Measurements are made of droplet size, size distribution, velocity, and spatial variation of the spray droplet field for designed injector elements that are representative of rocket engine injectors in terms of geometry and flow conditions. Phase/Doppler interferometry studies focus on the dilute spray region to characterize the atomization flowfield of swirl coaxial injectors.

2. A series of combusting studies with the same injector using hydrogen and liquid oxygen as the propellants are conducted in the Cryogenic Combustion Lab (CCL) at the Penn State Propulsion Engineering Research Center (PERC). This laboratory is capable of testing oxygen/hydrogen injectors with total flows up to 1 lbm/s over a wide range of oxidizer to fuel ratios. Injectors performance and stability characteristics are demonstrated in this work.

3.0 Research Accomplishments

3.1 Review of Coaxial Gas/Liquid Spray Literature

Atomization is generally regarded as the rate-controlling element in the atomization-vaporization-mixing-chemical reaction chain of events leading to energy release in rocket combustion devices (preburners and main combustion chambers). An understanding of atomization for coaxial gas/liquid injection is believed to be the key to providing designers with a means to optimize the rocket combustion processes as well as address combustion stability issues which are linked to injector atomization characteristics.

In order to survey the state-of-the-art, prior works in the spray literature on injection processes were reviewed for their applicability towards predicting spray atomization characteristics for liquid oxygen/gaseous hydrogen (LOX/GH_2) rocket injectors. It was found that the present data base on both the shear and swirl type of coaxial gas/liquid injectors consists solely of non-combusting (cold-flow) spray experiments with fluids which do not simulate the unique propellant properties of GH_2 and LOX, namely, GH_2 density at injection, and LOX surface tension and viscosity. Simulations of these properties is crucial to obtaining atomization results that are relevant to LOX/GH_2 injector sprays. Previously developed drop-size correlations for primary atomization, based upon cold-flow studies, do not apply to rocket injector conditions, and therefore cannot be used as a predictive tool. In order to extend the knowledge of sprays atomization to cover low viscosity and low surface tension liquids, such as LOX, a special set of cold-flow and hot-fire atomization studies are required. The experiments must simulate LOX/GH_2 rocket injection conditions of high flowrate, high Reynolds and Weber numbers, and need to be performed under combusting and non-combusting environments. Details of the literature review for shear coaxial injection are presented in Attachment A, which contains a reprint of an AIAA paper on this topic. Literature related to swirl coaxial injection is covered in another AIAA paper which is provided as Attachment B.

3.2 Swirl Coaxial Injector Combustion Studies

The paucity of information on rocket-scale injectors, particularly for the swirl coaxial type, led to an effort focused upon design, fabrication, and testing of a research swirl coaxial rocket injector element. Guidelines from industry were applied to achieve a design which replicated the geometry of actual rocket injectors and operated at conditions similar to full-scale in terms of injector element flowrate, swirl strength, Reynolds number, Weber number, and chamber pressure. The designed injector, illustrated in Figure 1, is patterned after RL10A engine main propellant injectors utilized by Pratt and Whitney, and is almost identical to an industry research injector.[1] A windowed research combustor employed to evaluate injector characteristics is shown in Figure 2.

Rapid implementation of the research injector for combustion characterizations was the first significant achievement of this AASERT program. In particular, combustion studies performed at the Propulsion Engineering Research Center at Penn State successfully demonstrated the high performance characteristics of LOX/GH_2 swirl coaxial injection on a single-element basis over a wide range of oxidizer to fuel ratios from 3 to 175. High c*-efficiencies of 90% or better are

achieved as indicated in Figure 3. Excellent ignition characteristics, as well as stability and flameholding, were verified in this work. Peak-to-peak pressure fluctuations of less than 6% of the measured chamber pressure were indicative of stable combustion (see Figure 4). The result that high performance and stability are possible for oxygen-rich combustion[2] of LOX/GH_2 propellants was helpful for establishing the feasibility of oxygen-rich combustion devices for advances rocket engine cycles[3] such as that recently envisioned for Reusable Launch Vehicle application. The oxygen-rich studies were discussed in a JANNAF meeting paper which is provided as Attachment C.

Pursuant to the research objective of characterizing LOX swirl atomization, cold-flow and hot-fire visualization studies were performed with the injector. As shown in Figure 4, simulation of the swirl spray with water and air provided an analog for understanding the basic atomization phenomenon for this design. The distribution of LOX drops within the conical flame zone, visualized by laser-light scattering, was seen to be consistent with cold-flow spray visualizations. This first *in situ* observation of a combusting swirl coaxial injector flowfield, mixing and burning more rapidly than its non-swirled counterpart,[4] provides the fundamental reason for improved c*-efficiencies for this type of injector. More details on the visualization studies may be found in Attachment B.

3.3 Scaling Methodology for Swirl Coaxial Atomization

A phase/Doppler interferometry instrument was employed for quantitative measurements of atomization for the designed injector in cold-flow. The most relevant previous study in this vein is by Hautmann.[1] In the present research, however, a more fundamental approach was taken in an experiment designed to study the role of Weber number in particular since it is known to be a key parameter governing atomization processes. Simultaneous drop size and drop velocity measurement data were obtained for two different size injectors of the same design where water was employed to generate a swirl spray with no coaxial gas. Flow conditions were chosen to equate the liquid injection Weber number of the two injectors. After normalizing the measured results, using appropriate length and velocity scales of the flow, comprehensive atomization similitude was revealed between the two sets of results (see Figure 5). Remarkably, normalized values of Sauter mean diameter, drop velocity components, drop distributions, and other parameters, were found to be equivalent for the two cases.

The similarity provides a powerful yet simple means to scale the results for one injector to other injectors of different sizes, assuming equivalent Weber number, based only upon knowledge of the length and velocity scales of liquid injection. This is of direct benefit to industry where the scaling methods can be incorporated into injector sizing activities. Work in progress indicates a potential for similitude in swirl sprays with coaxial gas flow based upon gas to liquid momentum ratio. Attachment D documents these findings in a manuscript to be submitted to the journal *Physics of Fluids.*

4.0 Conclusion

A research focus on rocket-scale swirl coaxial gas/liquid injection has led to detailed characterizations of a single-element research injector that will benefit the rocket combustor design community. Noteworthy developments include the following:

1) A research swirl coaxial injector element, patterned after industry designs, was fabricated and studied in a windowed combustion chamber using actual liquid oxygen/gaseous oxygen propellants. A complementary capability for cold-flow studies was developed employing water and air as convenient propellant simulants to investigate the spray flowfield behavior for this type of injector.

2) Favorable ignition, flameholding, and stability characteristics of swirl coaxial injection were demonstrated and visualized in the windowed combustor over a wide range of oxidizer to fuel mixture ratios (3 to 175), and chamber pressures (200 to 700 psia), at single-element flowrates comparable to actual rocket injectors. In particular, efficient combustion at extreme mixture ratios is a feature of the present injector which can be exploited in the design of oxygen-rich combustion devices for advanced rocket cycles.

3) The nature of swirl coaxial spray phenomena, which allow for efficient combustion, was elucidated through cold-flow studies employing the Phase/Doppler interferometry technique for drop sizing and velocimetry. The critical role of Weber number as the key determinant of swirl atomization behavior was revealed. In particular, the demonstration of atomization flowfield similitude based upon Weber number leads to a scaling methodology which can be used by designers to estimate drop size and velocity for swirl injectors of varying sizes.

5.0 References

1. Hautman, D. J., "Spray Characterization of Liquid/Gas and Liquid/Liquid Coaxial Injectors with the Center Liquid Swirled," Report No. UTRC89-31, United Technologies Research Center, East Hartford, CT. June 1990.

2. Knuth, W. K., and Crawford, R. C., "Oxygen-Rich Combustion Process Applications and Benefits," AIAA Paper 91-2042, AIAA/SAE/ASME 27th Joint Propulsion Conference, Sacramento, CA., June 24-26, 1991.

3. Jensen, R. J., Farhangi, S., Tuegel, L., and Roberts, T., "Oxygen-Rich Preburner Technology for Full Flow Cycle Applications," *Proceedings of 2nd International Conference on Liquid Rocket Propulsion*, ONERA, Paris, France, June 1995.

4. Beisler, M., Pal, S., Moser, M. D., and Santoro, R. J., "Shear Coaxial Injector Atomization in a LOX/GH_2 Propellant Rocket," AIAA Paper 94-2775, *30th AIAA/ASME/SAE/ASEE Joint Propulsion Conference*, Indianapolis, IN, June 27-29, 1994.

6.0 Publications

Rahman, S., A., and Santoro, R. J., "A Review of Coaxial Gas/Liquid Spray Experiments and Correlations," AIAA Paper 94-2772, *30th AIAA/ASME/SAE/ASEE Joint Propulsion Conference*, Indianapolis, IN, June 27-29, 1994.

Rahman, S., A., Pal, S., and Santoro, R. J., "Swirl Coaxial Atomization: Cold-Flow and Hot-Fire Experiments," AIAA Paper 95-0381, *33rd Aerospace Sciences Meeting and Exhibit*, Reno, NV, January 9-12, 1995.

Rahman, S., A., Pal, S., and Santoro, R. J., "Coaxial Swirl Injector Studies at High O/F Ratios," *Proceedings of the 32nd JANNAF Combustion Subcommittee Meeting*, Huntsville, AL, October 23-27, 1995.

Rahman, S., A., Pal, S., and Santoro, R. J., "Atomization Study of Swirl Coaxial Rocket Injectors," *Proceedings of the 9th Annual Conference on Liquid Atomization and Spray Systems (ILASS-96)*, San Francisco, CA, April 19-23, 1996.

Rahman, S., A., Pal, S., and Santoro, R. J., "Similitude in pressure-swirl atomizer sprays," to be submitted to *Physics of Fluids* for publication.

7.0 Interactions and Acknowledgments

During the course of the program we have had several interactions with industry and government laboratories regarding our work on rocket injectors, in general, and swirl coaxial injectors, in particular. Below, the major contacts related to these interactions are listed:

UTRC -	Don Hautmann
Pratt and Whitney -	George Cox, Combustion Technology Manager
Aerojet -	Mr. Jerry Pieper, Manager, Product Analysis Group, and Mr. Jim Hulka
Rocketdyne -	Steve Fisher, Manager, Advanced Combustion Devices
NASA Marshall -	Mr. John Cramer, and Mr. John Hutt, Combustion Physics Branch

Initial assistance was received from Aerojet, Pratt & Whitney, and UTRC engineers and researchers who provided technical guidance in injector design, as well as some sample injector hardware. The present research injector design reflects their inputs.

Successful implementation of the injector in hot-fire experiments has provided an impetus for further study of oxygen-rich combustion with LOX/GH_2 swirl coaxial elements at NASA-Marshall. Two identical units of the present research swirl coaxial injector were fabricated and provided to the Combustion Physics Branch, NASA-Marshall, for high pressure mixing and combustion studies which are now in progress. This research has also complemented the concurrent oxygen-rich studies with impinging elements at Rocketdyne.

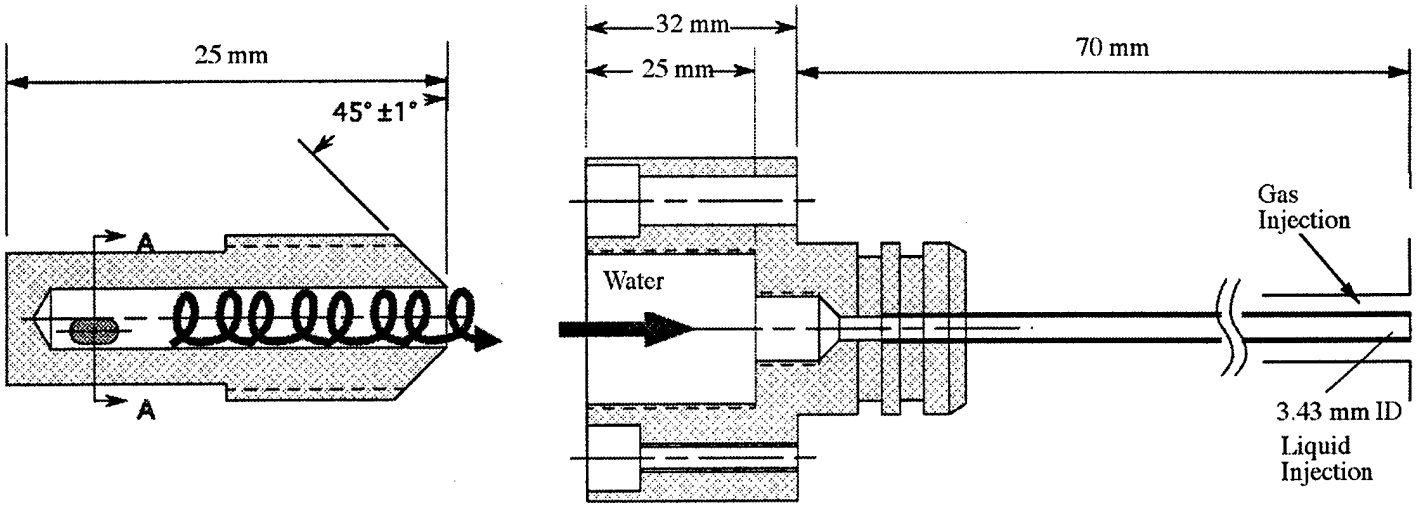

Swirl Insert
(enlarged for clarity)

Swirl Coaxial Injector

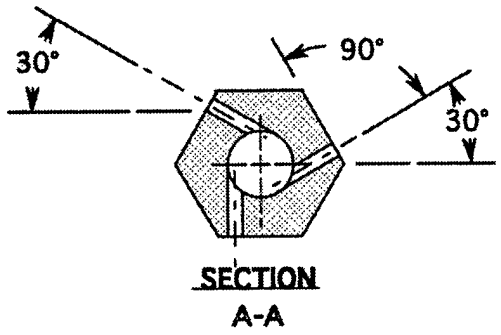

Figure 1. Design of research swirl coaxial injector element. Swirl is imparted to the liquid in the center post tube by means of three tangential-entry slots (section A-A) in the swirl insert piece.

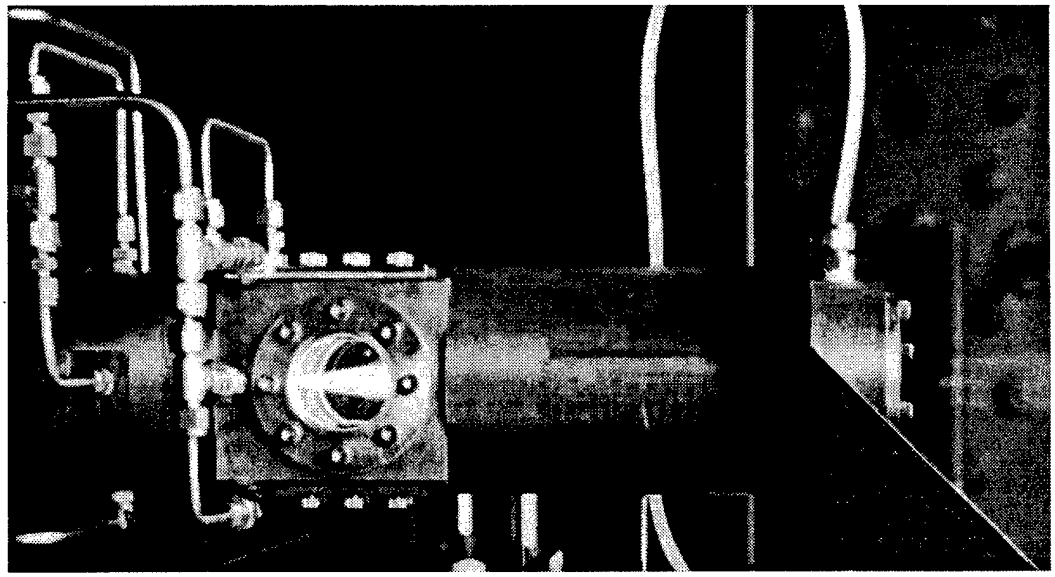

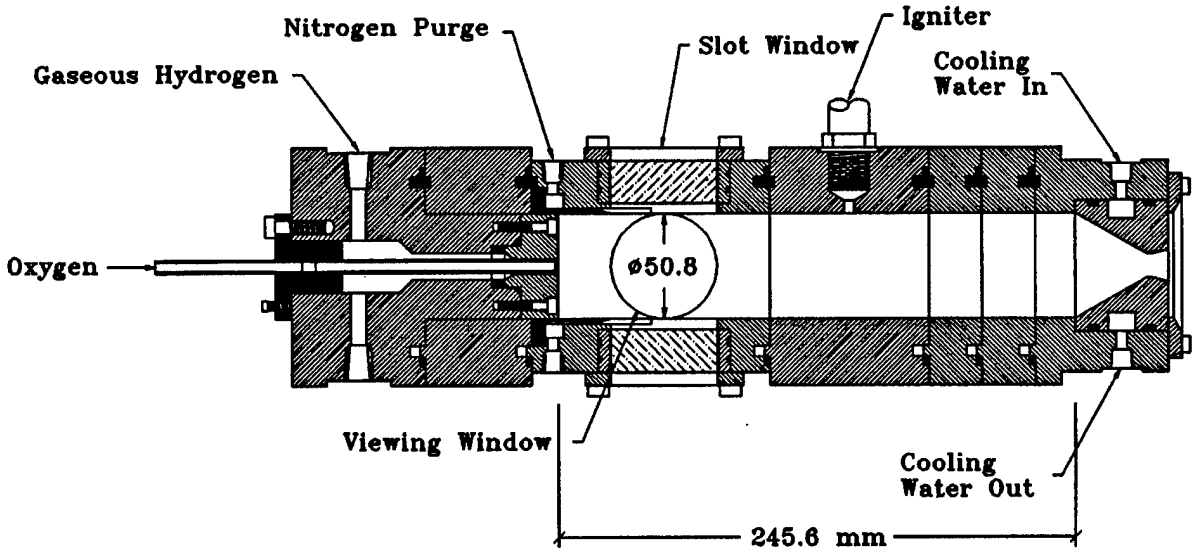

Figure 2. View of combustion chamber for single-element injector studies (top), and schematic cross-section of the same chamber (bottom). Optical access is provided by 50.8 mm round windows. A conventional coaxial injector element is shown.

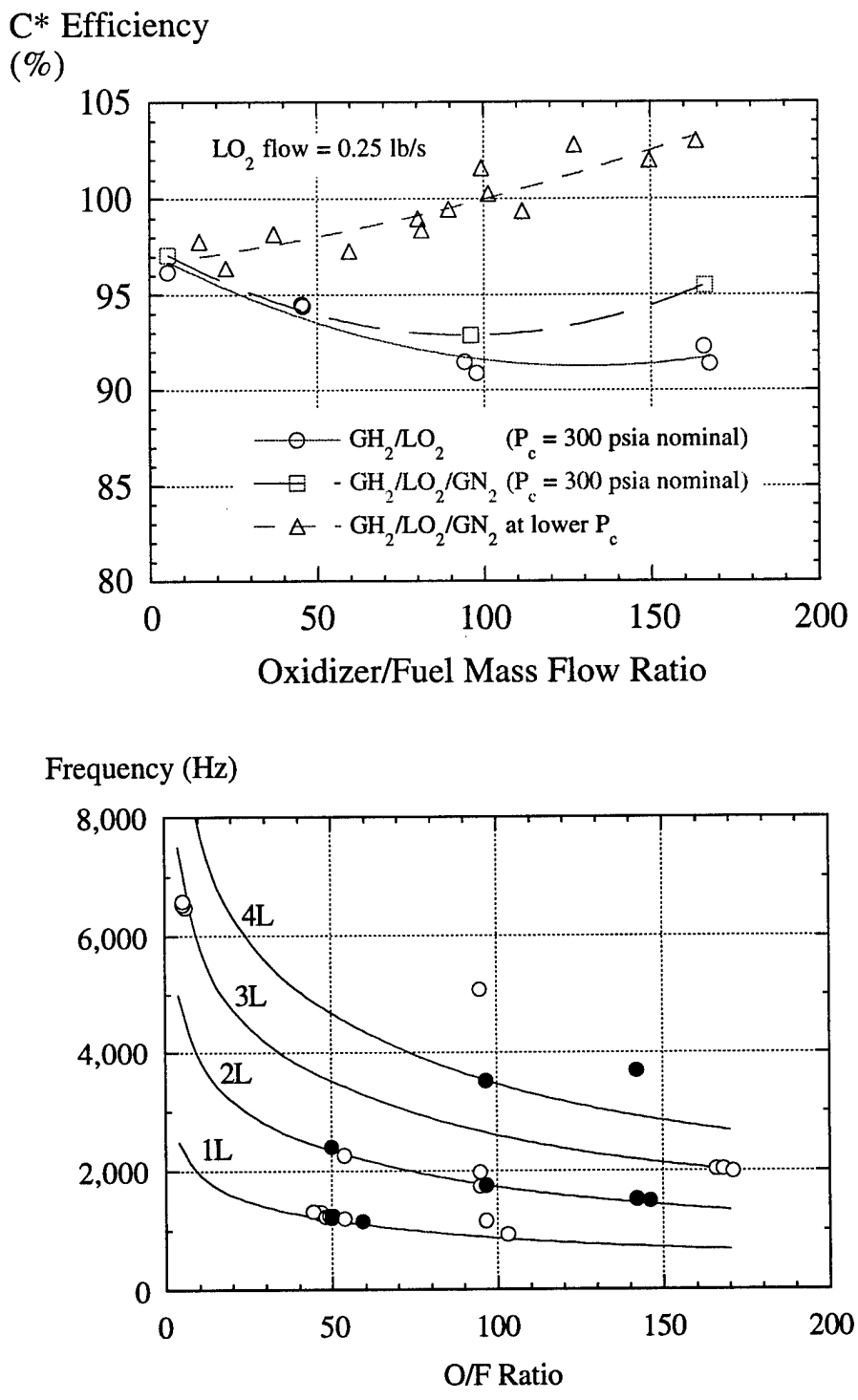

Figure 3. High c*-efficiency (top) and combustion stability (bottom) over a range of O/F ratios are features demonstrated for the research swirl coaxial injector element in the windowed rocket chamber. Peak-to-peak pressure fluctuations during combustion were less than 6% of chamber pressure and restricted to longitudinal modes 1L, 2L, 3L, 4L. Stability results are for the designed injector, and a larger twice-scale version (small o, and large •)

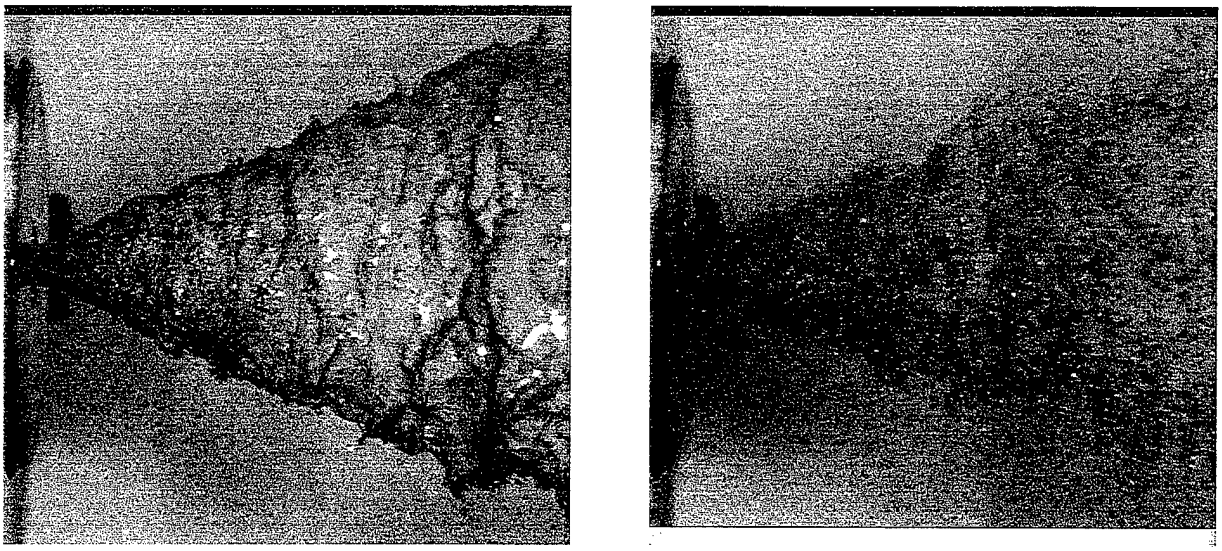

Figure 4a. Near-injector spray visualization with the research swirl coaxial injector element. Flow is from left to right (51 mm field of view). Water and air are used as propellant simulants. Image on left, with no coaxial air flow, exhibits a contiguous liquid sheet, and the image at right, with coaxial air flow, demonstrates rapid sheet breakup and atomization which are favorable for propellant mixing and combustion (see below).

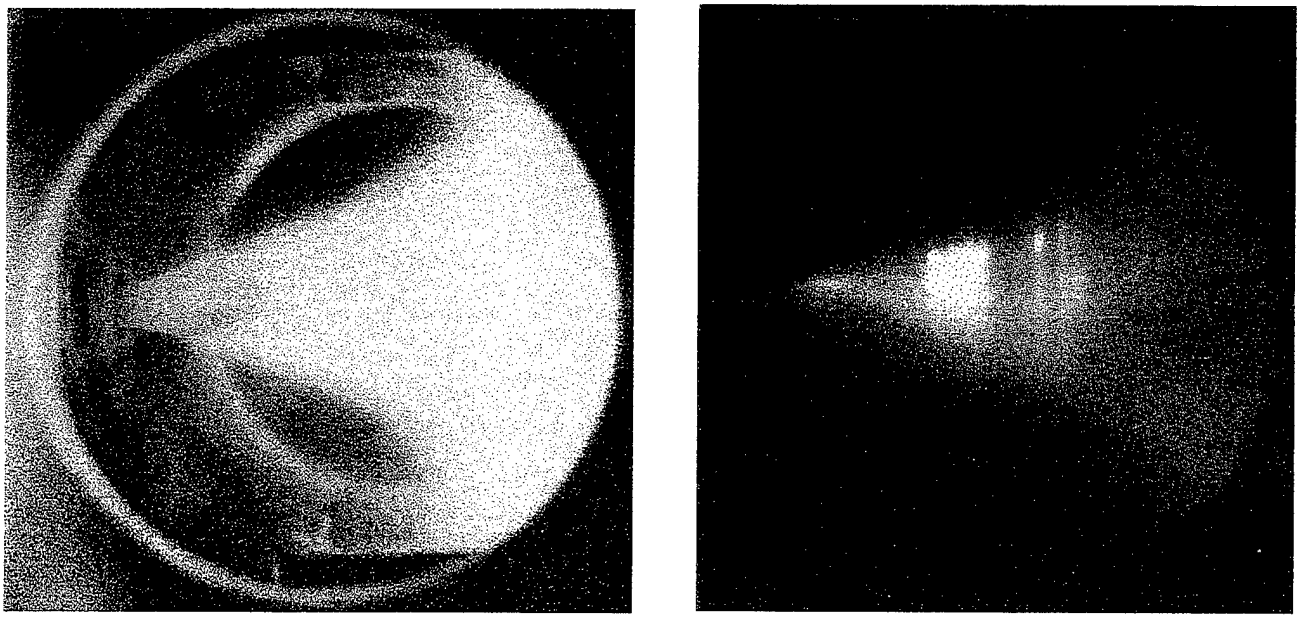

Figure 4b. Near-injector combustion flowfield visualization with the same injector element as seen through 51 mm quartz windows. Propellants are LOX/GH_2. Chamber pressure is 2.75 MPa (400 psia). Image on the left demonstrates that an effect of LOX swirling is to rapidly expand the combustion zone. Image on the right is scattered laser light (514.5 nm) from combusting LOX spray. This images shows a technique which can be effectively used to distinguish the presence of LOX drops.

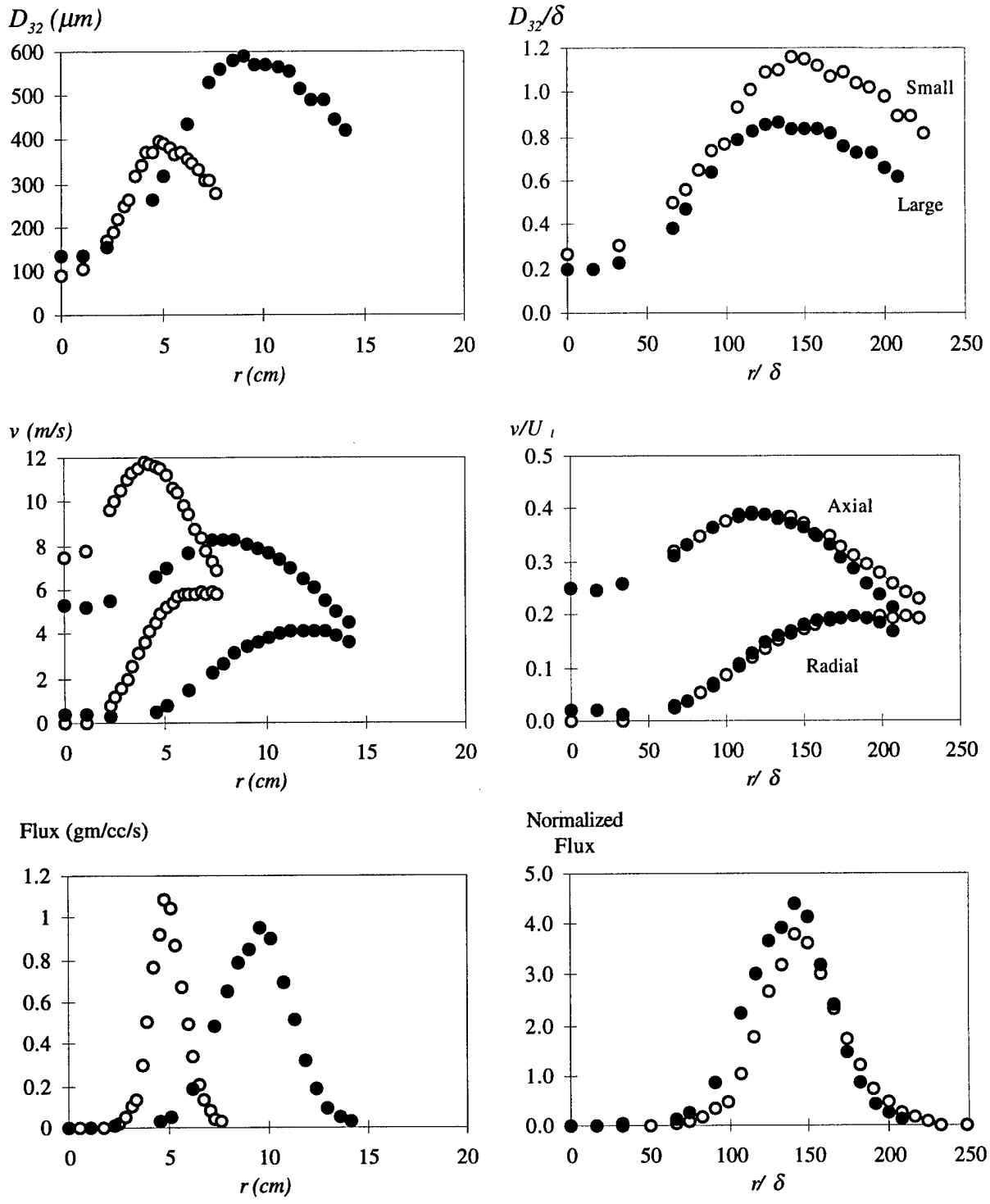

Figure 5. Phase/Doppler interferometry results for the research swirl injector (case of no coaxial gas) include drop size, velocity, and mass flux radial distributions for water sprays produced by two different size injectors: small o, and large • (figures at left). Similitude is demonstrated, based upon Weber number, by normalizing the data using appropriate liquid injection length and velocity scales (figures at right).

Attachment A

A Review of Coaxial Gas/Liquid Spray Experiments and Correlations

by

S. A. Rahman and R. J. Santoro
(AIAA Paper 94-2772)

30th AIAA/ASME/SAE/ASEE Joint Propulsion Conference
Indianapolis, IN
27-29 June 1994

AIAA 94-2772

A Review of Coaxial Gas/Liquid Spray Experiments and Correlations

S. A. Rahman and R. J. Santoro

The Pennsylvania State University
University Park, PA

30th AIAA/ASME/SAE/ASEE Joint Propulsion Conference
June 27-29, 1994 / Indianapolis, IN

A REVIEW OF COAXIAL GAS/LIQUID SPRAY EXPERIMENTS AND CORRELATIONS

S. A. Rahman* and R. J. Santoro†

Propulsion Engineering Research Center
and
Department of Mechanical Engineering
The Pennsylvania State University
University Park, PA. 16802-2320

Abstract

Published literature on shear coaxial injector atomization was reviewed for information that would be relevant to predicting spray drop-sizes from liquid oxygen/gaseous hydrogen (LOX/GH_2) rocket injectors. It was found that the present data base on shear coaxial injectors consists solely of non-combusting (cold-flow) spray experiments with fluids which do not simulate the unique propellant properties of LOX and GH_2, namely, GH_2 density at injection, and LOX surface tension and viscosity. Simulation of these properties is crucial to obtaining atomization results that are relevant to LOX/GH_2 injector sprays. Previously developed drop-size correlations for primary atomization, based upon cold-flow studies, also do not apply to such rocket injector conditions, and therefore cannot be used as a predictive tool. In order to extend the knowledge base on spray atomization to low viscosity and low surface tension liquids such as LOX, a unique set of cold-flow and hot-fire primary atomization studies are required. Such experiments must simulate the high flowrates, high Reynolds and Weber numbers, as well as the propellant properties of LOX/GH_2 rocket injectors and be performed under both non-combusting and combusting environments. Some issues pertaining to designing the experiments are presented in this paper.

Nomenclature

A	area of cross-section
d	liquid jet diameter
D	gas annulus outer diameter
D_h	hydraulic diameter of gas flow
$\overline{D}$	spray-average drop-size
$\dot{m}$	flowrate
P	pressure
r,z	radial and axial coordinates
R	specific gas constant
Re	Reynolds number, gas - $Re_g = \rho_g U_g D_h / \mu_g$, liq - $Re_l = \rho_l U_l d / \mu_l$
t	wall thickness of post tube
T	temperature
U	velocity
V_r	relative velocity, $\lvert U_g - U_l \rvert$
MMD	mass median diameter, ($\overline{D}_{V0.5}$)
SMD	Sauter mean diameter, ($\overline{D}_{32}$)
We	Weber number, gas - $We_g = \rho_g \left(U_g - U_l\right)^2 d / \sigma$

Greek Symbols

ρ	density
μ	dynamic viscosity
σ	surface tension

Subscripts

ac	acoustic
c	chamber
crit	critical
g	gas
l	liquid
10	arithmetic mean
32	Sauter mean

Introduction

Spray atomization is of interest to the propulsion community from the standpoint of propellant injector design for liquid rocket engine combustion chambers and gas generators. Propellant injection and atomization from a shear coaxial jet refers to the breakup of the core liquid jet by shear forces due to a coflowing, high velocity, annular gas jet surrounding the core liquid stream (see

---

* Graduate Student, Mechanical Engineering, Member AIAA

† Professor, Mechanical Engineering, Member AIAA

Fig. 1). An appreciable experimental data base on this type of atomization process is available in the published literature. The purpose of the review was to determine whether this published atomization literature is pertinent to the special case of shear coaxial LOX/GH_2 propellant injection into the combustion chamber of a liquid rocket engine. The ultimate objective of this effort is to advance the understanding of atomization in rocket chambers such as the RL10A-1, J-2, and the SSME (Space Shuttle Main Engine), all of which were designed for shear coaxial injection of LOX/GH_2 propellants.[1]

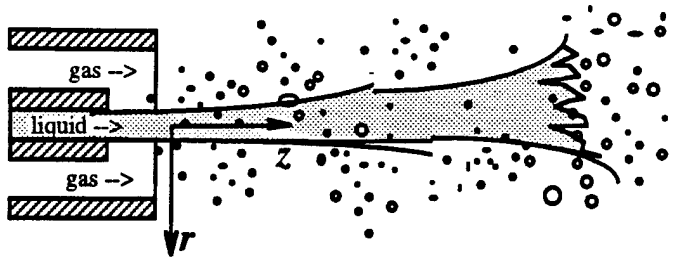

Fig. 1. Schematic of a Shear Coaxial Gas/Liquid Spray

The evaluation of shear coaxial atomization literature amounted to a comparison of several uni-element cold-flow (non-combusting) spray studies since there is virtually no atomization data under combusting (hot-fire) conditions for this injector. Hence, some of the more unique and comprehensive cold-flow spray experiments in the literature were analyzed with a view towards their applicability to rocket propellant injection and atomization. Specifically, two tasks were performed:

1. cold-flow experimental conditions of several studies were compared to typical LOX/GH_2 rocket injector conditions (in terms of injection velocity, flowrate, Reynolds number, etc.), and,
2. published correlations for primary atomization were exercised to predict LOX drop-size in rocket combustion chambers.

In this manner, several deficiencies in the atomization knowledge base became apparent. After a cursory introduction to the shear coaxial atomization literature, these deficiencies will be explained in following sections.

Overview of Shear Coaxial Spray Literature

Previous reviews have provided comprehensive publication lists of the work done in industry, universities, and government laboratories on gas/liquid coaxial sprays (also known as two-fluid, twin-fluid, pneumatic, or airblast atomization). Among these, the reviews of Ferrenberg et al.,[2] Nurick[3] and Lefebvre[4] are sufficiently recent and fairly thorough in covering all previous experimental work on the *shear* coaxial type of spray atomization process --- there were over one-hundred articles and reports cited. However, none of the reviews have specifically addressed the relevance to the unique situation of atomization in rocket chambers employing cryogenic propellants like LOX/GH_2. In view of this, some of the more systematic and interesting experiments on atomization were selected from the extensive bibliographies of previous reviewers for the purpose of this study. An examination of the experimental conditions and results of a carefully selected subset of articles, given chronologically in Table 1, helps to identify the areas where knowledge of atomization needs to be improved in order to predict atomization in rocket chambers. Most of the ensuing discussions in this paper are focused on the works listed in the table.

Table 1
Selected Atomization Studies on Shear Coaxial Injectors

Investigators	Technique	Result Reported	Results Correlated?
Weiss,[5] 1959	Wax	MMD	yes
Kim,[6] 1970	Wax	MMD	yes
Burick,[7] 1974 Falk,[8] 1973	Wax	MMD	no
Lorenzetto,[9] 1977	Light-Scattering	SMD	yes
Ingebo,[10,11] 1990	Light-Scattering	SMD	yes
Zaller,[12] 1991	Phase Doppler Interferometry	SMD vs. z, r	yes (unpublished)
Hardalupas,[13] 1992	Phase Doppler Interferometry	SMD vs. z, r	no

It should be noted that the selected works are all experimental in nature, and the associated articles/reports document test conditions and results of experiments involving atomization of a core liquid jet by a coannular, high velocity gas jet in a non-combusting environment.

The experiments of Table 1 were studied specifically for the insights each provided on atomization. The uniqueness of each study should be noted here. First, the experiments by Weiss and Worsham,[5] Kim and Marshall,[6] and Lorenzetto and Lefebvre,[9] conducted at universities, are relatively important because they attempted to characterize liquid property effects (viscosity, density, and surface tension) on atomization, drop-size and provided engineering correlations of their results. Among them, Lorenzetto's work was the most systematic since all three properties were more or less isolated in turn. Next, the work of Hardalupas et al.[13] and Zaller and Klem[12] is noted since their experiments were designed to address rocket injectors using water and air as

simulants. Their atomization results are also spatially resolved because they employ state-of-the-art, non-intrusive drop-sizing techniques in their ongoing work. The work of Burick[7] and Falk[8] using heated wax as the liquid simulant is noteworthy because they also focused on rocket injector design issues and generated a substantial data set on atomization. Their results along with those of Zaller and Klem[12] were recently correlated by Nurick.[3] Finally, the experiments of Ingebo[10,11] were included for comparison with the others since those studies, unlike the rest, involved a systematic investigation of gas property effects, and also made use of liquid nitrogen which is a good simulant for liquid oxygen. Correlations were developed by Ingebo,[10,11] and will be discussed with the other correlations in a later section.

Before reviewing and comparing these experiments in detail, some general points should be mentioned. Comparison of the above works must be viewed in light of several caveats. First, the coaxial injection process was achieved in quite different manner by geometrically different injectors in these experiments as shown in Fig. 2. Given the various sizes, shapes, and length-to-diameter ratios of these injectors, atomization results from one may not be universally applicable to other injectors. Ingebo's injector is particularly unlike the typical rocket injector shown in Fig. 1. Similarly, the variety of fluid simulants used (water, kerosene, wax, alcohol mixtures) also precludes a more general interpretation of the results, or even the trends in the results, since the phenomenology of coaxial atomization is not yet established. The results may also be biased by the

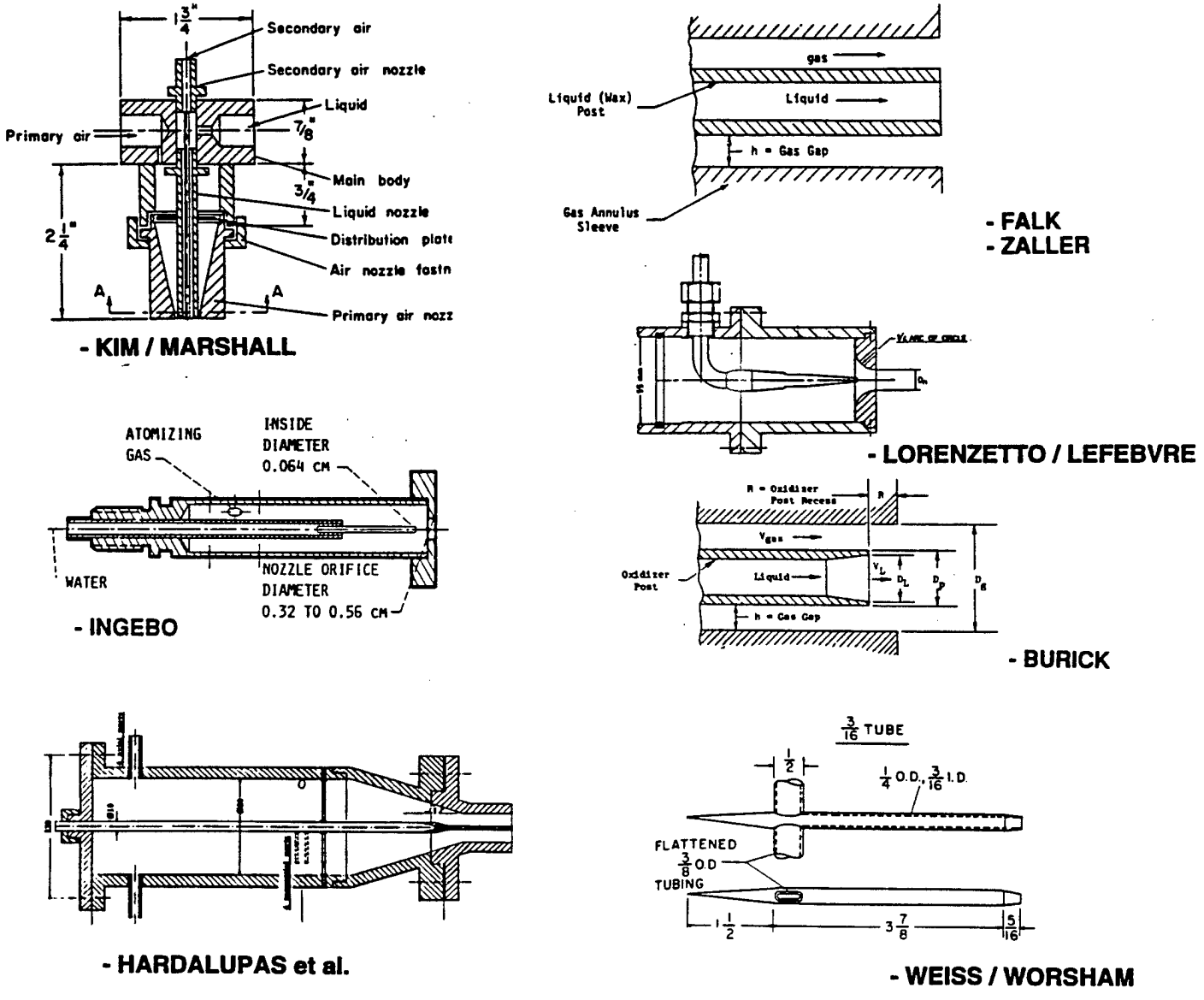

Fig. 2. Various kinds of Coaxial Gas/Liquid Atomizers Studied Previously (Refs. 5-13)

drop-sizing technique itself, especially if the method was intrusive. Finally, as mentioned earlier, the studies themselves focused on a limited set of variables, either scale, fluid property, or flowrate effects, and therefore do not overlap sufficiently to properly verify the other's results and conclusions.

Given these caveats, the shear coaxial atomization "data base" is an assorted collection of laboratory results that cannot be readily applied to any injector flow or fluid combination. Nevertheless, when taken collectively, the studies cited in Table 1 begin to provide some guidance towards the understanding of liquid rocket chamber atomization, as the following discussions will attempt to show.

Comparison of Shear Coaxial Spray Experiments

Cold-flow atomization experiments of Table 1 were compared in terms of the physical parameters that were varied in the testing, namely, injector scale, flowrates, velocities, fluid properties, and Reynolds number, *Re* and Weber number, *We*, which are the global quantities that are believed to control the atomization process. This was done to examine the physical "parameter space" in which atomization data are available. The extent of the parameter variation of the experiments is reviewed in a series of figures, Figs. 3 - 10, that illustrate both liquid and gas side injection conditions. For instance, liquid post diameter, and the corresponding gas annulus hydraulic diameter, for all injectors tested are indicated in Fig. 3 in a plot of d vs. D_h. Fig. 4 similarly presents all injection velocities in a plot of U_l vs. U_g, and so forth.

Operating conditions of typical LOX/GH_2 shear coaxial rocket injectors, the RL10A-1, J-2, and the SSME, were also assembled and compared in the figures. Thus, it was possible to determine which parameters of LOX/GH_2 injection were approximately matched in cold-flow atomization studies. This was a first step in ascertaining the relevance of cold-flow results to atomization in rockets. The three flight-proven rocket engines were selected as a representative sample for comparison with the cold-flow studies. Their operating chamber pressures are 300, 900, and 3300 psia, respectively, spanning a range of pressures from sub-critical (RL10A-1), to near-critical (J-2), to super-critical (SSME) in terms of the thermodynamic states of liquid oxygen (P_{crit}=730 psia). The findings from the comparisons are discussed below.

Atomizer Scale and Injection Velocity

The various injector sizes used by experimenters are summarized in Fig. 3. This plot clearly differentiates studies with respect to the sizes of posts and annuluses. The annulus hydraulic diameter D_h equates to twice the annulus gap dimension, and the liquid post size refers to the inner diameter d of the LOX post. The three injectors employed by Burick are shown as points connected by lines, while other studies employing several combinations of posts and annuluses (e.g. Lorenzetto: 4 posts and 10 annuluses of varying sizes) are indicated by a box drawn around the largest and smallest sizes. In this representative sample of atomization experiments, the liquid posts are seen to range from 0.4 mm to 5.6 mm, while gas hydraulic diameters D_h range from 0.25 mm to 20 mm. Note from this figure that typical rocket injector liquid posts are from 2 to 5 mm in diameter, while D_h are approximately 2 to 3 mm. Evidently, a few of the

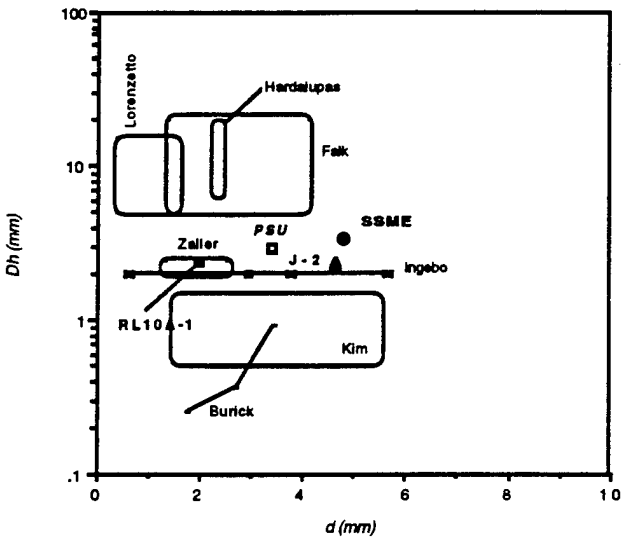

Fig. 3. Comparison of sizes for shear coaxial injectors

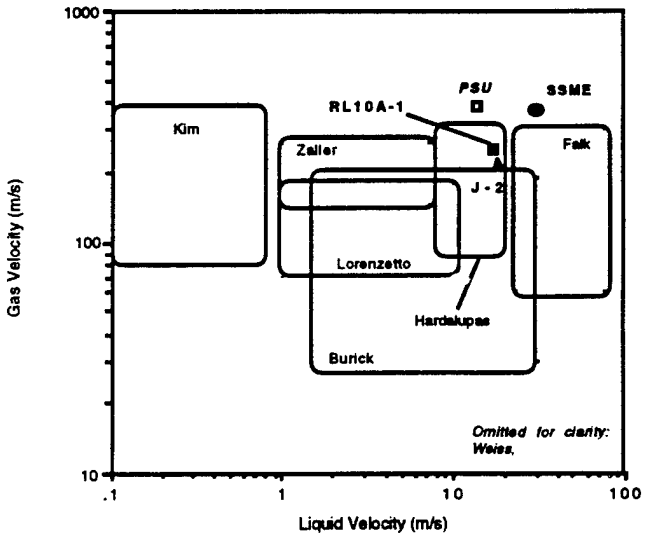

Fig. 4. Comparison of shear coaxial injector velocities

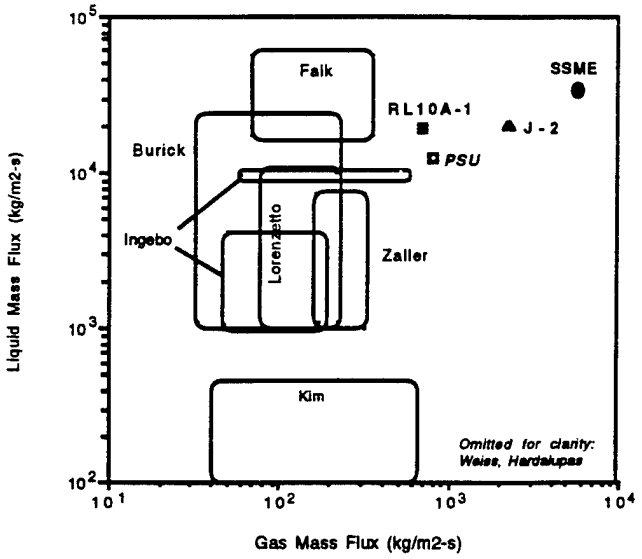

Fig. 5. Comparison of shear coaxial injector mass fluxes

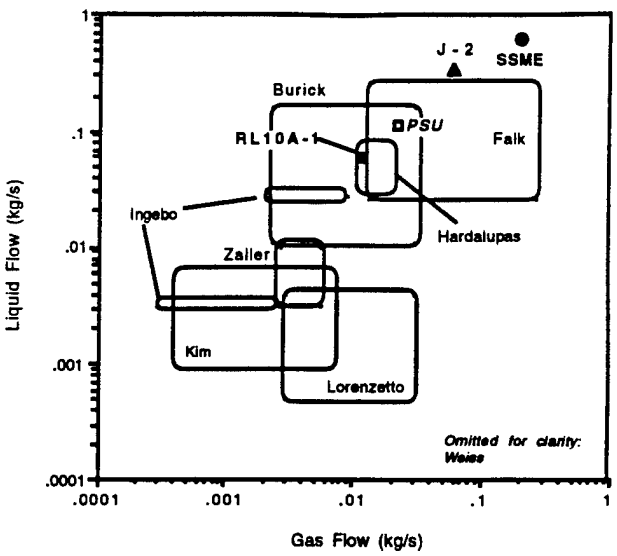

Fig. 6. Comparison of shear coaxial injector flowrates

laboratory injectors were similar in scale to typical rocket injectors.

A research LOX/GH_2 injector studied at Penn State University (PSU) is also shown in Fig. 3 designated as "PSU." This injector and its combustion chamber were designed specifically for non-intrusive diagnostic studies under realistic rocket conditions. Pal et al.[14] are currently employing this injector to measure LOX drop-size; typical injection conditions for these tests will also be compared in subsequent figures.

In Fig. 4 the bulk velocities, and velocity ratio, at the exit of the injectors are compared. Note that the axes are logarithmic, and that lines of constant velocity ratio run diagonally across the plot. This figure further differentiates the studies with respect to the coaxial injection velocities. This comparison showed that some of the work of Burick,[7] Falk,[8] and Hardalupas et al.[13] simulated the velocities of LOX and GH_2 propellant injection, as well as the gas-to-liquid velocity ratio. The rocket injector velocities were generally higher than the cold-flow studies, with velocity ratios of 10 or greater.

Atomizer Flow and Gas Injection Density

Further comparisons in Figs. 5 - 7 compare density, mass fluxes, and mass flowrates, for both gas and liquid streams. They also appeared to show that the experiments of Burick,[7] Falk,[8] and Hardalupas et al.[13] were more representative of rocket injector flows. The shear force in shear coaxial atomization is due to both the velocity *and density* of the gas stream. Hence it would seem reasonable to compare the gas density, mass flux (density-velocity product), and mass flowrate (density-velocity-scale product) of laboratory sprays to propellant injection in rockets. Comparisons revealed that flowrates and fluxes in cold-flow studies were usually lower than LOX/GH_2 rocket injection conditions, by approximately one order-of-magnitude in some cases (cf. Fig. 5 and 6).

From closer examination of cold-flow conditions it was found that an inability to simulate gas injection density of rockets causes the flux and flowrate differences highlighted above. High pressures in the RL10, J-2, and SSME combustors lead to GH_2 injection densities ranging from 0.0025 to 0.015 kg/m^3 (gas density $\rho_g = P_c/RT_g$). By comparison, cold-flow studies have typically employed air or nitrogen (for convenience) as simulants at a density of only 0.0012 kg/m^3, a factor of 8 or more lower as compared to the corresponding J-2 and SSME values shown in Fig. 7. This implies a proportionally lower gas mass flux ($\rho_g U_g$) or gas mass flow ($\dot{m}_g = \rho_g A_g U_g$) even when the gas injection velocity is high enough to simulate a rocket injector. In fact, a proper simulation of the shearing effect of the gas stream on the liquid core requires a simultaneous simulation of all four parameters in the continuity equation $\dot{m}_g, \rho_g, A_g, U_g$. When any one of the four is not simulated, at least one other parameter is also not simulated and a hydrodynamic matching of gas injection is rendered impossible.

In light of the above, the Burick[7] and Falk[8] experiments did not adequately simulate LOX/GH_2 rocket injectors in spite of the fact they covered the range of rocket element flowrates and velocities. Gas density and injector scale were quite different from the rocket injectors shown in the figures. It was found that Ingebo was the only investigator to experimentally isolate and correlate the important effect of gas injection density. This was done by employing helium, nitrogen, air, and

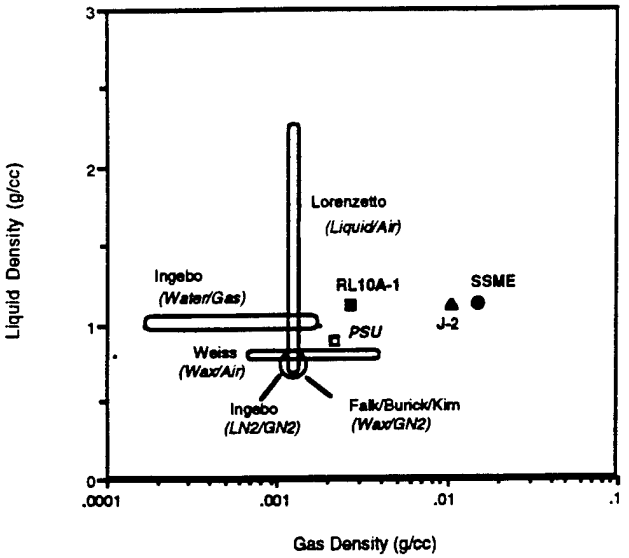

Fig. 7. Comparison of injection densities of simulants with liquid oxygen and gaseous hydrogen

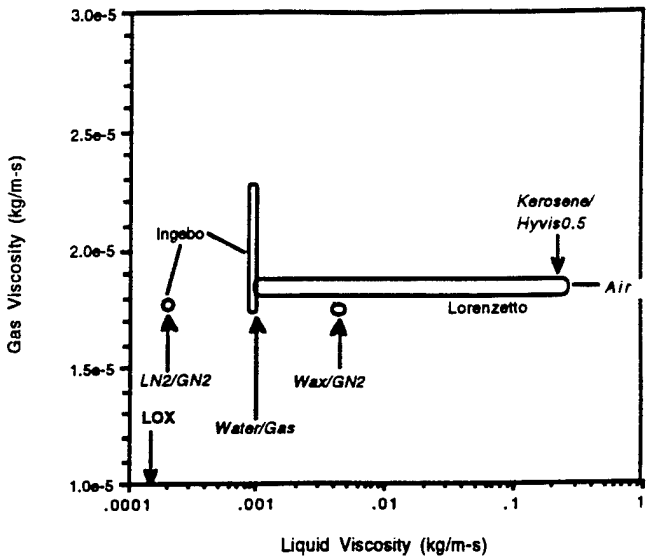

Fig. 8. Comparison of propellant and simulant viscosities

argon (gases of successively higher molecular weights) to obtain a variation in gas density at atmospheric pressure. The experiments were done at low flowrates, however, but the results are still important since they are the only data addressing this crucial parameter. The PSU hot-fire atomization experiment was performed at a pressure of approximately 2.7 MPa (400 psia) and a gas injection density of 0.0021 kg/m^3. Note that with the higher gas injection density and velocity (Fig. 4), this experiment was more representative of the LOX/GH_2 rocket injector spray in terms of velocity, mass flux, and flowrates as well.

Liquid Properties, Reynolds and Weber Number

Two additional crucial parameters in LOX/GH_2 atomization are liquid viscosity and surface tension. They represent the two forces resisting the breakup of the liquid core. Upon examining the studies in Table 1, it was found that the LOX values of viscosity and surface tension were not simulated by water, kerosene, or molten wax, convenient simulants that were generally used in cold-flow studies. No atomization studies with low surface tension and viscosity fluids were available in the literature. LOX values are approximately one order-of-magnitude lower than the values for water. However, some useful data characterizing liquid property effects were obtained by Lorenzetto and Lefebvre.[9] The viscosity ranges covered in his experiments and others is shown in Fig. 8. Although the data were taken with low flowrates (See Fig. 6), and with fluids of viscosity and surface tension much higher than LOX, it is the only available information from which to extrapolate.

A final comparison of cold-flow and hot-fire experimental conditions was performed in terms of Reynolds numbers *Re* and Weber numbers *We*, two of the non-dimensional parameters that are obtained from dimensional analysis of the atomization parameter set. As defined in Giffen,[15] *Re* and *We* combine the effects of gas and liquid densities, velocities, and properties, into dimensionless ratios of atomization-enhancing forces and atomization-resisting forces. An important atomization parameter is the gas Weber number $We_g = \rho_g \left(U_g - U_l\right)^2 d / \sigma$, which is a ratio of the disruptive force of gas momentum to the cohesive surface tension force. Again, a significant disparity between cold-flow and hot-fire studies was found as illustrated in Figs. 9 and 10. Cold-flow *Re* and *We* were an order-of-magnitude lower than for rocket injectors, primarily due to the properties of LOX (affecting Re_l and We_g), and high GH_2 injection density (affecting Re_g and We_g). It was also found that liquid injection Reynolds number Re_l of cold-flow experiments, $Re_l \leq 10^4$, implied laminar or transitional flow hydrodynamics (developing or fully-developed), as compared to the developing turbulent flow conditions for LOX injection in rockets (cf. Fig. 9). Such a basic difference between cold-flow and hot-fire flow hydrodynamics alone could invalidate the extrapolation of laboratory drop-size results to rocket applications.

Recent cold flow shear coaxial experiments (Hardalupas et al.,[13] Zaller and Klem,[12] Pal et al.[14]) have been performed with water and air since these are inexpensive and convenient simulants. These studies, compared in Fig. 10, indicated that the injection *Re* and *We* for these injectors remained an order-of-magnitude lower than rocket injectors. The experiments done at the higher flowrates with modern non-intrusive diagnostics

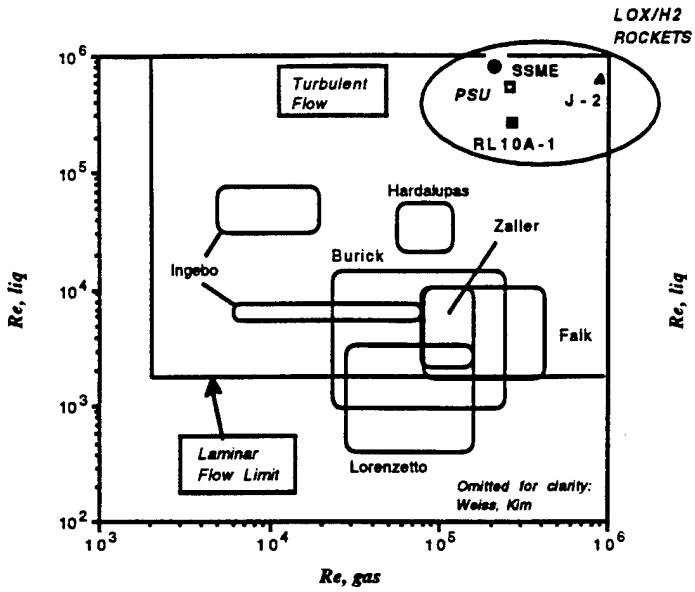

Fig. 9. Shear coaxial injection gas and liquid Reynolds numbers --- cold flow studies vs. LOX/GH_2 rockets

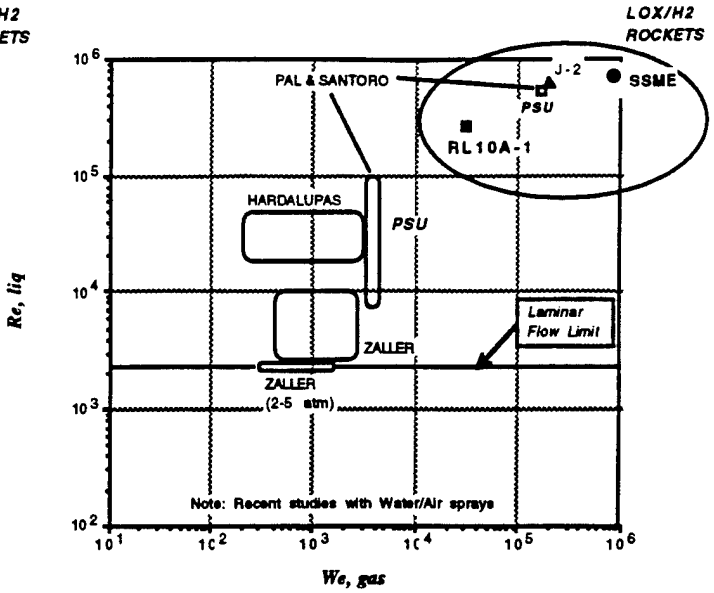

Fig. 10. Shear coaxial injection Reynolds and Weber numbers --- cold-flow studies vs. LOX/GH_2 rockets. Since the surface tension of LOX is undefined above the critical pressure, Weber numbers for J-2 and SSME were evaluated using the same properties as for the RL10A-1.

(Hardalupas et al.[13], Pal et al.[14]) are useful, however, since they complement the work done at similar flowrates with wax (Burick,[7] Falk[8]) and also can serve as a basis for verifying and improving correlations of previous studies.

The Figs. 9 and 10 essentially summarize the challenge of designing an experiment that can adequately characterize atomization phenomena for LOX/GH_2 rocket injector sprays, i.e. employing a suitable LOX simulant, and matching the injection gas density in a rocket chamber. They also suggest that correlations derived from these studies are highly unlikely to predict atomization in rocket combustion chambers. Since no other data exist, however, designers still attempt to extrapolate drop-size correlations derived from cold-flow experiments to predict hot-fire atomization. In the following section, several atomization correlations are evaluated at rocket injection conditions to compare the magnitudes and trends in drop-size predictions, and hence gauge their potential as predictive tools.

Atomization Correlations for Shear Coaxial Injectors

In addition to the correlations indicated in Table 1, correlating equations were also developed by Nukiyama and Tanasawa,[16] Mayer,[17] and Nurick.[3] Nukiyama and Tanasawa's formula was based on experiments conducted in the 1930s with wax and water. Mayer's formula was derived from a theoretical analysis, and calibrated to Weiss' experimental results. Nurick's formula was based on the data taken by Burick,[7] Falk,[8] and more recently by Zaller,[12] as cited in Table 1.

All correlations were compared by evaluating them at a typical LOX/GH_2 rocket injector operating condition, that of the RL10A-1 shear coaxial injector element. The formulae were not intended for rocket conditions and LOX propellant, but extrapolating them was a means of gauging their utility. They have been previously studied for rocket applications by Zaller[18] (which motivated some of this work), but a more extensive comparison of their strengths and weaknesses was performed in this study and is reported here. The correlations are listed below:

Nukiyama and Tanasawa[16] (1939) - English units (given in Ref. 6, Eq. 1)

$$\overline{D}_{32} = \frac{585}{V_r}\sqrt{\frac{\sigma}{\rho_l}} + 597\left(\frac{\mu_l}{\sqrt{\sigma\rho_l}}\right)^{0.45}\left(1000\frac{\dot{m}_l}{\dot{m}_g}\frac{\rho_g}{\rho_l}\right)^{1.5}$$

Weiss[5] (1959) - SI units

$$\overline{D}_{V0.5} = 0.61\left(1+1000\frac{\rho_g}{\rho_l}\right)\left(\frac{V_r\mu_l}{\sigma}\right)^{\frac{2}{3}} \times\left(\frac{\sigma}{\rho_g V_r^2}\right)\left(\frac{\rho_l\sigma\mu_g}{\mu_l^4}\left(\dot{m}_l+\dot{m}_g\right)\right)^{\frac{1}{12}}$$

Mayer[17] (by theory, 1961) - SI units

$$\overline{D}_{V0.5} = 9\pi\sqrt[3]{16}B\left(\frac{\mu_l\sqrt{\sigma}}{\rho_g V_g^2\sqrt{\rho_l}}\right)^{\frac{2}{3}}$$

Kim and Marshall[6] (1971) - mixed units

$$\overline{D}_{V0.5} = 249\frac{\sigma^{0.41}\mu_l^{0.32}}{\left(\rho_g V_r^2\right)^{0.57} A_g^{0.36}\rho_l^{0.16}} + 1260\left(\frac{1}{V_r^{0.54}}\right)\left(\frac{\dot{m}_l}{\dot{m}_g}\right)\left(\frac{\mu_l^2}{\sigma\rho_l}\right)^{0.17}$$

Lorenzetto and Lefebvre[9] (1977) - SI units

$$\overline{D}_{32} = 0.95\left(\frac{\sigma^{0.33}\dot{m}_l^{0.33}}{V_r\rho_l^{0.37}\rho_g^{0.3}}\right)\left(1+\frac{\dot{m}_l}{\dot{m}_g}\right)^{1.7} + 0.13\mu_l\left(\frac{d}{\sigma\rho_l}\right)^{0.5}\left(1+\frac{\dot{m}_l}{\dot{m}_g}\right)^{1.7}$$

Ingebo[10] (for cryogenic LN_2, 1991) - SI units

$$\overline{D}_{32} = \frac{d}{8.1\left\{\left(\frac{\rho_g}{\rho_l}\right)\frac{\rho_g^2 d^2 V_{ac}^3}{\mu_l\sigma}\right\}^{0.44}}$$

Nurick[3] (1991) - SI units

$$\overline{D}_{V0.5} = 3.3\times10^5\left(\frac{V_l^{0.61}}{\left(V_g - V_l\right)^{1.4}}\right)\left(\frac{d}{D}\right)$$

Analysis of Correlations

The underlying premise of the above correlations and other formulae in the literature is that the average drop-size from primary atomization, mean diameter $\overline{D}_{10}$ or Sauter diameter $\overline{D}_{32}$, or mass median diameter (denoted $\overline{D}_{V0.5}$) can be estimated based solely on knowledge of the fluid properties and spray kinematics at the point of injection, that is,

$$\overline{D} = fn\left\{d, U_l, \rho_l, \mu, \sigma, \ldots, D, U_g, \rho_g, \ldots\right\}$$

Such correlating equations are simple, non-physical mathematical expressions that usually contain the above injection parameters raised to a power. Specifically, they model the gross physical trends of their source data sets over the ranges of test variables, and, they essentially represent the results of the many cold-flow spray studies that were performed. The parameter *exponents* in the expressions indicate the *degree* to which drop-size was proportional to a given physical parameter, such as density, surface tension or viscosity, in a given investigation. For example, in the Mayer[17] expression, drop-size is proportional to surface tension to the one-third power --- $\overline{D}_{V0.5} \propto \left(\sqrt{\sigma}\right)^{\frac{2}{3}}$, or $\overline{D}_{V0.5} \propto \sigma^x$ where the exponent x = 1/3. The exponents of the various formulae are therefore informative to compare, especially when the objective is to extrapolate to conditions beyond laboratory experience. Note that an exponent for σ is not unique in the two-term formulae of Nukiyama and Tanasawa,[16] Kim and Marshall,[6] and Lorenzetto and Lefebvre[9] since σ appears in both terms but raised to different powers. For such cases, a locally valid exponent was mathematically determined at the conditions where the formula was evaluated. The exponents and drop-sizes are compared in a series of figures, Figs. 11 - 15, with respect to the common baseline of the RL10A-1 shear coaxial injector. All equations were evaluated at RL10A-1 injection flowrates and propellant properties (given in Table 2, and discussed later).

Scale Effects on Drop-Size

The average LOX drop-size predicted by the formulae for the RL10A-1 injector spray is listed at the bottom of the graphs. A direct evaluation of the formulae for LOX/GH_2 resulted in a wide range of results, spray-average LOX drop-size as high as 922 μm and as low as 0.1 μm. This was already noted by Zaller.[18] For this reason, a comparison of the trends predicted by the correlations is more meaningful and interesting. Additionally, it was more useful to study the equation exponents that caused this large divergence upon extrapolation. Fig. 11 compares the exponents on injector post size and annulus size. Positive exponents indicate that drop-size increases with post diameter ($\overline{D} \propto d^x$), and the negative exponents show that drop-size decreases with increasing annulus size ($\overline{D} \propto 1/D_h^x$), where x represents the magnitude of any correlation exponent. These trends should carry over to LOX/GH_2 atomization, but it is impossible to predict the magnitude of the exponents without further study. In the correlations by Nukiyama and Tanasawa,[16] Kim and Marshall,[6] and Lorenzetto and Lefebvre[9] the proportionality is strong with the exponent x ranging from one to three. However, in contrast, the formulae by Weiss and Worsham,[5] Mayer,[17] and Ingebo,[10] propose that drop-size is virtually independent of injector scale (exponents are zero or near-zero). Both the Weiss and Worsham[5] and Ingebo[10] experiments varied liquid post diameter d, but did not show a pronounced effect on drop-size. Their work did not involve varying the gas annulus size, and hence the effect is omitted in their correlations.

Velocity Effects on Drop-Size

The exponents on injection velocity of both liquid and gas streams are compared in Fig. 12. All formulae showed good agreement on the strong effect of gas velocity in reducing drop-size, $\overline{D} \propto 1/V_g^x$. However, a discrepancy with respect to the importance of *liquid* velocity is observed. The Nukiyama and Tanasawa,[16] Kim and Marshall,[6] and Lorenzetto and Lefebvre[9]

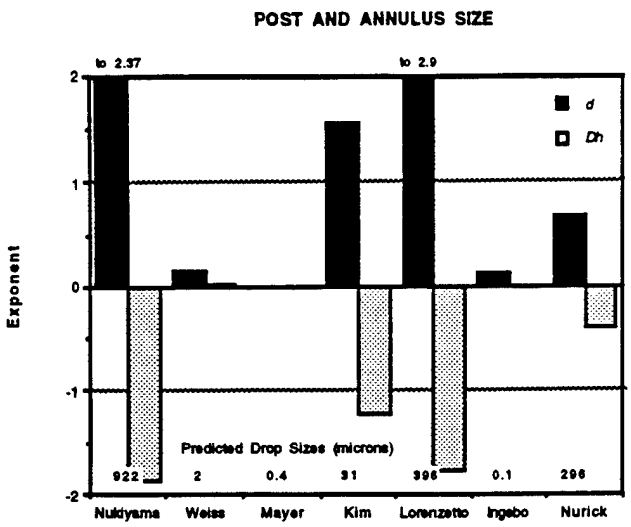

Fig. 11. Effect of shear coaxial injector size on spray drop-size as indicated by correlation exponents

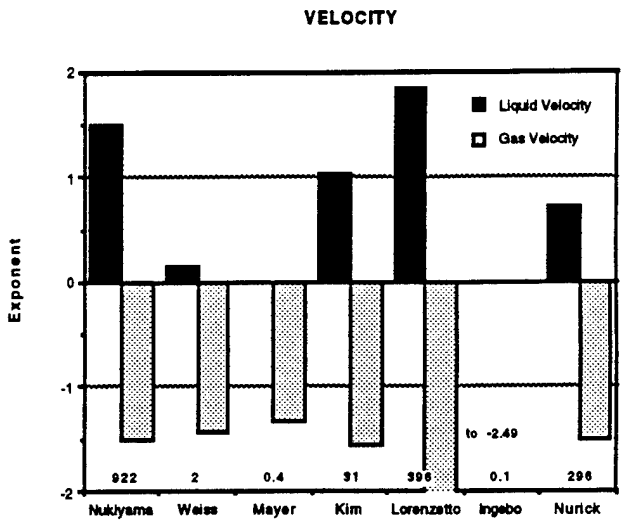

Fig. 12. Effect of gas and liquid injection velocity on spray drop-size as indicated by correlation exponents

formulae all propose a strong dependence of drop-size on liquid velocity, while the Weiss and Worsham[5] and Mayer[17] formulae show weak dependence. Differences in simulants or test conditions might account for these results. Ingebo[10] chose not to correlate to injection velocity at all, but employs an acoustic velocity instead. This is a property of the gas, and serves primarily as a velocity scale in the formula. Some correlations do not explicitly contain liquid velocity raised to an exponent. The dependence is implicit in the liquid flowrate term raised to a power since $\dot{m}_l^x = (\rho_l A_l)^x U_l^x$. Analogously, note that the gas and liquid flowrate terms in the equations also implicitly contain dependence on density and injector size (e.g. $A_l = \pi d^2 / 4$). In all figures, the explicit and implicit exponents were collected together in giving the total dependence of drop-size on any parameter.

Fluid Property Effects on Drop-Size

The effect of density on drop-size in the correlations is shown in Fig. 13. Even though only Ingebo's experiments varied gas density, others have also included it in their correlations either implicitly or explicitly. From the Ingebo[10] experiments, an inverse proportionality with drop-size is expected ($\overline{D}_{32} \propto 1/\rho_g^x$). The effect of liquid density was studied by Lorenzetto and Lefebvre[9] where it was found that $\overline{D}_{32} \propto \rho_l^x$. Other correlations suggest the opposite effect on drop-size although density was not independently varied.

The effects of liquid viscosity, μ_l, and surface tension, σ, are given in Figs. 14 and 15. Both are critical parameters for LOX atomization, since fluids of lower μ_l and σ would generally be expected to atomize into smaller drops. However, only Lorenzetto and Lefebvre were systematic in varying liquid jet surface tension, viscosity, and density, in turn (using fluid mixtures), such that the independent effect of each was properly isolated. The viscosity formula given earlier summarizes their results.[9] The formula contains two terms that describe the behavior of low viscosity liquids (first term dominant) and high viscosity fluids (second term dominant). When extrapolating the equation for LOX, the formula would suggest that viscosity would become unimportant, but surface tension effects would be significant. The two-term formulae by Nukiyama and Tanasawa,[16] and Kim

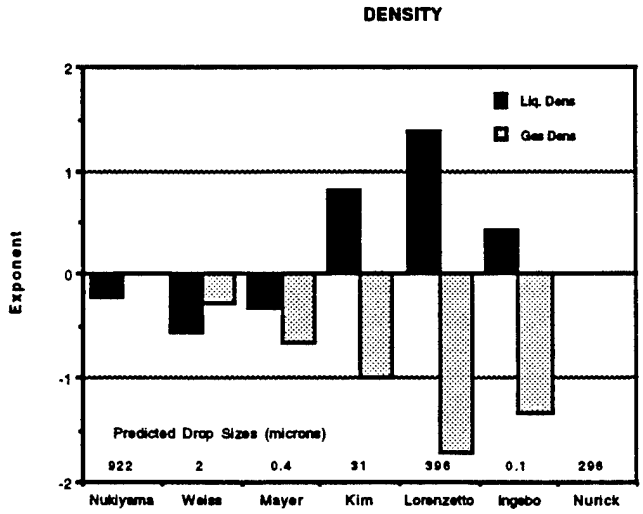

Fig. 13. Effect of gas and liquid density on spray drop-size as indicated by correlation exponents

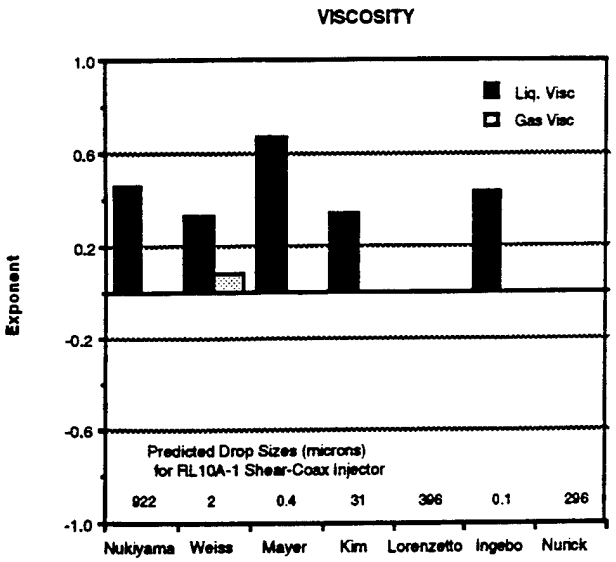

Fig. 14. Effect of liquid viscosity on spray drop-size as indicated by correlation exponents

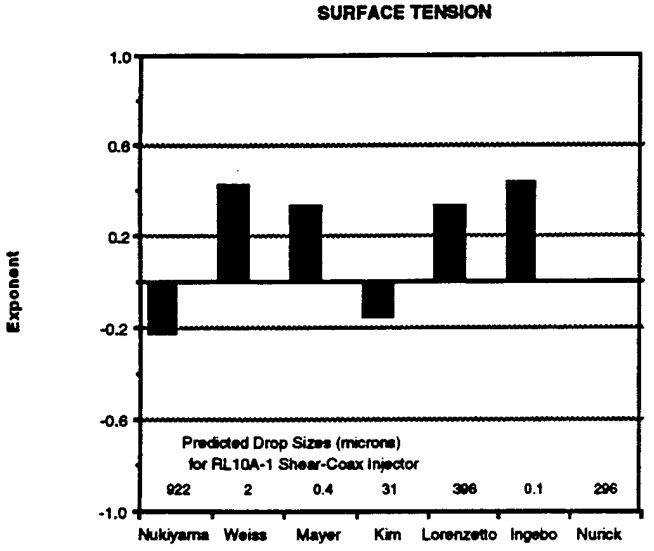

Fig. 15. Effect of liquid surface tension on spray drop-size as indicated by correlation exponents

and Marshall[6] give an inverse trend for surface tension. Both these formulas have surface tension terms appearing in the denominator as well as the numerator. Since only the work of Lorenzetto and Lefebvre[9] isolated μ_l and σ (with μ_l varied by a factor of 200, and σ by a factor of three), those results are probably more reliable. Weiss and Worsham[5] also varied liquid properties to find that $D_{V0.5} \propto \mu^{2/3}$ and $D_{V0.5} \propto \sigma^{1/3}$. Gas viscosity is generally ignored as not being germane to atomization, except in the case of Weiss and Worsham[5] who have proposed a small dependence that was arrived at by dimensional analysis.

In view of the differences in correlations with respect to the physical parameters affecting atomization, the large variation in drop-size upon extrapolation is to be expected. It appears that there is at least rough agreement as to the parameters that increase drop-size (d, U_l, μ_l, σ) and those that decrease drop-size (D_h, U_g, ρ_g). It is also interesting to compare the correlations for a spray that is more conventional, such as a water/air spray at relatively low liquid flowrate. The injector conditions for both the LOX/GH_2 and water/air spray from the same RL10A-1 shear coaxial element are given in Table 2. For a water/air spray, the predictions were much closer relatively (see Table 3); average predicted drop-size ranged from 7 μm to 100 μm. This is still a significant variation, but expected when considering the differences in injector hardware and fluids that were employed in developing the correlations.

Table 2
Propellant Injection Parameters for the RL10A-1 Shear Coaxial Element

	LOX/GH_2	Water/Air
Scale		
d (mm)	2.01	2.01
D_h (mm)	2.32	2.32
Flow		
$\dot{m}_l$ (kg/s)	0.060	0.003
$\dot{m}_g$ (kg/s)	0.012	0.003
$\dot{m}_l/\dot{m}_g$	5	1
V_l (m/s)	17	1
V_g (m/s)	255	147
Properties		
Pressure (atm)	20	1
Gas Temp (K)	185	300
Liquid Temp (K)	105	300
ρ_g (kg/m^3)	2.7	1.17
ρ_l (kg/m^3)	1130	1000
μ_l (kg/m-s)	0.00015	0.001
σ (N/m)	0.01	0.0735

Table 3
Predicted Spray-Average Drop-Size

	LOX/GH_2	Water/Air
Nukiyama	922	44
Lorenzetto	396	97
Nurick	296	100
Kim	31	22
Weiss	2	23
Mayer	0.4	10
Ingebo	0.1	7

Therefore, it is clearly the extrapolation to the high rocket injector flowrates, and to the unique LOX properties that invalidates the correlations for LOX/GH_2 injectors such as the RL10A-1 shear coaxial.

A first step towards obtaining an atomization correlation valid for LOX/GH_2 rocket injectors must involve experiments that simulate the physical parameters discussed previously, as well as Reynolds numbers and Weber numbers. Cold-flow atomization data with more appropriate simulants would provide a baseline set of information. A set of hot-fire rocket injector experiments would then be needed to explore the difference between cold-flow and hot-fire primary atomization phenomena.

Proposed Cold-Flow and Hot-Fire Experiments on Shear Coaxial Atomization

A specially designed cold-flow experiment could involve a pressurized LN_2/helium spray at 2 MPa (300 psi) to simulate a LOX/GH_2 rocket injector spray. An appropriate experiment could be conducted to simulate the RL10A-1 injection element, where liquid and gas flowrates, injector size and geometry would be identical to the rocket element. Since the LN_2 transport properties are very similar to LOX, good simulation of Re_l and We_g would be achieved. The only drawback of LN_2 would be its lower density (25% lower than LOX) which would result in a corresponding higher injection velocity. The elevated chamber pressure would suppress liquid cavitation in the injector which is a concern with cryogenic liquids at room temperature. On the gas side, room temperature helium at the elevated pressure of 2 MPa would adequately simulate injection density and velocity (within 30%), and Reynolds number. A non-intrusive drop-sizing investigation similar to that of Hardalupas could be performed to survey the spray statistics. Even though the above is not a perfect matching of the RL10A-1 rocket conditions, it is much improved relative to the cold-flow experiments done to date.

A hot-fire experiment could also be performed at these same injector conditions. The previously cited experiment of Pal et al.,[14] with non-intrusive drop-sizing, was performed with a similar but larger injector, and employed ambient temperature hydrogen. With cold hydrogen capability, the RL10A-1 conditions of coaxial injection could be closely approached in a hot-fire test. This type of data is critical for extending the correlations described earlier to predict drop-size in combustion chambers.

Conclusions and Recommendations

The present data base on shear coaxial atomization consists solely of cold-flow spray experiments. The data base does not contain any experiments that simulate the unique propellant properties of LOX/GH_2, namely, GH_2 injection density and LOX surface tension and viscosity. Simulation of these properties is crucial to obtaining atomization results that are directly relevant to LOX/GH_2 injector sprays. A review of the drop-size correlations in the literature provides some guidance towards expected trends in drop-size at rocket conditions. However, the available correlations differ significantly when evaluated at (i.e. extrapolated to) such rocket injector conditions, and therefore cannot be used as a predictive tool.

In order to extend the knowledge base on spray atomization to low viscosity and surface tension liquids such as LOX, a unique set of cold-flow or hot-fire primary atomization studies is required. It is recommended that further work involve both of the following experiments: cold-flow atomization experiments at pressure using LN_2 to simulate LOX, and gaseous helium to simulate hydrogen injection; hot-fire atomization experiments with LOX/GH_2 for the identical injector. Modern non-intrusive diagnostics would be employed in both experiments to obtain drop-size and velocity data that could be used to extend a current atomization correlation or to develop a new one for LOX/GH_2 shear coaxial injectors.

Acknowledgment

Funding by Aerojet Propulsion Division and the Air Force Office of Scientific Research, Air Force Systems Command, USAF, under grant number F49620-93-1-0365 is gratefully acknowledged. The US Government is authorized to reproduce and distribute reprints for Governmental purposes notwithstanding any copyright notation thereon.

References

[1] *Liquid Rocket Engine Injectors*, NASA SP-8089, 1976.

[2] Ferrenberg, A. J., Hunt, K., and Duesberg, J., "Atomization and Mixing Study," (Rocketdyne Report RI/RD85-312), NASA-CR-178751, December 1985.

[3] Personal Communication. Nurick, W. H., "A Review of Shear Coaxial Element Atomization," W. J. Schafer Assoc., May 20, 1992.

[4]Lefebvre, A. H., "Airblast Atomization," *Progress in Energy and Combustion Science*, Vol. 6, 1980, pp. 233-261.

[5]Weiss, M. A., and Worsham, C. H., "Atomization in High Velocity Airstreams," *ARS Journal*, Vol. 29, No. 4, 1959, pp. 252-259.

[6]Kim, K. Y., and Marshall, W. R., "Drop-Size Distributions from Pneumatic Atomizers," *AIChE. Journal*, Vol. 17, No. 3, May 1971, pp. 575-584.

[7]Burick, R. J., "Space Storable Propellant Performance Program - Coaxial Injector Characterization," NASA-CR-120936, October 1972.

[8]Falk, A. Y., "Coaxial Spray Atomization in Accelerating Gas Streams - Final Report," NASA-CR-134825, June 1975.

[9]Lorenzetto, G. E., and Lefebvre, A. H., "Measurements of Drop Size on a Plain-Jet Airblast Atomizer," *AIAA Journal*, Vol. 15, No. 7, July 1977, pp. 1006-1010.

[10]Ingebo, R. D., "Drop Size Correlation for Cryogenic Liquid-Jet Atomization," NASA TM-102432, March 1990.

[11]Ingebo, R. D., "Gas Property Effects on Dropsize of Simulated Fuel Sprays," *Journal of Propulsion*, Vol. 7, No. 4, July-August 1991, pp. 467.

[12]Zaller, M. M., and Klem, M. D., "Coaxial Injector Spray Characterization Using Water/Air as Simulants," NASA-TM-105322, November 1991.

[13]Hardalupas, Y., McDonald, H., and Whitelaw, J. H., "Two Fluid Mixing," NASA-CP-3174, Vol. II, *Advanced Earth-to-Orbit Propulsion Technology Conference*, May 19-21, 1992.

[14]Pal, S., Moser, M. D., Ryan, H. M., Foust, M. J., and Santoro, R. J., "Flowfield Characteristics in a Liquid Propellant Rocket," AIAA Paper No. 93-1882, AIAA/SAE/ASME/ASEE 29th Joint Propulsion Conference, June 28-30, 1993.

[15]Giffen, E., and Muraszew, A., *Atomisation of Liquid Fuels*, Chapman and Hall, 1953.

[16]Nukiyama, S., and Tanasawa, Y., "Experiments on the Atomization of Liquids in an Airstream," *Transactions of the Society of Mechanical Engineers (Japan)*, Vol. 5, No. 18, 1939, pp. 68-75.

[17]Mayer, E., "Theory of Liquid Atomization in High Velocity Gas Streams," ARS Journal, December 1961, pp. 1783-1785.

[18]Zaller, M. M., "LOX/Hydrogen Coaxial Injector Atomization Test Program - Final Report," NASA-CR-187037, October 1990.

Attachment B

Swirl Coaxial Atomization: Cold-Flow and Hot-Fire Experiments

by

S. A. Rahman, S. Pal, and R. J. Santoro
(AIAA Paper 95-0381)

33rd Aerospace Sciences Meeting and Exhibit
Reno, NV
9-12 January 1995

AIAA 95-0381

Swirl Coaxial Atomization: Cold-Flow and Hot-fire Experiments

S. A. Rahman, S. Pal, and R. J. Santoro

The Pennsylvania State University
University Park, PA

33rd Aerospace Sciences Meeting and Exhibit
January 9-12, 1995 / Reno, NV

SWIRL COAXIAL ATOMIZATION: COLD-FLOW AND HOT-FIRE EXPERIMENTS

S. A. Rahman,* S. Pal,† and R. J. Santoro††

Propulsion Engineering Research Center
and
Department of Mechanical Engineering
The Pennsylvania State University
University Park, PA. 16802-2320

Abstract

The design and testing of a research swirl coaxial gas/liquid injector for rocket application are described. Cold-flow visualizations of the spray field issuing from this injector are presented showing the effect of flowrate, injector length, and coaxial gas flow, on spray atomization. Results with the same injector in hot-fire testing employing liquid oxygen (LOX) and gaseous hydrogen (GH_2) propellants are also presented.

Stable ignition and combustion are demonstrated with this injector in a uni-element rocket chamber over a wide range of oxidizer-to-fuel ratios (3 to 166), for chamber pressures between 140 and 500 psia. The measured c*-efficiencies associated with these tests are 92 to 100%. The first hot-fire test visualizations of the near-injector swirling flame zone and of the LOX atomization region, obtained by photography in the windowed rocket combustion chamber, are discussed. These provide evidence of flameholding, and LOX atomization under hot-fire conditions. In light of good performance results at extreme oxidizer-to-fuel ratios, this injector is expected to be a viable candidate for an oxidizer-rich preburner employing LOX/GH_2, such as that envisioned in the current Reusable Launch Vehicle (RLV) engine technology program.

Nomenclature

d	liquid jet diameter
D_h	hydraulic diameter of gas flow
D	drop size
$\overline{D}$	spray-average drop-size
$f(D)$	drop size probability density function
$\dot{m}$	flowrate
P	pressure
O/F	oxidizer-to-fuel mass ratio
Re	Reynolds number
t	wall thickness of LOX post tube
T	temperature
V	liquid sheet velocity
We	Weber number

Greek Symbols

ρ	density
μ	dynamic viscosity
η_{c^*}	c*-efficiency
θ	total included swirl cone angle

Subscripts

af	adiabatic flame
c	chamber
g	gas
l	liquid
$tang$	tangential
ax	axial

Introduction

A comprehensive research program to characterize propellant injection, atomization, mixing, and combustion for typical rocket injector elements is ongoing at the Propulsion Engineering Research Center (PERC) at The Pennsylvania State University.[1,2,3,4] Impinging jet and coaxial jet injector elements, both shear and swirl, are under study for gaseous and liquid propellant injection schemes. In this paper, experimental results obtained for one of the injector designs, the swirl coaxial injector element for a LOX/GH_2 rocket engine system are presented.

---

* Graduate Student, Mechanical Engineering, Member AIAA
† Research Associate, Mechanical Engineering, Member AIAA
†† Professor, Mechanical Engineering, Member AIAA

This project is focused on investigating the near-injector region of the swirling and combusting spray flame issuing from a single swirl coaxial element (fuel + oxidizer) in an optically accessible combustion chamber. The experiments are being conducted at chamber pressures, temperatures and flowrates representative of a rocket injector and combustor at the single element level. The research for the swirl coaxial injector project, as well as for the other cited projects within the broader program, is being conducted at the PERC's Cryogenic Combustion Laboratory.

The swirl coaxial injector has demonstrated effectiveness in achieving atomization and mixing, and therefore stable combustion in rocket engines. It has been successfully employed for decades in the RL10A rocket engine system[5] (an upper stage), and continues to be incorporated into current derivatives of this LOX/GH_2 engine technology. The swirl coaxial injector is also in wide use in liquid rocket engines employed in the Russian space program.[6] Inspite of its wide application, there is little fundamental understanding of the mechanism of swirl-induced atomization/combustion in rockets. Most of the current information on this injector is based on inferences from cold-flow, atmospheric pressure studies with single elements. Since extension of cold-flow atomization/mixing results to hot-fire conditions is tenuous at best, hot-fire data are needed to characterize the spray flame from this type of element *in situ* within a rocket chamber.

An immediate requirement for swirl coaxial injector research also derives from NASA's current Reusable Launch Vehicle (RLV) technology program. This program calls for a propulsion system employing full-flow, fuel-rich and oxidizer-rich preburners[7] that supply gaseous propellants to the main combustion chamber. One of the propellant combinations being considered for an oxidizer-rich preburner is LOX/GH_2, for which the injector design of choice has been either the shear coaxial or swirl coaxial element.[8] However, the data base in the United States for high O/F rocket combustion of LOX is very limited.[9] Issues that need to be addressed at high O/F (in excess of 100) include propellant atomization/mixing, ignition, combustion stability, and the homogeneity of exhaust gas. Hence, demonstrations with the swirl coaxial injector (as a candidate element) in high O/F rocket experiments are relevant for the RLV engine research and development activity.

In the present paper, the hot-fire experiments with a swirl coaxial injector in a uni-element rocket chamber are discussed. These results are complemented by findings from cold-flow experiments where water and air were employed as simulants to examine the spray breakup mechanism. A description of the swirl coaxial injection process and relevant literature on swirl atomizers is presented first.

Background and Literature

A typical swirl coaxial rocket injector is illustrated in Fig. 1. Liquid is introduced tangentially into the center post through passages (holes or slots). The liquid stream's tangential velocity creates a swirling vortex flow within the center post tube. If properly designed, the tube does not flow full, but instead contains a thin swirling film along the inner wall with a hollow gas core as shown in the figure. The swirling film exits the tube in the form of a hollow cone sheet. While this sheet readily self-atomizes, a coaxial flow of gas greatly enhances and accelerates the sheet breakup process by disturbing the liquid film that emerges from the injector post. The atomization process is therefore a combination of two factors: the tendency of the conical liquid sheet to disintegrate as it swirls and stretches, and the tendency of the coaxial gas flow to accelerate sheet breakup due to its momentum transfer to the conical sheet emerging at the exit of the post.

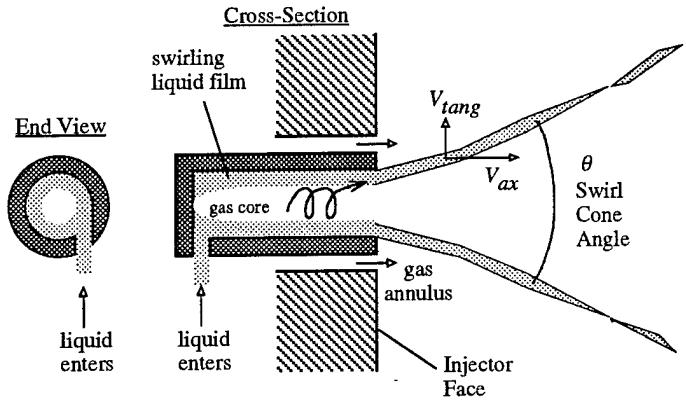

Figure 1. Schematic of a swirl coaxial gas/liquid injector

The resultant drop size distribution and mean drop size for such an injection process is a function of several variables. Giffen[10] determined by dimensional analysis arguments that a spray's drop field in an unconfined, quiescent environment (non-combusting) depends upon the following six parameters (deduced from 9 variables) that represent injector scale, fluid inertia, and fluid property effects:

$$\frac{\overline{D}}{d} \text{ or } f(D) = fcn\left(\frac{\rho_l}{\rho_g}, \frac{\mu_l}{\mu_g}, We_g, \mathrm{Re}_l, \theta\right)$$

where, $\overline{D}$ and $f(D)$ represent a characteristic spray drop size and distribution function, respectively. Swirl strength is represented by θ in this parameter set. For the swirl coaxial injection case, the parameters D_h/d and Re_g would be added on the right-hand-side. For a combusting spray, additional parameters related to the spatially varying combustion chamber conditions (density, velocity, etc.) also enter into the equation. Also, the sub-critical or super-critical nature of the combusting flowfield affects the atomization process. However, for the present, studies in the literature have avoided these additional complexities and focused strictly on investigating the relationship given in the above equation for the case of primary atomization. A majority of this work addresses the non-combusting (cold-flow) spray situation in anticipation that much of the combusting spray behavior can be interpreted from those results. The particular literature cited below provides guidance, in the writers' opinion, towards researching atomization of LOX by *swirl* coaxial injection for a LOX/GH_2 rocket application. Therefore, relevant academic and industry work is outlined below as a brief summary of the state-of-the-art.

Fundamental Studies

The process of liquid swirl injection alone has been described in detail in quite early literature by Novikov[11] and Giffen.[10] Such injectors have been extensively applied in gas turbine combustion and spray drying, albeit by a different name. (They have been referred to as simplex nozzles or atomizers, pressure swirl nozzles or atomizers, or as centrifugal pressure nozzles.) Parametric investigations have produced data sets that describe how drop sizes in swirling sprays are affected by changes in atomizer dimensions or fluid properties (for instance, see Tate and Marshall[12]). Both inviscid[13] and viscous[14] theories/models have also been developed to predict injector discharge coefficient and swirl cone angle from first principles. An up-to-date discussion of the inviscid theory, which is particularly simple to apply, was presented recently by Yule and Chinn.[15] In the authors' views, the best discussions of the phenomenology of a swirling liquid cone spray have been given by Giffen,[10] and by Dombrowski and Hasson[16], who have assembled and reviewed significant results of several investigators.

In contrast, the case with coaxial liquid/gas injection (also known as "air-assisted" simplex) has not been investigated in as much detail. Simmons[17] has performed experiments to show parametric effects of liquid and gas properties, and atomizer scale, but there seem to be no other systematic studies in this vein. Furthermore, there is no analysis to assist in interpreting the experimental data or to extrapolate from it. Hence, it appears that significant research remains to be done for gas/liquid swirl coaxial injection.

Rocket-Injector Related Studies

While fundamental studies provide an essential frame-of-reference from which to design the swirling liquid portion of the rocket coaxial injector, additional issues need to be addressed for rocket injector design. First, the issue of scale arises since rocket injector elements necessarily must provide for higher flowrates per element than for most other applications. Much of the fundamental data was taken with low flowrate atomizers. Second, the understanding of fluid property effects (viscosity and surface tension) on atomization is critical since LOX viscosity and surface tension values are much lower than those of typical simulant fluids. Third, mixing of the coaxial liquid and gas streams becomes important since efficient combustion cannot be achieved with unmixedness. A few studies undertaken by rocket engine industry researchers start to address such issues and are summarized below.

A comprehensive set of swirl coaxial injector studies have been reported by researchers at United Technologies (Pratt & Whitney Rocket Engines) who incorporate swirl coaxial injectors into virtually every engine that they produce. A noteworthy set of cold-flow studies performed by them as part of the Air Force Reusable Rocket Engine Program (also known as the XLR129 program)[18] served to determine optimum injector geometries that produced stable spray patterns with both water and liquid nitrogen (employed to simulate the liquid oxygen propellant). The injector post size of elements tested ranged from 1.91 to 3.15 mm ID (0.075 to 0.124 inches). While the Air Force XLR129 study focused on injector discharge coefficients and spray stability, a research study carried out by Hautman[19] on Pratt & Whitney injectors employed state-of-the-art diagnostics to measure drop sizes for swirling sprays. Larger injectors were characterized in this study and liquid property effects were also investigated.

Further studies of mixing and atomization for larger injectors of varying geometries were carried out by Hulka et al.[20] of the Aerojet Propulsion Division under the technology development efforts for the Space Transportation Main Engine (STME) program. Their results showed good mixing and atomization for the injector designs that were studied. All the above rocket

injector data sets served as important guideposts in the development of the present swirl coaxial injector. Further details on these studies will be presented later in context of the results reported in this paper.

Experimental

Single element cold-flow and hot-fire studies are being performed to characterize the swirl coaxial injection/atomization process for liquid rocket engine application. The focus of the work, as already mentioned, is combusting LOX/GH_2 spray characterization at chamber pressures and injector flowrates representative of full-scale rockets at the single element level.

At the crux of the experimental effort is the choice of an injector design. From the outset, an attempt was made to design an injector which had stable hydrodynamic characteristics, was verified in cold-flow, and which was similar in scale and flowrates to proven injectors used by industry researchers. Such an injector was designed with guidance from industry.[21] The choice of injector design is explained below, followed by the relevant details of the hot-fire facility in which the injector was tested.

Swirl Coaxial Injector Design

For the given propellant combination, there were four primary choices to be made with respect to the injector design: size of the post, size of the annulus gap, swirl strength, and length of the injector. All four are geometry considerations, including the swirl strength which is dictated primarily by the ratio of tangential inlet area to post area. The choice of post and annulus size was influenced by several factors.

First, it was desirable to use an element of identical scale to a shear coaxial injector[3] recently tested in the present rocket facility, of 3.43 mm post (0.135 inch), and 1.46 mm (0.0575 inch) annulus gap, to allow for direct shear coaxial to swirl coaxial element comparison. Second, an element similar to an industry designed and tested element was preferable to assure successful hot-fire application. Third, similarity to actual rocket injector elements was desirable so that any results obtained with this research injector had relevance and application beyond the present laboratory studies. A design that satisfied all three "requirements" is shown in Fig. 2. As indicated in Table 1, the geometry of this element corresponds closely to elements reported by Atherton et al.[18] for the XLR129 program, and by Hautman.[19] Both sets of industry data helped established confidence *a priori* that this element, of 3.43 mm post diameter and slot-to-post area ratio of 0.65, would provide for good atomization and combustion of LOX/GH_2. The element itself is also somewhat larger than the RL10A-3 engine element, and hence covers the single-element injection flowrate of this Centaur upper stage LOX/GH_2 engine.

Table 1
Geometric Comparison of Selected Swirl Injectors

	Shear Coax (Ref. 3)	Swirl Coax	Hautman Inj. 3 (Ref. 19)	XLR129 Elem. F (Ref. 18)	RL10A (Ref. 8)
Post ID, mm	3.43	3.43	3.45	3.15	2.0
Gas gap, mm	1.46	1.46	1	n/a	0.43
Wall thick, mm	0.38	0.38	0.51	n/a	
Slot/Post area ratio	-	0.65	0.63	0.57	
Post length, mm	121	141	48	43, 75	
Post L/d	35	41	14	14, 24	
Slot size, mm					
height	-	2.79	3.8	2.74	
width	-	0.76	0.5	0.81	
area (mm^2)	-	6.1	6.1	4.45	
No. of slots	none	3	3	2	

The findings from cold-flow studies with water and liquid nitrogen, under the XLR129 program,[18] were particularly useful for selecting an injector to study. First, those experiments showed that certain injectors maintained a stable gas core within the post tube much better that others, namely those with slot-to-post area ratios near 0.5. Under that program, tests were also conducted with liquid nitrogen (simulating LOX) spraying into elevated back pressure, and showed in direct visualizations that a stable gas core is formed with a cryogenic fluid. The injector listed in the above table, element F of the XLR129 study, was found to have such favorable hydrodynamic characteristics for a slot-to-post area ratio of 0.57. As a consequence, the 3.43 mm ID (0.135 inch) post was chosen since it was fairly close to the size of the XLR129 element F of 3.15 mm ID (0.124 inch). With regard to the design of the tangential slots, the same XLR129 program results indicated that an aspect ratio (width to height) of 0.2 was optimal. This was incorporated into the Penn State swirl coaxial element. A three-slot configuration was chosen since mixing tests by Hulka et al.[20] indicated that this was a superior design.

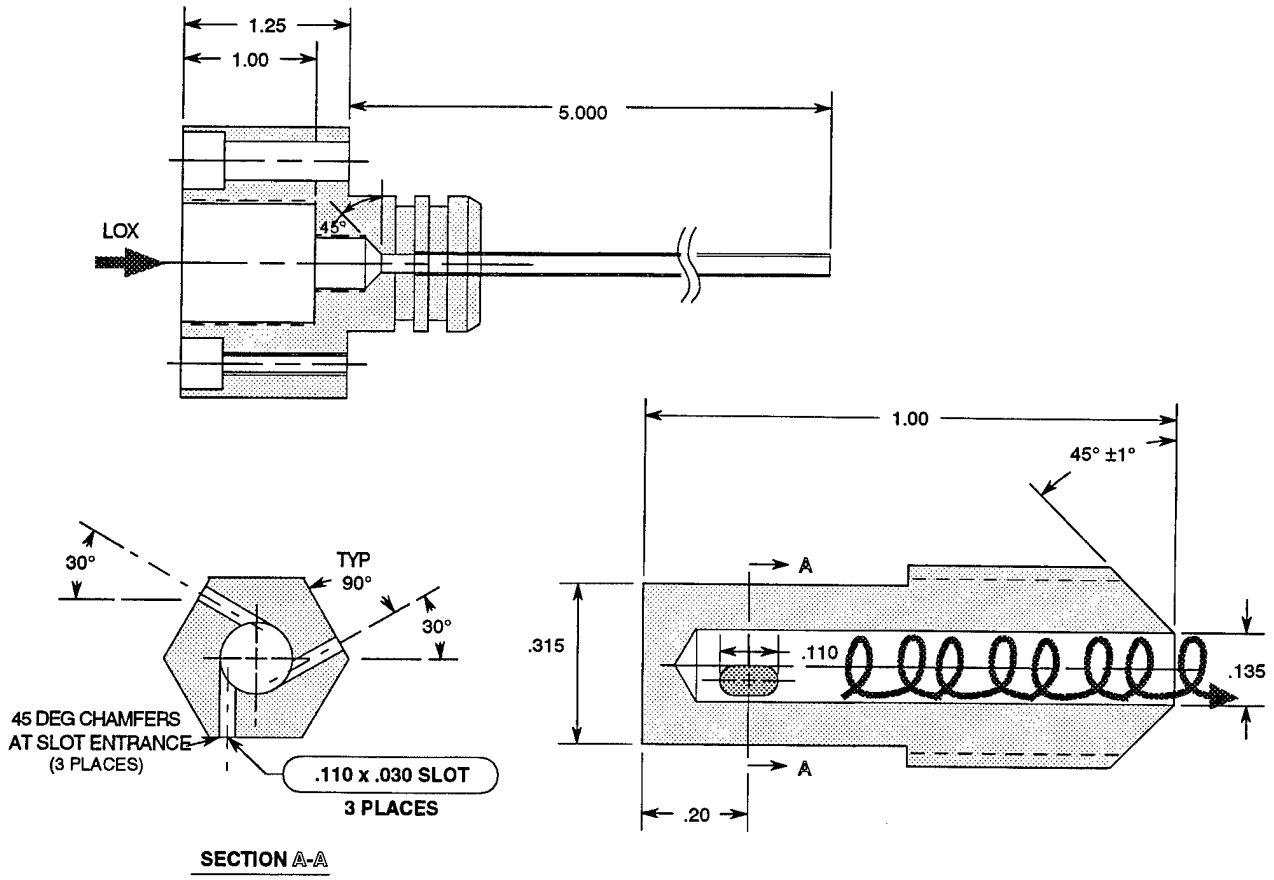

Figure 2. Design of the single element swirl coaxial rocket injector. LOX is injected into the center post tube via the swirl insert, both shown in cross-section (but at different scales, insert is enlarged for clarity). Swirl is imparted by means of tangential entry slots placed at 3 azimuthal positions around the post, 120 degrees apart. Dimensions are given in inches.

Finally, it was also shown in the XLR129 work that shorter post tubes allowed for better swirl cones and atomization. This parameter was varied under cold-flow conditions for the swirl coaxial element and findings will be discussed later in this paper.

A comparison of the present injector with several other injectors characterized by industry is shown in Fig. 3. Most injectors tested by Hulka et al.[20] and in the XLR129 report[18] are given. Inviscid theory predicts that the swirl angle of the liquid conical sheet (in the absence of gas co-flow) is determined by the ratio of total slot area to post area. Hence, cone angles of various injectors are implied by the values shown on the ordinate of the figure: the smaller the tangential slots relative to the post, the higher the swirl within the injector and hence the greater the swirl cone angle. The Penn State swirl coaxial injector was designed to be within the family of injectors used in industry. The abscissa indicates the non-dimensional post tube length. In cold-flow tests, it was observed that post L/d diminishes the cone angle. Three post lengths are shown for the Penn State element (3.43 mm or 0.135 inch ID). Present experiments are being carried out with a long post (L/d of 41), however, this may be a parameter to modify in the future.

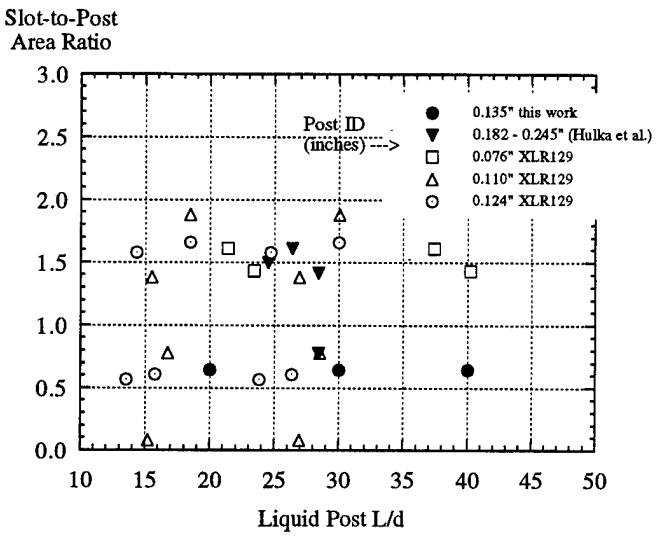

Figure 3. Geometrical comparison of present swirl coaxial injector design with selected industry tested injector elements.

Injector slots in the Penn State injector were designed to be 0.76 mm wide by 2.79 mm long end-to-end (0.030 by 0.11 inch), and placed at 3 azimuthal positions (cf. Fig. 2). The slots were machined by an EDM process (electric discharge machining) for accuracy. The entrance region to the slots were chamfered (as recommended by Nurick[22]) to avoid local cavitation at this location. In this respect also, Table 1 shows the similarity of this injector with other tested injectors. Overall, it is envisioned that cold-flow or hot-fire results with the current swirl coaxial element should therefore be comparable to results from the Hautman[19] and Hulka et al.[20] atomization studies.

Uni-Element Rocket

The experiments were conducted at the Cryogenic Combustion Laboratory at Penn State University. The laboratory provides the capability for firing both gaseous and liquid propellant rockets at the single element level. The flowrate capabilities for this laboratory are 0.45 kg/s (1 lb/s) for liquid oxygen and 0.11 kg/s (0.25 lb/s) for gaseous hydrogen. The rocket chamber used for the experiments has been described elsewhere, but most design particulars are also given here for completeness.[1,3]

The rocket chamber used for these experiments is modular by design and provides optical access for laser-based diagnostic approaches. A cross-sectional view of the chamber is shown in Fig. 4. The chamber consists of an injector assembly section, a window-section, an ignitor section, several blank sections and a nozzle section, which are all held in place by a hydraulic jack. The middle sections of the chamber may be interchanged, allowing placement of the window section at any location along the chamber. This arrangement provides for optical access along the entire length of the chamber. For the experiments reported here, the length of the chamber was 349 mm (13.75 inch). The window-section includes two diametrically opposed round quartz windows, 50.8 mm in diameter (2 inch), that provide optical access to the 50.8 mm diameter square cross-section combustion chamber. The other two sides of the window feature slot windows measuring 6.25 x 50.8 mm which provide additional optical access. All of the windows are thermally protected from the hot combustion gases by a curtain purge of nitrogen which flows across the windows. The injector section also has a modular design for convenient interchange of injector type and/or geometry. For these experiments, the swirl coaxial injector shown in Fig. 2 was used. The inner diameter of the LOX post was 3.43 mm (0.135 inch) with no recess. The inner diameter of the fuel annulus was 4.19 mm (0.165inches) and the outer diameter was 7.11 mm (0.28 inches).

The ignitor section of the rocket is equipped with an ignition chamber (not shown in Fig. 4) that provides a spark-ignited gaseous hydrogen/oxygen torch for ignition

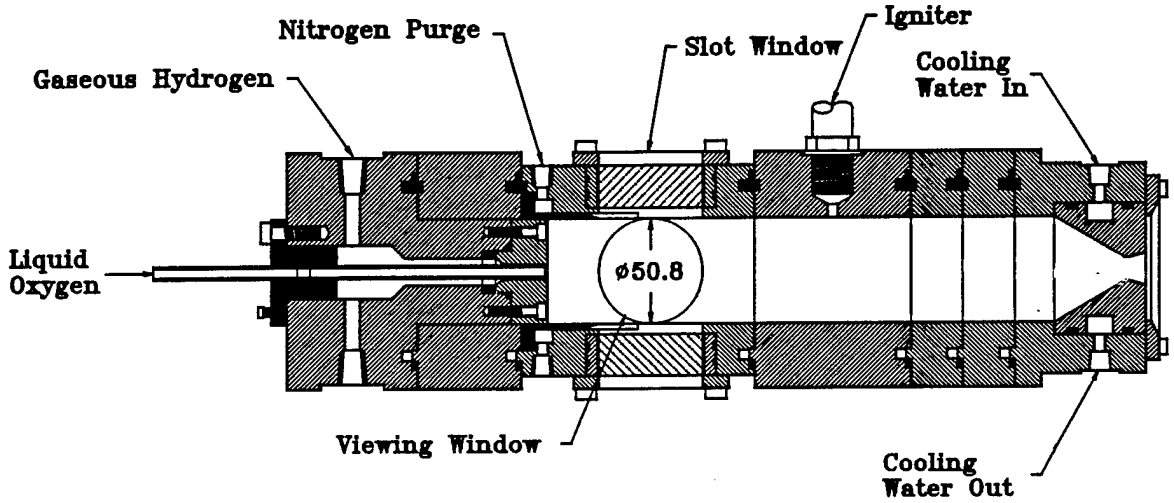

Figure 4. Cross-sectional view of the optically accessible rocket chamber. The chamber is modular in design and allows for varying the chamber length, injector assembly, window-section location, and nozzle. The interior of the chamber is 50.8 x 50.8 mm (2 inches square). For the results presented here, the length of the chamber was 349 mm (13.75 inches). Various nozzles with throat sizes ranging from 6.3 to 13.7 mm (0.25 to 0.54 inches) were used.

in the main combustion chamber. Finally, the water-cooled nozzle of the rocket can be easily changed between tests to vary the chamber pressure. For the present experiment, nozzles with throat diameters ranging from 6.3 to 13.7 mm (0.25 to 0.54 inch) were used to vary the chamber pressure. The setting and monitoring of the flowrate of the gaseous (GH_2) and liquid propellants (LOX) was accomplished with the aid of a critical orifice and a cavitating venturi, respectively, that were instrumented at both upstream and downstream locations with pressure transducers and thermocouples. The nominal LOX flowrates ranged from 0.11 to 0.18 kg/s (0.25 to 0.4 lb/s), whereas the nominal hydrogen flowrates were varied between 0.7 and 45 gm/s (0.0015 and 0.1 lb/s). The resulting range of O/F mass flow ratios was 3 to 166. These flowrates, coupled with the nozzles used, resulted in chamber pressures that ranged from 0.97 to 3.4 MPa (140 to 500 psia).

The duration of a test run was nominally four seconds, with shorter runs being used at near-stoichiometric conditions. The duration of a test is a compromise between the time required to achieve a steady chamber pressure and survivability of the quartz windows. For these tests, it takes approximately two seconds for the chamber pressure to stabilize. After this period, stable chamber pressures are achieved for the programmed duration of the hot-fire test.

Experimental Results with the Swirl Coaxial Injector

Cold-flow and hot-fire experimentation with the present injector element is described below. While, the primary objective was to characterize this element under hot-fire conditions, this work was preceded by cold-flow laboratory simulations of the injector spray using water and air. This served to confirm the injector's hydrodynamic characteristics (pressure drop, flowrate) prior to hot-fire, as well as demonstrate its ability to form the swirling spray cone typically reported for this type of injector. These cold-flow results are discussed first.

Cold-Flow Studies

A visualization technique was employed to obtain instantaneous images of the swirl coaxial liquid spray with and without a coaxial flow of gas. Images were acquired by a CID (charge injection device) solid state camera under microsecond strobe flash illumination (backlit), and subsequently stored as digital pixelized intensity information. Instantaneous images were obtained for the matrix of flow conditions summarized below in Table 2. The cold-flow tests were for water/air spray injection into an unconfined, ambient pressure and temperature environment.

Table 2
Summary of Cold-Flow Visualizations
with the Swirl Coaxial Rocket Injector

Flow liquid	(lb/s) gas	Post L/d 20	27	30	40	41*	Sheet velocity (m/s)
0.1	-	x					17
0.2	-	x	x	x	x	x	34
0.3	-	x					51
0.4	-	x					68
0.5	-	x					85
0.2	0.002		x				34

* Hot-fire injector post L/d is 41.

The first series of visualizations, shown in Fig. 5, are for water flow only. The field of view of each image is 51 mm (2 inches) in width. In the absence of gas flow, a hollow conical sheet of water is formed as the water film inside the post exits the injector (flow going from right to left). In each image, it is seen that the conical sheet develops instabilities that eventually form fluid ligaments which in turn breakup into drops. (The photographs also illustrate that gravitational effects at these flowrates are negligible compared to the momentum forces driving the formation of the spray cone.) Estimates of the liquid sheet velocity (resultant of the axial and tangential components) at the injector exit are indicated in the Table 2. They were computed according to the procedure of Doumas and Laster.[13] Actual velocities for the liquid sheet will be somewhat lower since boundary layer development within the injector post diminishes both the axial and tangential components along the length of the post. The images are consistent with well documented fluid dynamic behavior for this kind of injector. It is noteworthy that the classical process of sheet breakup for this kind of injector (pictured in Album of Fluid Mechanics[23]) for injectors where typically L/d < 2, was also found for the L/d > 20 cases reported here.

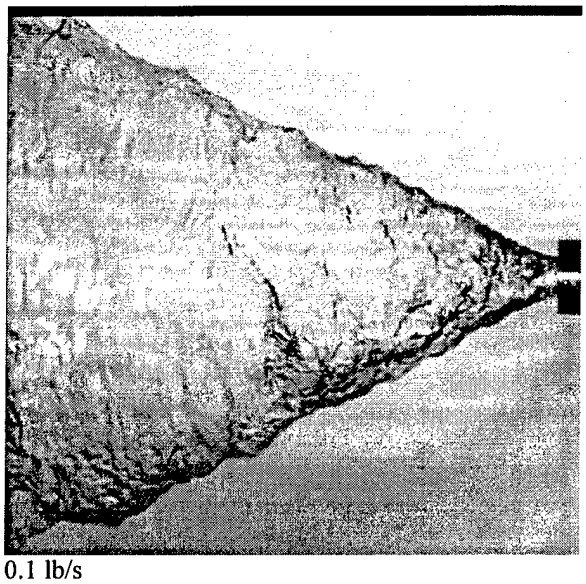

0.1 lb/s

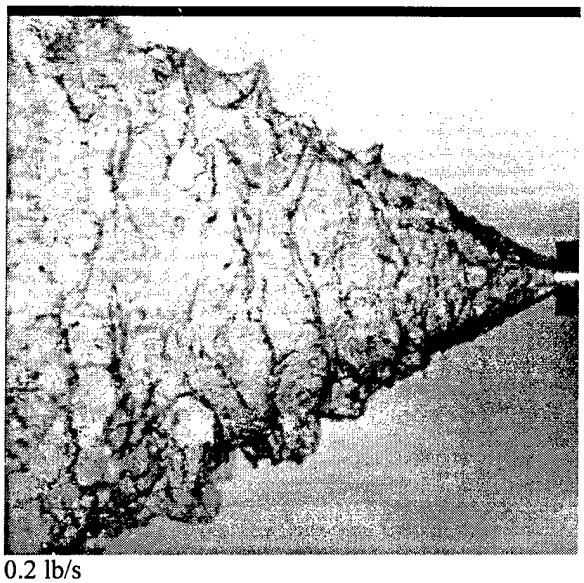

0.2 lb/s

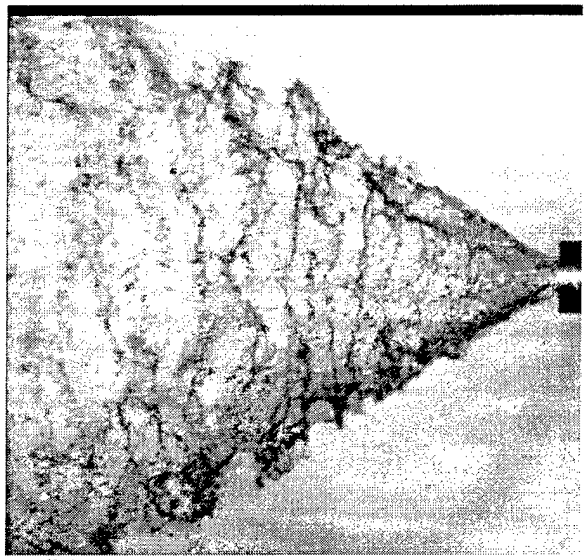

0.3 lb/s

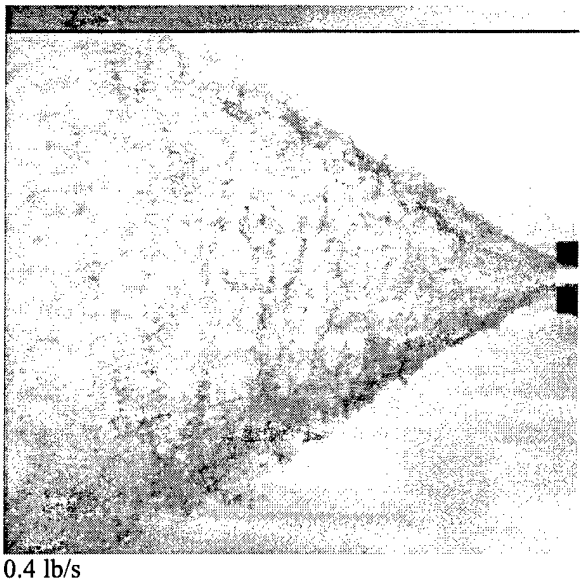

0.4 lb/s

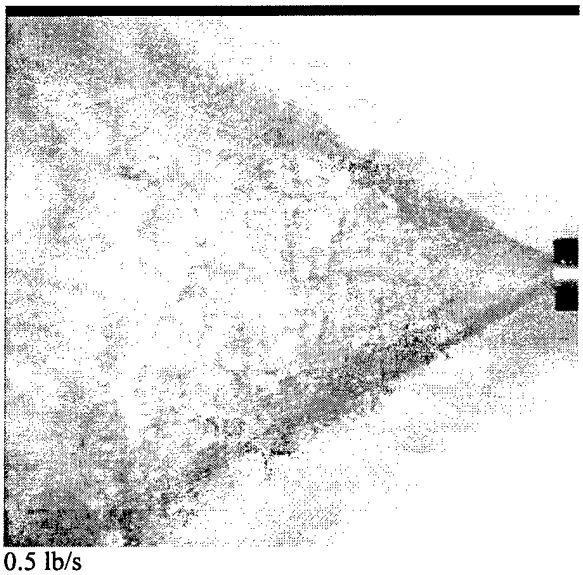

0.5 lb/s

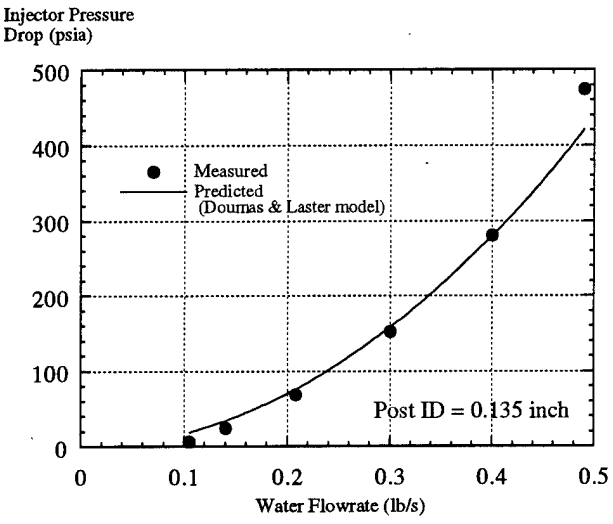

Figure 5. Instantaneous images of a swirling coaxial injector spray showing the effect of liquid flowrate on the breakup of the spray. Water flowrate is varied from 0.045 to 0.227 kg/s (0.1 to 0.5 lb/s); there is no coaxial gas flow. Flow is from right to left into an unconfined, ambient environment. The field of view of each image is 51 mm (2 inches) in width.

The series of images in Fig. 5 shows the effect of water flowrate in enhancing the breakup and self-atomization of the liquid sheet in the region close to the injector exit. The near-injector region is visualized since this is also the region of interest in hot-fire testing. While the unconfined sprays shown in the images would be somewhat different for LOX sprays at the same flowrate (due to transport property differences), it is important to make the following two observations from the images. First, the angle at which the liquid exits the injector remains constant in spite of the significant variation in flowrate. The cone angle is effectively fixed by the ratio of tangential-to-axial velocity component of the fluid leaving the post, which in turn is fixed by the injector dimensions. Second, the point of sheet breakup into ligaments and drops appears to occur closer to the injector with increasing flowrates. This trend is more easily visualized at the lower flowrates where clearer images were obtained. For a given flowrate, the sheet breakup is expected to occur closer to the injector for a LOX spray (as compared to the water spray) due to the combined effects of lower surface tension and viscosity.

The pressure drop across the injector was also measured during the imaging experiments and agreed reasonably with inviscid theory predictions in both magnitude and trend. The discharge coefficient of this injector was calculated to be 0.32 from the inviscid theory/model described by Doumas and Laster.[13]

A second series of visualizations show the effect of injector post length-to-diameter ratio (L/d) on the liquid spray cone (cf. Fig. 6). The shape of the spray cone

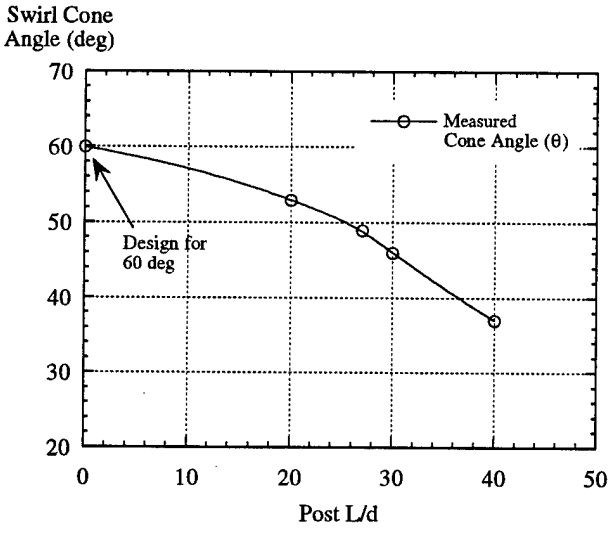

Figure 6 Instantaneous images of swirling liquid spray of water, with no gas co-flow, show the effect of injector post length-to-diameter ratio (at right). Flow is from right to left into an unconfined, ambient environment. θ is the total included cone angle (graphed in above figure).

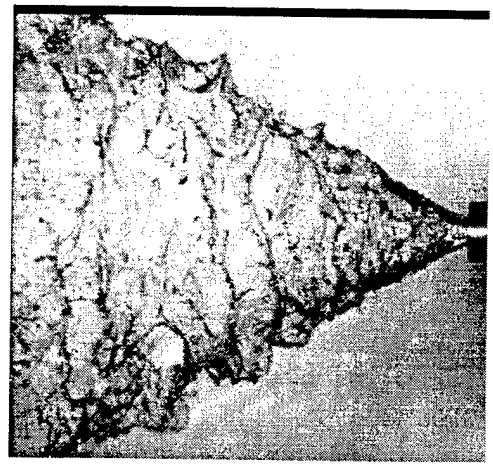

Post L/d = 20
θ = 53 deg

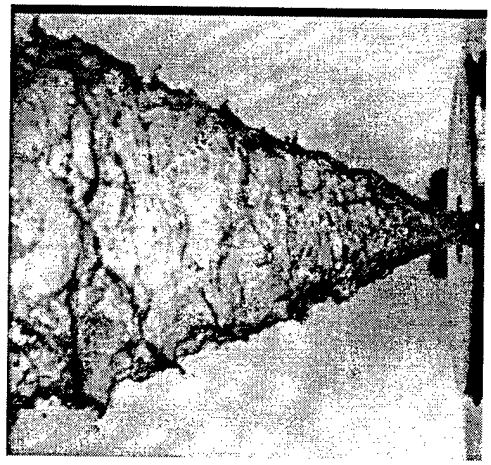

Post L/D = 27
θ = 49 deg

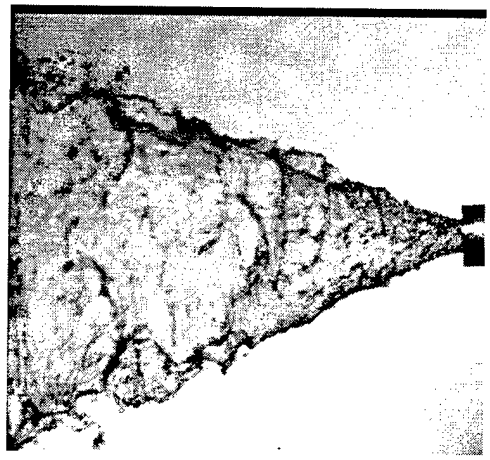

Post L/D = 30,
θ = 46 deg

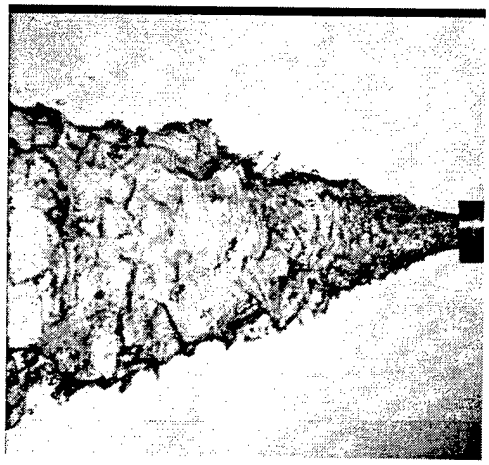

Post L/D = 40,
θ = 37 deg

is itself a direct and important indication of the potential of the spray to atomize. The greater the cone angle, the thinner the liquid sheet that is formed, and hence the smaller the drop sizes formed in the spray. This implies better mixing characteristics and higher c*-efficiencies under combusting conditions. These images show that, for a given liquid mass flowrate, the spray cone angle decreases with increasing L/d. The cone angle predicted by inviscid theory is 60 degrees which is significantly greater than the 37 degree cone angle measured for the L/d of 40 case (injector used in hot-fire experiments). Dombrowski and Hasson[16] noted that measurable friction losses occurred within the post tube when they studied injectors of L/d less than 5. They further noted that a reduction of swirl cone angle implied that tangential velocity was reduced proportionally more than the axial velocity, since the cone angle is given approximately by the relationship: $\tan\theta/2 = V_{tang} / V_{ax}$. Dombrowski's[16] data base however did not include larger L/d's. Hautman[19] noted that for larger L/d posts the discharge coefficient was proportional to $(L/d)^{-0.2}$. Their findings, in conjunction with the results described in Fig. 6, indicate that this parameter needs to be studied further to establish its effects on the drop size field, and corresponding effects on rocket c*-efficiency.

A final pair of visualizations indicates the effect of coaxial gas flow (air) on the liquid sheet atomization process. Fig. 7 indicates that even very small amounts of gas flow causes significant increases in atomization of the conical liquid sheet. This visualization is probably most indicative of the nature of the spray flowfield in hot-fire, particularly for high oxidizer-to-fuel mass flow ratio conditions (that is, oxygen-rich conditions). It is encouraging to see the rapid breakup of the spray even with a modest amount of coflowing gas.

Hot-Fire Studies

The following presents the first swirl coaxial injector results obtained for LOX/GH_2 propellants in a single-element, hot-fire rocket chamber over a wide range of oxidizer-to-fuel ratios (3 to 166). Owing to the recent renewed interest in oxidizer-rich combustion for rocket engine preburner applications, two series of tests covering very high mixture ratios were performed. Specific operating conditions of hot-fire testing are given in Table 3. The LOX flowrate was held constant for all tests at 0.11 kg/s (0.25 lb/s). Stable and repeatable ignition and combustion was achieved at the conditions listed in the table, with measured c*-efficiencies (η_{c*}) between 92 and 103% (based on recorded chamber pressures).

The c*-efficiency results of the present work are shown in Fig. 8. Four typical chamber pressure traces, for tests listed in Table 3, are also given in the figure. The chamber pressure traces indicate stable burning after the ignition period. LOX temperature, measured at the entrance to the injector, was between 117 and 128 degrees K (-230 and -250 degrees F) for all tests. Rocket c*-

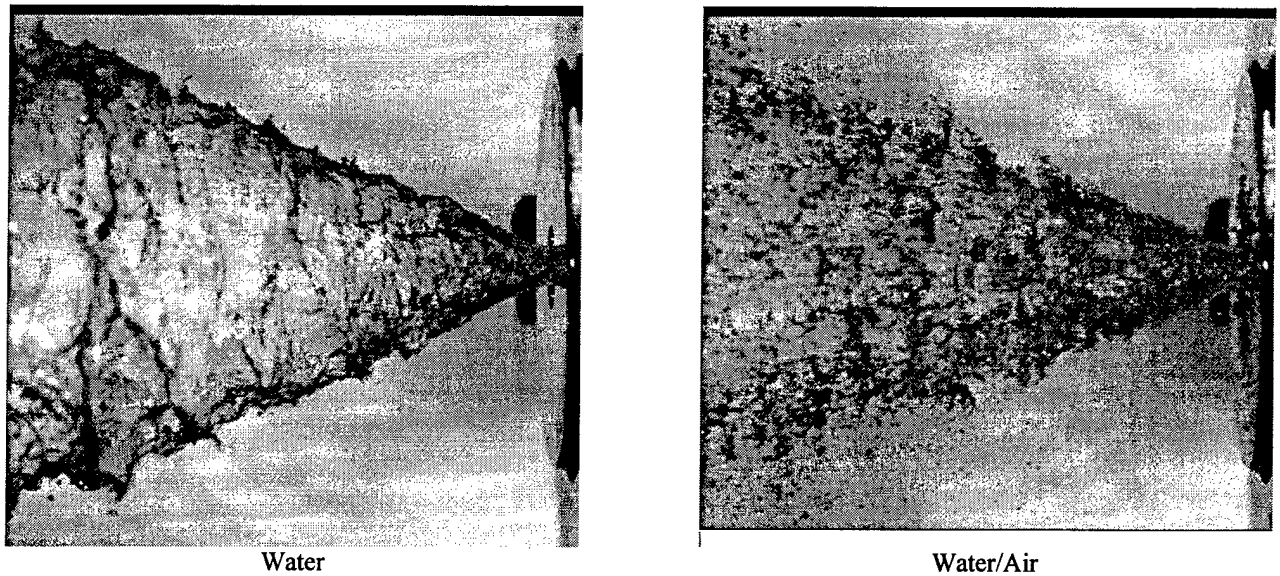

Water Water/Air

Figure 7. Instantaneous images of swirl coaxial spray showing the effect of gas flow on atomization. Water flowrate was held constant at 0.091 kg/s (0.2 lb/s). Air flowrate for water/air case was 0.91 gm/s (0.002 lb/s). Flow is from right to left into an unconfined, ambient environment.

Table 3
Representative Hot-Fire Tests with the
Swirl Coaxial Rocket Injector

	O/F (LO_2/H_2)	P_c (psia)	T_{af}† (K)	η_{C^*} (%)	GN_2 purge
Near-Stoich.	3.62	339	2815	95.2	x
	3.72	346	2854	96.9	x
	3.61	343	2815	96.1	x
	5.38	340	3308	97.1	x
	5.37	319	3347	96.2	
Ox-rich Series 1	14.8	205	2985	97.8	x
	22.7	262	2557	96.4	x
	37.0	214	1923	98.2	x
	59.7	269	1351	97.3	x
	80.2	241	1060	99	x
	81.3	238	1049	98.4	x
	89.5	229	966	99.5	x
	101.4	220	868	100.3	x
	99.3	199	968	101.6	x
	111.5	183	870	99.4	x
	127.3	175	767	102.8	x
	149.6	156	653	102	x
	163.6	141	594	103	x
Ox-rich Series 2	45.7	255	1929	94.4	
	45.3	258	1942	94.5	
	97.7	281	1032	90.9	
	96.1	307	975	92.9	x
	165.8	308	611	92.3	
	166.1	348	577	95.5	x

†Adiabatic flame temperatures based on chemical equilibrium calculations are given as T_{af}

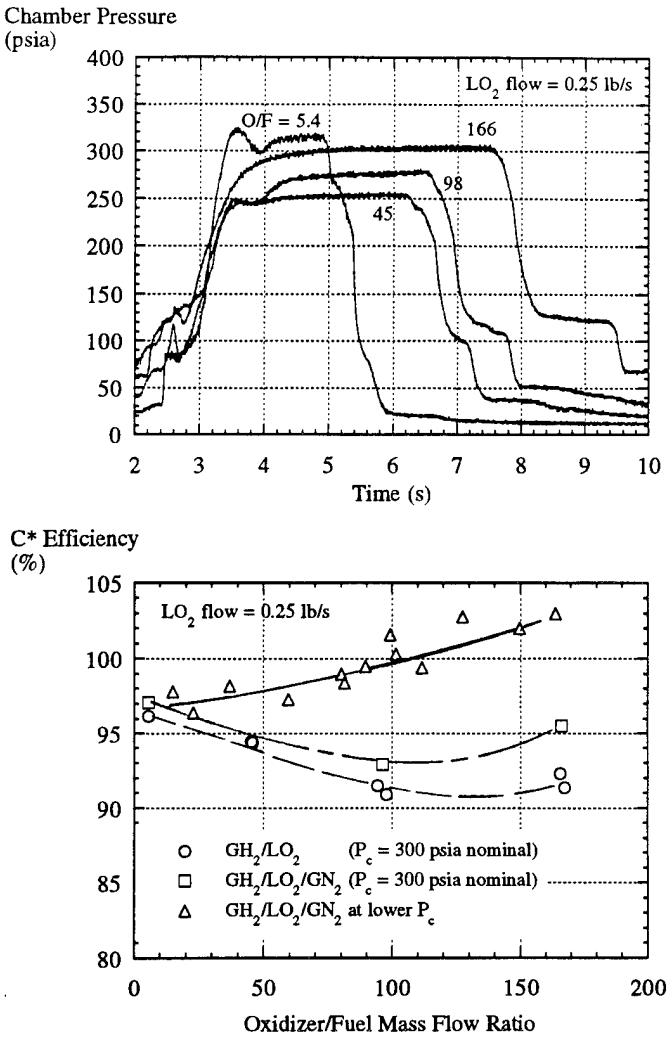

Figure 8. Performance of the single-element swirl coaxial injector in a uni-element rocket is demonstrated. Typical chamber pressure traces are shown in top graph. The measured c*-efficiencies are presented as a function of O/F mixture ratio in bottom figure. The data sampling rate for the chamber pressure transducers was 200 Hz.

efficiencies of better that 92% were measured for all tests. Near-stoichiometric tests indicated consistent c*-efficiencies of 95-97%. Series 1 tests, which were conducted at pressures ranging from 0.97 to 1.86 MPa (140 to 270 psia), indicated the highest c*-efficiencies of the data set. Series 2 tests covered a higher range of pressures from 1.72 to 2.41 MPa (250 to 350 psia), and resulted in somewhat lower c*-efficiencies. This is particularly noticeable at the highest mixture ratios. An explanation for this trend is decreased hydrogen injection velocity at higher P_c (all other things being equal), and the associated degradation in atomization, and oxidizer/fuel mixing which tend to reduce c*-efficiency. For higher chamber pressures, the hydrogen injection density is proportionally increased, and causes the reduced injection velocity for given flowrate. (For the highest O/F tests in Series 1, the c*-efficiencies of greater than 100% are non-physical. As little as 4 psia bias in the transducer measuring P_c can result in 2-3% over-estimate of η_{C^*}).

The oxidizer-rich test series are compared to other investigations in Table 4. Previous demonstrations of high mixture ratio combustion with rocket elements include only those of Bailey,[9] and very recent tests by Farhangi et al.[24] The three data sets appear to be complementary in several aspects. The three studies employed different elements: shear coaxial, swirl coaxial, and impinging elements. Also, they spanned different ranges in chamber pressures from subcritical at 140 psia

to supercritical at 3000 psia. The present study was for a single-element injector while the cited studies in Table 4 were for multi-element rocket chambers of somewhat larger chamber size. Nevertheless, they all indicate combustion over a very wide range of O/F ratios, and overall, the data indicate a potential for high performance with LOX/GH_2, even at the extreme mixture ratios listed in Table 4.

In the present experiments, the optical access of the rocket chamber was exploited in the single element test series (done at higher chamber pressures, not listed in Table 4). Flame visualizations and corresponding LOX visualizations, performed at the near-stoichiometric hot-fire conditions, are shown in Fig. 9 and 10. In Fig. 9, a composite photograph of the flame just downstream of the injector exit (1/1000th sec exposure) is constructed from photos taken of two rocket firings, one with the window positioned at 0 to 2 inhes, and another with it positioned at 2 to 4 inches. Several such photographs were taken during the steady chamber pressure portion of the hot-fire test; the photos shown are typical of what was seen. To the authors' knowledge, these are the first visualizations of a swirl coaxial injector spray flame obtained at rocket operating conditions and flowrates. Interesting features are observed in these photographs.

First, it is observed in Fig. 9 that a conical flame

Table 4
Comparison of Oxidizer-Rich Rocket Experiments with LOX/GH_2 Propellants

	No. of Elements	O/F	P_c (psia)	η_{C^*} (%)
Bailey[9] (25 tests)	69 shear coax	20 - 150	~1000	65 - 85
Farhangi et al.[24] (8 tests)	multiple imping.	117 - 173	2000 - 3000	100
Present work (>20 tests)	single swirl coax	3 - 166	140 - 350	92 - 100

Note:-
Bailey's rocket chamber was of 3.7 inch diameter
Farhangi's rocket chamber was of 3.5 inch diameter

is formed at the exit of the injector with the flame being held at the thin wall of the injector post (wall thickness of only 0.38 mm or 0.015 inches). The flame is the luminous region of the photograph. This observation indicates that the LOX stream is immediately mixed with hydrogen and a flame is established just downstream of

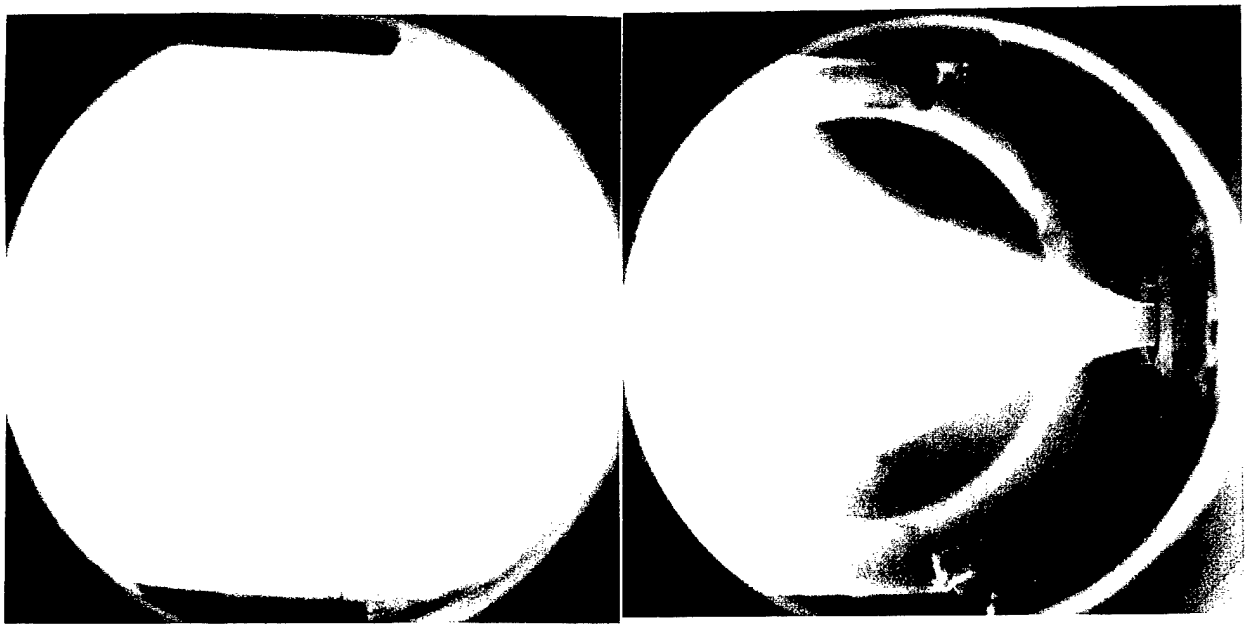

Figure 9. Swirl coaxial injector spray flame as visualized by taking 35 mm photograph at 1/1000th sec exposure. Flow is from right to left. Composite of two photographs shows the flame at 0 to 2 inches downstream of the injector face (right), and 2 to 4 inches downstreams of the injector face (left). Propellants are liquid oxygen and gaseous hydrogen at a mixture ratio of 5.7. The measured chamber pressure was 440 psia, and a rocket c*-efficiency of 97% was achieved.

Figure 10. Visualization of LOX droplets and ligament structures from photograph taken with window location at 0 to 2 inches downstream of the injector face. Flow is from right to left. Laser light at 514.5 nm, passed through the flame zone, is scattered towards the 35 mm camera (1/1000th sec exposure). Test conditions are identical to those in the previous figure.

the injector at this firing condition. Post-test inspections of the oxygen post indicated discolorations and oxidation at the injector tip, which corroborates the flameholding shown in Fig. 9. Second, it is observed that the spreading angle of the flame is similar to the spreading angle of the conical sheet for cold-flow tests with water and air, and more importantly, the spreading angle was seen to be significantly greater than for *shear* coaxial injector tests with LOX/GH_2 for identical conditions.[4] Finally, the flame is seen to fill the chamber somewhere between the two photographs that make up the composite. At a position approximately 3 inches (76 mm) downstream of the injector face, the flow attaches to the wall of the chamber and flows parallel to it. The photo at 2 to 4 inches indicates a zone of continued atomization, mixing and combustion that is representative of the remainder of the chamber.

A laser-based visualization technique was also applied in the hot-fire chamber to determine the presence of LOX in the flame zone. A continuous, argon-ion laser sheet at 514.5 nm wavelength (green) was passed through the axis of the conical flame (Fig. 9, right). The scattered laser light from LOX drops and ligaments was detected by a 35 mm camera. A 10 nm band pass filter centered at 514.5 nm wavelength was used to reject light from the luminous flame. One such photograph is shown in Fig. 10. Directional streaks that indicate drop or ligament motion are seen in the photograph due to the long exposure time. The presence of unvaporized LOX just downstream of the injector is inferred from this photograph which shows a conical distribution of LOX that is consistent with the extent of the conical flame zone pictured in Fig. 9. It is also consistent with the cold-flow image of Fig. 7 with water/air. Thus, this technique provides a glimpse of LOX atomization under hot-fire conditions.

In summary, the present single-element cold-flow and hot-fire studies confirm the utility of swirl coaxial rocket injectors as a means to achieving good performance in rockets, and demonstrate that this element is an excellent candidate for performing non-intrusive, laser-based studies in the windowed rocket chamber with LOX/GH_2. Future studies will focus on non-intrusive drop-size measurements in the flame zone to further explore the fundamental process of LOX atomization under rocket chamber conditions.

Conclusions

The hot-fire results which are presented in this paper, demonstrate the viability of the present swirl coaxial injector for both near-stoichiometric and high mixture ratio rocket combustion. In particular, the present injector provides for stable ignition, combustion, and flame holding at any oxidizer-to-fuel mixture ratio (by mass) from 3 to 166, and chamber pressures from 140 psia to 500 psia.

The first visualizations of a swirl coaxial rocket injector flame zone, and near-injector LOX spray field, are presented. These indicate immediate oxidizer/fuel mixing and combustion upon injection, as well as a stable flame attached to the LOX post tip. Complementary cold-flow visualizations with water and air show the mechanism of atomization from this type of injector for a representative rocket injector design, and are consistent with the LOX spray field visualized in hot-fire tests.

The present results, in conjunction with other high mixture ratio studies, have programmatic implications that favor the development of LOX preburners for operation at high mixture ratios. High c*-efficiencies are obtained in a uni-element rocket chamber; and hence justify further experimentation at higher chamber pressures and flowrates with a swirl coaxial element. The present injector and optically-accessible rocket is to serve as a necessary test bed in which to apply non-intrusive spray visualization and characterization

techniques to provide fundamental data in addition to single element performance results.

Acknowledgments

Funding by Dr. Mitat Birkan of the Air Force Office of Scientific Research, Air Force Systems Command, USAF, under grant number F49620-93-1-0365 is gratefully acknowledged. G. Cox and D. Hautman of United Technologies, J. Hulka of Aerojet Propulsion Division, C. Dexter of NASA (Marshall Space Flight Center), and Mr. D. Harrje are acknowledged for their comments with respect to the swirl injector design. Finally, the assistance of L. Schaaf, M. Moser, H. Ryan III, and M. Foust (Penn State Propulsion Engineering Research Center) in conducting the experiments is also gratefully acknowledged.

References

[1]Moser, M. D., Merenich, J. J., Pal, S., and Santoro, R. J., "OH-Radical Imaging and Velocity Field Measurements in a Gaseous Hydrogen/Oxygen Rocket," AIAA Paper 93-2036, AIAA/SAE/ASME/ASEE 29th Joint Propulsion Conference & Exhibit, Monterey, CA., June 28-30, 1993.

[2]Ryan III, H. M., Anderson, W. E., Pal, S., and Santoro, R. J., "Atomization Characteristics of Impinging Liquid Jets," AIAA Paper 93-0230, 31st Aerospace Sciences Meeting & Exhibit, Reno, NV., Jan. 11-14, 1993.

[3]Pal, S., Moser, M. D., Ryan, H. M., Foust M. J., and Santoro, R. J., "Flowfield Characteristics in a Liquid Propellant Rocket," AIAA Paper 93-1882, AIAA/SAE/ASME/ASEE 29th Joint Propulsion Conference & Exhibit, Monterey, CA., June 28-30, 1993.

[4]Beisler, M. A., Pal, S., Moser, M. D., and Santoro, R. J., "Shear Coaxial Injector Atomization in a LOX/GH_2 Propellant Rocket," AIAA Paper 94-2775, AIAA/SAE/ASME/ASEE 30th Joint Propulsion Conference & Exhibit, Indianapolis, IN., June 27-29, 1994.

[5]Brown, J. R., "Cryogenic Upper State Propulsion - RL10 and Derivative Engines," NASA Conference Publication 3112, Vol. 2, Space Transportation Propulsion Technology Symposium - Proceedings Vol. 2, held at Penn State University, State College, PA., June 25-29, 1990.

[6]Andreyev, A. V., Chepkin, V., and Fanciullo, T. J., "Investigation of Oxygen/Hydrogen Combustion Stability in Staged Combustion Liquid Rocket Engines," AIAA/SAE/ASME/ASEE 30th Joint Propulsion Conference, Indianapolis, IN., June 28-30, 1994.

[7]Knuth, W. K., and Crawford, R. C., "Oxygen-Rich Combustion Process Applications and Benefits," AIAA Paper 91-2042, AIAA/SAE/ASME 27th Joint Propulsion Conference, Sacramento, CA., June 24-26, 1991.

[8]Anon., *Liquid Rocket Engine Injectors*, NASA SP-8089, March 1976.

[9]Bailey, C. R., "A Preliminary Investigation of Oxidizer-Rich Hydrogen-Oxygen Combustion Characteristics," NASA TN D-3729, NASA Marshall Space Flight Center, December 1966.

[10]Giffen, E., and Muraszew, A., *The Atomisation of Liquid Fuels*, Chapman & Hall, 1953, Ch. V.

[11]Novikov, I. I., "Atomization of Liquids by Centrifugal Nozzles," (translated from Russian *Journal of Technical Physics*, Vol. 18, No. 3, 1948, pp. 345-354) *The Engineers' Digest*, Vol. 10, No. 3, March 1949, pp. 72-74.

[12]Tate, R. W., and Marshall, W. R., Jr., "Atomization by Centrifugal Pressure Nozzles - Part I and II," *Chemical Engineering Progress*, Vol. 49, No. 4, April 1953, pp. 169-174 (Part I), and Vol. 49, No. 5, May 1953, pp. 226-234 (Part II).

[13]Doumas, M., and Laster, R., "Liquid-Film Properties for Centrifugal Spray Nozzles," *Chemical Engineering Progress*, Vol. 49, No. 10, October 1953, pp. 518-526.

[14]Dumouchel, C., Bloor, M. I. G., Dombrowski, N., Ingham, D. B., and Ledoux, M., "Viscous Flow in a Swirl Atomizer," *Chemical Engineering Science*, Vol, 48, No. 1, 1993, pp. 81-87.

[15]Yule, A. J., and Chinn, J. J., "Swirl Atomizer Flow: Classical Inviscid Theory Revisited," International Conference on Liquid Atomization and Spray Systems (ICLASS-94), Rouen, France, July 1994.

[16]Dombrowski, N., and Hasson, D., "The Flow Characteristics of Swirl (Centrifugal) Spray Pressure Nozzles with Low Viscosity Liquids," *AIChe Journal*, Vol. 15, No. 4, July 1969, pp. 604-611.

[17]Simmons, H. C., "The Prediction of Sauter Mean Diameter for Gas Turbine Fuel Nozzles of Different Types," ASME Paper No. 79-WA/GT-5, *Journal of*

Engineering for Power, 1979, pp. 1-7.

[18]Atherton, R. R., et al., "Air Force Reusable Rocket Engine Program - Final Report," AFRPL-TR-71-1 Vol. 1 (Air Force Contract F04611-68-C-0002), Pratt & Whitney Aircraft, Division of United Aircraft Corp., January 1971.

[19]Hautman, D. J., "Spray Characterization of Liquid/Gas and Liquid/Liquid Coaxial Injectors with the Center Liquid Swirled," Report No. UTRC89-31, United Technologies Research Center, East Hartford, CT., June 1990.

[20]Hulka, J., Schneider, J. A., and Davis, J., "Single Element Injector Testing for STME Injector Technology," AIAA/SAE/ASME/ASEE 28th Joint Propulsion Conference and Exhibit, Nashville, TN., July 6-8, 1992.

[21] Private communications with: G. Cox of Pratt & Whitney, J. Hulka of Aerojet Propulsion Division, and D. Hautmann of United Technologies Research Center.

[22]Nurick, W. H., "Orifice Cavitation and its Effect on Spray Mixing," *Journal of Fluids Engineering*, Dec. 1976, pp. 681-687.

[23]Van Dyke, M., *Album of Fluid Motion*, The Parabolic Press, Stanford, CA., 1982 ed., pp. 115.

[24]Farhangi, S., Hunt, K., Tuegel, L., Matthews, D., and Fisher, S., "Oxidizer-Rich Preburner for Advanced Rocket Engine Application," AIAA Paper 94-3260, AIAA/SAE/ASME/ASEE 30th Joint Propulsion Conference & Exhibit, Indianapolis, IN., June 27-29, 1994.

Attachment C

Coaxial Swirl Injector Studies at High O/F Ratios

by

S. A. Rahman, S. Pal, and R. J. Santoro

32nd JANNAF Combustion Subcommittee Meeting
Huntsville, AL.
23-27 October 1995

Presented at 32nd JANNAF Combustion Subcommittee Meeting
Huntsville, AL, 23-27 October, 1995.

COAXIAL SWIRL INJECTOR STUDIES AT HIGH O/F RATIOS

S. A. Rahman,* J. M. Cramer,* S. Pal,† and R. J. Santoro‡

Propulsion Engineering Research Center
and
Department of Mechanical Engineering
The Pennsylvania State University
University Park, PA. 16802-2320

ABSTRACT

Current interest in reusable launch vehicles (RLV) has generated renewed interest in high oxygen to fuel ratio (O/F) preburner operation. In particular, full-flow preburner concepts for rocket engines require high O/F operating conditions. In the present work, the performance, stability, and heat transfer characteristics of a swirl coaxial injector over an O/F range of 5 to 170 are investigated. These experiments were conducted in an optically-accessible rocket chamber operating with liquid oxygen and gaseous hydrogen at a nominal pressure of 2.1 MPa (300 psia), with some additional studies at 4.8 MPa (700 psia). The studies show that high c*-efficiency (> 90%) and stable combustion can be achieved over the O/F range examined. Concurrent heat flux measurements show that heat transfer to the walls decreases as O/F increases. Heating at both upstream and downstream chamber locations is characterized. Over this pressure range, the chamber pressure does not significantly affect the stability and heat transfer characteristics of the rocket. Extension of the present work to supercritical chamber pressures representative of a rocket preburner is planned to further examine operating chamber pressure effects. The findings of the present study are to be incorporated into CFD modeling activities at Penn State and the Marshall Space Flight Center in order to provide design methodologies for high O/F preburners as related to this particular injector.

NOMENCLATURE

A_t	nozzle throat area
a	speed of sound
c	specific heat
c*	characteristic exhaust velocity $(=P_c A_t / \dot{m})$
f_{res}	chamber resonant frequency
k	thermal conductivity
$\dot{m}$	flowrate
P	pressure
P'	pressure fluctuation
q	heat flux
t	time
T	temperature

Greek Symbols

ρ	density
η_{c^*}	c*-efficiency

Subscripts

af	adiabatic flame
c	chamber
rms	root-mean-square
w	wall

Abbreviations

CFD	computational fluid dynamics
GH_2	gaseous hydrogen
ID	inner diameter
OD	outer diameter
LOX	liquid oxygen
O/F	oxidizer/fuel ratio by mass
RLV	reusable launch vehicle

---

* Graduate Research Assistant
† Research Associate
‡ Professor of Mechanical Engineering.

INTRODUCTION

In order to better understand combustion phenomena in current rocket engines, and to develop more advanced engines, it is often useful to first characterize a single rocket injector element under precisely controlled combustion conditions. This study concerns the swirl coaxial type of rocket injector which is currently undergoing just such a characterization, with a strong emphasis on high oxidizer-to-fuel ratio (O/F) combustion processes for H_2/O_2 propellants. The information obtained to date is to become part of a technology base on the feasibility of high O/F combustion in rocket chambers.

Combustion of liquid oxygen (LOX) at high O/F is of particular interest to the rocket combustion community under the Reusable Launch Vehicle (RLV) technology program. Proposed engine cycle concepts for the RLV call for full-flow of propellants through both fuel-rich and oxidizer-rich (high O/F) preburners with subsequent gaseous propellant injection into the main chamber of the rocket engine. Such an engine cycle is described for instance by Knuth.[1] There is presently great interest in the oxidizer-rich preburner component since the ability to operate LOX preburners at an O/F ratio greater than 100 is a critical technology that has had few demonstrations in the US.[2,3,4] Issues that need to be addressed at high O/F include propellant atomization/mixing, ignition, combustion stability, and the homogeneity of exhaust gas. As indicated in Figure 1, a distinguishing feature of the oxidizer-rich combustion process is the reduced temperature of the combustion products. Thus, operation at the ~~minimum~~ maximum possible O/F ratio will minimize thermal loads within the engine for components downstream of the preburner such as the LOX turbopump.

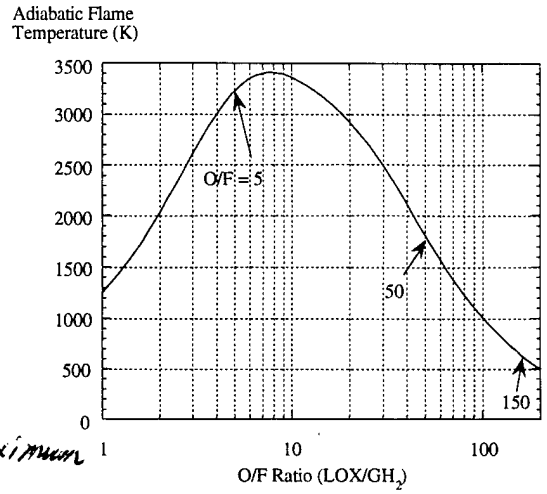

Figure 1. High O/F operation offers substantial reduction in the preburner flame temperature which would be beneficial for engine components downstream of the oxygen-rich preburner.

In the present paper, performance, stability and wall heat flux results from a series of LOX/GH_2 combustion experiments are discussed. The experimentation is performed with a swirl coaxial injector in a uni-element rocket chamber. The findings cover a range of O/F mass flow ratios from 5 to 170 (equivalence ratio of 1.6 to 0.047), at a nominal chamber pressure of 2.1 MPa (300 psia) with some further results at higher pressures up to 4.8 MPa (700 psia). The experiments are conducted at flowrates representative of a rocket injector and combustor at the single element level. The experimental study employed the Cryogenic Combustion Laboratory facility of the Propulsion Engineering Research Center (PERC). Introductory details regarding the injector, combustor, data acquisition, and data reduction are provided first.

SWIRL COAXIAL ROCKET INJECTOR

The development of the present swirl coaxial rocket injector element is described by Rahman et al.[4] The swirl coaxial type of injector has previously been demonstrated to be effective in achieving atomization and mixing, and stable combustion in rocket engines. This injector element, which has been successfully employed for decades on all Pratt & Whitney rocket engines and many Russian booster engines,[5] is designed to inject swirling LOX from the center tube and non-swirled gaseous hydrogen through an annulus surrounding the central tube. The present design follows current industry practice in employing tangential-entry slots to impart swirl within the LOX post tube (cf. Figure 2). The element design itself was guided by the findings in earlier injector characterization efforts reported by Atherton,[6] Hulka et al.[7] and Hautman.[8]

The mechanics of operation of this type of injector are as follows. The liquid stream's tangential velocity component causes a swirling vortex flow within the LOX post tube. This tube does not flow full, but instead contains a thin swirling liquid film along the inner wall with a hollow gas core. The swirling film exits the tube in the form of a hollow cone sheet which readily self-atomizes. However, the coaxial flow of gas (hydrogen in this case) greatly enhances and accelerates the sheet breakup process by disturbing the liquid film that emerges from the injector post.

Two such injectors are employed in this study. The smaller unit is nominally sized to deliver 0.114 kg/s (0.25 lbm/s) with an associated pressure drop of 0.76 MPa (110 psia),[4] i.e. discharge coefficient of 0.32 according to the calculation methodology of Doumas and Laster,[9] and Yule and Chinn.[10] The spray cone angle for the present injector was measured to be 40 degrees; this spreading of the spray has implications for the wall heat transfer results to be presented later. The post has an inner diameter (ID) of 3.43 mm (0.135 in.) and a wall thickness of 0.38 mm (0.015 in.). The film thickness of the liquid leaving this injector is estimated to be 10% of the injector diameter, or 0.34 mm (0.013 in.), thus occupying approximately 35% of the tube's cross-sectional area. The outer diameter (OD) of the coaxial gas annulus is 7.11 mm (0.28 in.) which results in a gas gap size of 1.46 mm (hydraulic diameter of 2.92 mm). A larger version of this injector has the following dimensions: post ID of 7 mm (0.277 in.), wall thickness of 1.24 mm (0.049 in.) and an annulus OD of 10.74 mm (0.423 in.). The larger element delivers liquid at the same discharge coefficient of 0.32, but provides four times the flowrate for the same pressure drop (since its post ID is twice as large).

The smaller element is similar in size and capacity to a current Pratt and Whitney rocket injection element design,[11] and also corresponds closely to elements verified in previous element characterization work by Atherton et al.[6] and Hautman.[8] The larger element is comparable in size to a booster engine element.[7]

RESEARCH ROCKET

The oxygen-rich experiments are conducted at the Cryogenic Combustion Laboratory at The Pennsylvania State University. The laboratory provides the capability for studying both gaseous and liquid propellant rocket combustion at the single element level. The flowrate capabilities for this laboratory are 0.45 kg/s (1 lbm/s) for liquid oxygen and 0.45 kg/s (1 lbm/s) for gaseous hydrogen. The rocket chamber used for the experiments has been described elsewhere, but design particulars are also given here for completeness.[12,13]

The rocket chamber is modular by design and provides optical access for laser-based diagnostic approaches. A cross-sectional view of the chamber is shown in Figure 2. The chamber consists of an injector assembly section, a window-section, an ignitor section, several blank sections and a nozzle section, which are all held in place by a hydraulic jack. The middle sections of the chamber may be interchanged, allowing placement of the window section at any location along the chamber. This arrangement provides for optical access, or instrumentation access, along the entire length of the chamber. For the experiments reported here, the length of the chamber was 349 mm (13.75 in.). The window-section includes two diametrically opposed round quartz windows, 50.8 mm in diameter (2 in.), that provide optical access to the 50.8 mm diameter square cross-section combustion chamber. The other two sides of the window feature slot windows measuring 6.25 x 50.8 mm which provide additional optical access. All of the windows are thermally protected from the hot combustion gases by a curtain purge of nitrogen which flows across the windows. In the present work, instrumentation is employed in place of the

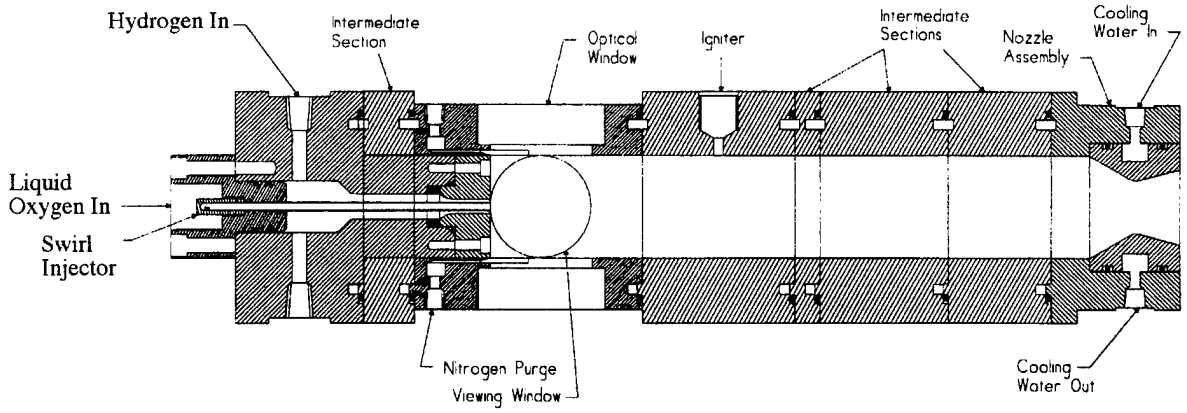

Figure 2. Cross-sectional view of the swirl coaxial injector and uni-element optically-accessible rocket chamber. LOX is injected into the center post tube via the swirl insert, while GH_2 enters (non-swirled) through a coaxial annulus surrounding the post. Liquid swirl is imparted by means of tangential entry slots placed at 3 azimuthal positions around the post, 120 degrees apart. The rocket chamber is modular in design and allows for varying the chamber length, injector assembly, window-section location, and nozzle. The interior of the chamber is 50.8 x 50.8 mm (2 in. square). For the results presented here, the length of the chamber was 349 mm (13.75 in.). Various nozzles with throat sizes ranging from 6.3 to 13.7 mm (0.25 to 0.54 in.) were used.

windows. Two heat flux gauges are adapted into the round window ports (on opposing sidewalls), and a high frequency pressure transducer is mounted into one of the slot window positions. Since optical access is not needed, the nitrogen curtain purge is turned off. The injector section of the rocket is also modular in design for convenient interchange of injector type and/or geometry. In this work, the swirl coaxial injector described earlier is used.

The ignitor section of the rocket is equipped with an ignition chamber (not shown in Figure 2) that provides a spark-ignited gaseous H_2/O_2 torch for ignition in the main combustion chamber. Finally, the water-cooled nozzle of the rocket is easily changed between tests to vary the chamber pressure. For the present experiments, nozzles with throat diameters ranging from 5.6 to 13.7 mm (0.22 to 0.54 in.) are used to vary the chamber pressure. The setting and monitoring of the flowrate of the gaseous (GH_2) and liquid propellants (LOX) is accomplished with the aid of a critical orifice and a cavitating venturi, respectively, that are instrumented at both upstream and downstream locations with pressure transducers and thermocouples. The nominal LOX flowrates ranged from 0.11 to 0.21 kg/s (0.25 to 0.46 lbm/s), whereas the nominal hydrogen flowrates are varied between 0.7 and 45 gm/s (0.0015 and 0.1 lbm/s). The resulting range of O/F mass flow ratios is 5 to 170. These flowrates, coupled with the nozzles used, allow for operating chamber pressures between 1.72 and 4.8 MPa (250 to 700 psia).

The duration of a combustion run is nominally four seconds, with shorter runs being used at near-stoichiometric conditions. The duration of a run is a compromise between the time required to achieve a steady chamber pressure and survivability of the quartz windows. In the present configuration, employing LOX/GH_2 propellants, it takes approximately two seconds for the chamber pressure to stabilize. After this period, stable chamber pressures are achieved for the programmed duration of the rocket firing.

INSTRUMENTATION

An overall view of the instrumentation layout for the present study is presented in Figure 3. The illustration indicates the four axial positions that are surveyed with the high frequency pressure transducers, 25, 76, 229, and 305 mm (1, 3, 9 and 12 in.), and the three axial positions where wall heat transfer measurements are made 25, 76, 229 mm (1, 3 and 9 in.). Two PCB pressure gauges (50 kHz sampling) supplied by PCB Piezotronics Inc., and two heat flux gauges built in-house are employed. One PCB transducer and two heat flux gauges are positioned at either the 25, 75 or 225 mm axial position for any given run, with the other PCB transducer permanently located at the 305 mm near-nozzle position. Two upstream positions near the flame zone are chosen (25 and 76 mm), as well as one downstream location (229 mm) where more uniform flow conditions are expected. Heat transfer gauges and a PCB gauge are mounted into the window section as described earlier. Standard chamber pressure measurements (Setra 204 transducers at 200 Hz sampling) are also made simultaneously for each combustion run at both upstream and downstream positions within the rocket chamber. These are required to estimate rocket c*-efficiency. Relevant details regarding the instruments and measurement technique are summarized below.

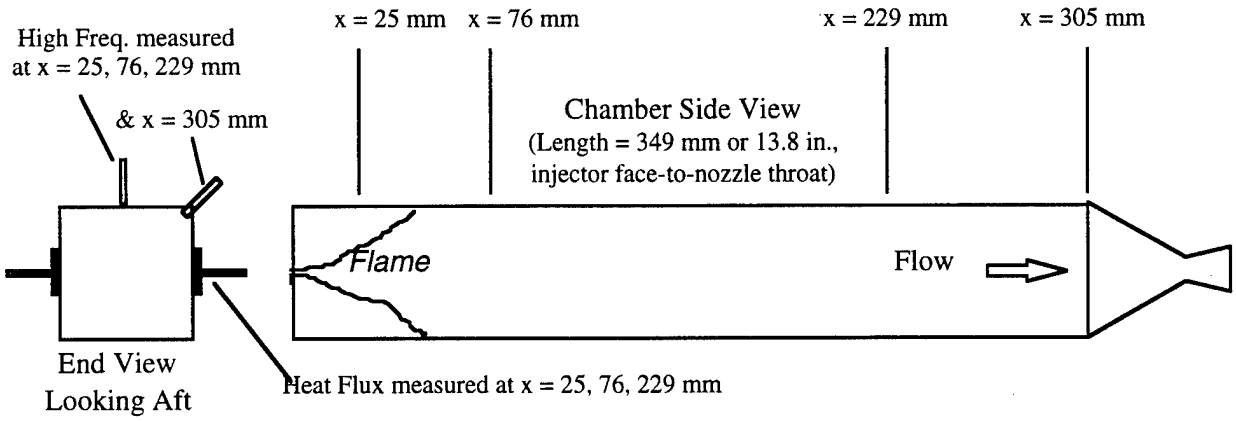

Figure 3. The illustration summarizes the chamber locations surveyed with high frequency pressure gauges and heat flux gauges. The rocket chamber is shown to scale. Experiments are repeated with the two opposed heat flux gauges located at the 25, 76, and 229 mm axial positions respectively. At each axial position, combustion runs at four nominal O/F ratios (5, 50, 100, 165) are conducted.

HIGH FREQUENCY PRESSURE GAUGE

The high frequency pressure transducers are PCB gauge Model 113A24 featuring 1 μs response with a 500 kHz natural frequency, well beyond any expected chamber frequencies. The gauge itself is mounted as close as possible to the inner wall of the rocket chamber. The mounting port is drilled to within 10 mm of the chamber side wall. A 1 mm hole is then drilled through to the chamber. Thus, direct impingement of combustion gases onto the sensing element is minimized while local pressure is measured through the 1 mm hole. For this combustion application, the gauge is encased in a water-cooling jacket (supplied by manufacturer) for thermal isolation from the hot chamber walls. Transducer signals (voltage output) are recorded by a LeCroy high speed data acquisition system in digital form. The PCB gauge is employed in an AC-coupled mode so that only the fluctuating component of pressure is recorded. In these experiments the data acquisition allowed for a full-scale range of ±276 kPa (±40 psi) with a bit resolution of 129 Pa (~0.02 psi). The typical time-history of the pressure oscillation consists of 10 s of data recorded at 50 kHz sampling rate by the PCB gauge. The conversion of this time domain signal into a frequency domain power spectrum provides the desired combustion stability information.

The period of data acquisition covers the ignition and shutdown transients as well as the steady-state portion of the combustion run. For purposes of this investigation, only the steady-state part is of interest. This steady period is determined from examination of the chamber pressure time-history (Setra 204 transducer output). At oxygen-rich conditions, several seconds of steady-state durations are possible. For near-stoichiometric conditions, only 0.5 s of a 3 s combustion period is steady-state owing to start transients; a longer firing duration to extend the steady-state period is precluded by chamber thermal constraints. In all cases, a subset of the steady combustion period is chosen for spectral analysis. A segment of the data towards the end of the steady combustion period is used.

The frequency content and energy spectrum of the time-domain pressure oscillation is determined by standard methods of Fourier analysis by Discrete Fourier Transform, as described for instance by Oppenheim and Schafer,[14] and Press et al.[15] In practice, the number of samples used in the analyses are 2^{14}, or 16384. This results in a 0.328 s period of combustion at 50 kHz sampling. After conversion of the data into the frequency-domain, a frequency bandwidth (resolution) for the power spectrum of 3 Hz is achieved. This provides sufficient accuracy to ascertain the frequency content of the pressure oscillations.

HEAT FLUX GAUGE

The measurement of transient heating within a rocket chamber is possible with a heat flux gauge developed by Liebert[16] at the NASA Lewis Research Center. As demonstrated by Liebert, the time-histories of multiple in-depth thermocouples may be used to deduce the wall heat flux provided that the heat flow near those thermocouples is one-dimensional. Two such gauges are employed in this study. As shown in Figure 4, the gauge consists of four Type K thermocouples soldered to a copper rod (designated T1--T4). Since an air gap exists between the rod and the remainder of its housing, the heat flow from the hot wall approximates one-dimensional heat flow with an adiabatic backface condition. The entire gauge is constructed of Oxygen-Free High-Conductivity Copper. The thermocouple positions ranged from 1.6 mm to 22 mm in-depth (nominally) with equal spacing between them.

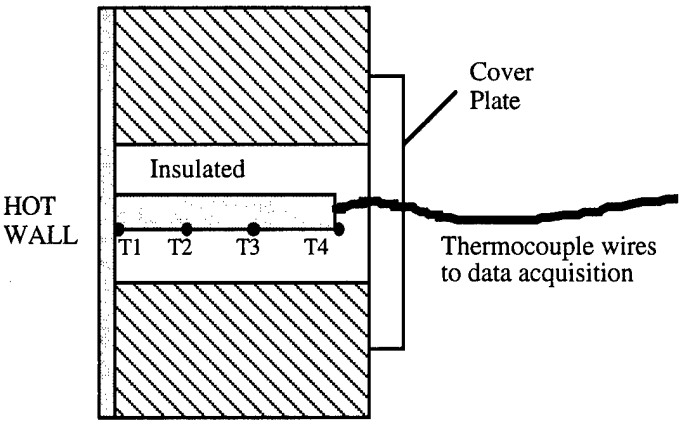

Figure 4. Schematic of heat flux gauges. Four in-depth thermocouples (Chromel-Alumel Type K) record the transient temperatures which are subsequently processed to obtain transient heat flux during the combustion run.

Surface heat flux $q_w(t)$ is estimated by integrating the one-dimensional heat conduction equation with respect to the spatial dimension x as shown below: (ρ, c, k are the copper density, heat capacity, and conductivity, respectively)

$$\int_0^L \left(\rho c \frac{\partial T}{\partial t}\right) dx = \int_0^L \frac{\partial}{\partial x}\left(k \frac{\partial T}{\partial x}\right) dx$$

$$\int_0^L \left(\rho c \frac{\partial T}{\partial t}\right) dx = \left(k \frac{\partial T}{\partial x}\right)\Bigg|_0^L = q(0) - q(L)$$

where $q \equiv -k\,\partial T / \partial x$. Since the backface is insulated (i.e. $q(L) = 0$), this results in

$$q_w \equiv q(0) = \int_0^L \left(\rho c \frac{\partial T}{\partial t} \right) dx$$

In practice, the measured time-histories *T1(t)*, *T2(t)*, *T3(t)*, *T4(t)*, are curve-fitted by fifth-order polynomial functions. The time-history of wall temperature, which is needed for the above integration, is estimated by linear extrapolation of the near-wall temperatures *T1(t)* and *T2(t)*. All temperatures are then differentiated numerically to obtain *dT1/dt*, *dT2/dt*, *dT3/dt*, *dT4/dt*. A trapezoidal rule integration in space is finally performed, accounting for temperature dependent properties, to get the desired wall heat flux. The above computations are restricted to the steady-state combustion portion of each rocket firing.

RESULTS

The discussions below address the combustion performance, stability, and wall heat transfer characteristics for oxidizer-rich combustion of LOX/GH_2. As mentioned already, three axial locations within the combustion chamber are surveyed with the instrumentation, and each location at four O/F ratios ranging from 5 to 170. For the studies of the small swirl coaxial injector, the LOX flowrate is maintained for all combustion runs at a nominal value of 0.11 kg/s (0.25 lbm/s) with a nominal chamber pressure P_c of 2.1 MPa (300 psia). This value of P_c is chosen to be significantly above the local vapor pressure at the injector so that LOX inlet quality is assured. The LOX injection temperature (typically 120 K) is monitored to verify this. For the studies of the larger injector, the LOX flowrate is maintained at 0.21 kg/s nominally (0.46 lbm/s) with a nominal chamber pressure of 4.8 MPa (700 psia). In terms of the critical pressure of LOX, which is 5.03 MPa, the pressures given above correspond to reduced pressure P_r of 0.42 and 0.96. O/F ratio variation for these oxidizer-rich combustion studies is achieved by reducing the hydrogen flowrate. It is noteworthy that in this manner total flowrate is also approximately constant for the oxidizer-rich O/F ratios since hydrogen constitutes a relatively small fraction of the injected mass.

PERFORMANCE

A visualization of the near-injector combustion zone as seen through 50.8 mm round viewing windows is provided in Figure 5. For this injector, the spray flame attaches to the LOX post for this injector/rocket flowfield, and rapidly expands to fill the chamber cross-section (cone angle is 38 degrees). This flame behavior is observed at near-stoichiometric conditions as well as oxidizer-rich conditions for this injector.

Chamber pressure is monitored and recorded by a pair of transducers, one at each end of the rocket. The chamber pressure time-histories for four typical combustion runs are shown in Figure 6. Ignition and shutdown transients are also included. The firing duration is limited by thermal constraints at the near-stoichiometric O/F ratio of 5.4 (flame temperature of 3350 K), but this is not a problem for oxidizer-rich cases where longer durations are employed to maximize the data collected. The traces indicate that steady combustion is achieved approximately 1.5 to 2 s after ignition.

Table 1 provides a list of the combustion runs specific to this study. The actual values of flowrates, chamber pressures, c*-efficiencies (characteristic exhaust velocity η_{C^*}) and instrumentation are given. C*-efficiencies of 95% and greater are achieved at the near-stoichiometric O/F ratio condition. For oxidizer-rich conditions, η_{C^*} is 90-95% at the lower chamber pressures, and 80-87% at the higher pressures. The present research injector is not optimized to maximize c*-efficiency. Higher values can be achieved by tailoring the injector annulus to increase the gas injection velocities for instance. The

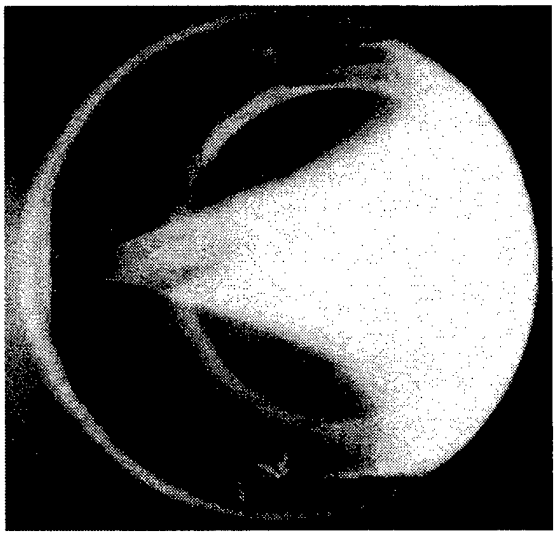

Figure 5. Swirl coaxial injector spray flame of LOX/GH_2 is visualized in a 35 mm photograph taken at 1/1000th sec exposure. The flame is seen through the circular rocket windows. Flow is from left to right. Photograph shows flame at 0 to 51 mm (0 to 2 in.) downstream of the injector face. Propellant O/F is 5.7, the chamber pressure is 3 MPa (440 psia), and a rocket c*-efficiency of 97% is achieved. *(reproduced from Ref. 4)*

purpose here is to report the specific c*-efficiencies for this oxidizer-rich series of combustion runs, and show that performance is *not* significantly degraded at high O/F ratio for the swirl coaxial injector. It should be noted that the length of the rocket chamber for these experiments is 349 mm. The chamber volume allows for a propellant residence time of approximately 7 ms at near-stoichiometric mixture ratios, and approximately 100 ms at the highest mixture ratios for either injector.

Performance at oxidizer-rich conditions has also been previously reported by Bailey[2] ($\eta_{C^*} \sim 80\%$), and more recently by Farhangi et al.[3] ($\eta_{C^*} \sim 100\%$). These studies are complementary to the present results. First, the chamber pressures were higher (5.5 to 20.5 MPa). Also, multi-element rocket injectors were employed in somewhat larger size chambers (shear coaxial element by Bailey,[2] and impinging elements by Farhangi et al.[3]). Nevertheless, LOX/GH_2 is the propellant combination for each of them, and taken together the studies demonstrate ignition/combustion over a wide range of O/F ratios and chamber pressures for this propellant combination.

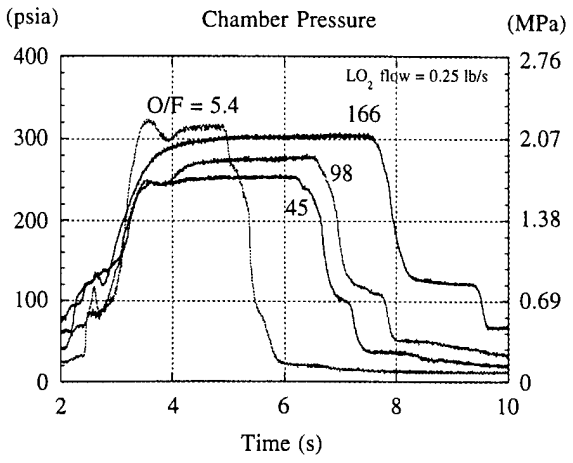

Figure 6. Chamber pressure time-history is shown for four typical combustion runs with the single-element swirl coaxial injector in the uni-element rocket. Ignition and shutdown transients are shown in the traces. *(reproduced from Ref. 4)*

Table 1. List of Run Conditions for Oxidizer-Rich Combustion Studies

†LOX Flow kg/s	O/F Ratio	Chamber Pressure, P_c MPa (psia)	Est. Flame Temp., T_{if} K	C*-Eff. (%)	Instrument Locations: Heat Flux Gauges A&B x = 25	x = 76	x=229	High Frequency Pressure Xdcrs. x=25	x=76	x=229	x=305
0.116	**6.1**	2.03 (295)	3420	95.6	×			×			×
0.116	**46.4**	1.81 (262)	1905	94.9	×			×			
0.118	**103**	1.72 (249)	980	84.3	×			×			
0.118	**166**	2.07 (301)	610	90.3	×			×			
0.117	**5.31**	2.32 (336)	3340	100		×			×		×
0.117	**46.6**	1.78 (258)	1905	93.2		×			×		
0.117	**96.5**	1.91 (277)	1045	91.5		×			×		
0.117	**168**	2.08(302)	605	92.7		×			×		
0.117	**5.32**	2.17 (315)	3340	95.7			×			×	×
0.112	**44.2**	1.75 (254)	1975	93.5			×			×	
0.117	**94.8**	1.82 (264)	1060	86.5			×			×	
0.120	**171**	2.12 (308)	590	92.7			×			×	
0.110	**48.1**	2.25 (327)	1860	80.2			**			×	×
0.112	**49.3**	2.33 (338)	1825	81.8			**			×	×
0.115	**50.2**	4.33 (628)	1800	80.9			**			×	×
‡ 0.117	**53.7**	4.37 (634)	1710	83.2			×			×	×
0.215	**50**	2.99 (434)	1810	87.4			×			×	×
0.213	**59.3**	4.16 (603)	1585	84.7			×			×	×
0.215	**49.9**	4.54 (658)	1810	84.2			×			×	×
0.206	**96.6**	4.51 (655)	1040	81.7			×			×	×
0.211	**146**	4.88 (708)	610	84.2			×			×	×
0.208	**142**	4.99 (724)	720	86			×			×	×
0.212	**144**	4.97 (721)	660	84.6	×					*	*
0.209	**97.8**	4.76 (691)	1020	85.6	×					*	*

* High frequency pressure data not available.

** Heat transfer data not available.

† Note that the two halves of the table represent studies at low chamber pressures and high chamber pressures respectively. Smaller injector is employed where the LOX flowrate is approximately 0.12 kg/s, and larger injector where flow is 0.21 kg/s.

‡ In this combustion run a smaller annulus was used to increase hydrogen injection velocity (OD of 0.218 mm).

STABILITY

The stability of rocket combustion at very high O/F ratio has not been addressed in previous work. Although the combustion performance and chamber pressures suggest smooth and stable combustion, this is specifically verified through the use of high frequency pressure measurements (PCB gauges described earlier). The magnitude of the pressure oscillation levels for all combustion runs is summarized in Figure 7. The root-mean-square of the fluctuation P'_{rms} is shown as a percentage of the chamber pressure P_c. In most cases, the root-mean-square fluctuations are less than 2% of P_c, while the peak-to-peak fluctuations are below 6% of P_c. Oscillations which are lower than 5% of P_c are generally associated with stable combustion.

The frequency content of the pressure fluctuations is also shown in Figure 7 and listed in Table 2. In most of the combustion runs, it appears that the fluctuation energy is concentrated in a single longitudinal mode of the combustion chamber. Agreement between both PCB gauges as to the excited frequencies is also excellent. The sampling and data reduction methods allow for a frequency resolution of 3 Hz; therefore the frequencies reported Table 2 should be interpreted to be accurate to 3 Hz.

A prediction of chamber resonant frequencies f_{res} (during combustion at a particular O/F ratio) is possible based upon the speed of sound, a, through the equation $f_{res} = (a/2)\sqrt{(n_x/l_x)^2 + (n_y/l_y)^2 + (n_z/l_z)^2}$. Predictions of the longitudinal mode frequencies are given in Figure 7 along with the data. In the above prediction formula, the chamber dimensions are given by l_x, l_y, l_z while the mode numbers (1st, 2nd, 3rd etc.) are indicated by n_x, n_y, n_z in the respective coordinate x, y, z. The analysis shows that either the 1L or the 2L mode is the most excited at O/F ratios of 50 and 100, with a small amount of resonant energy being found in higher order longitudinal mode subharmonics. At O/F ratios of 5 and 165, it is the 3L mode which is the most energetic. At high O/F ratios (45, 100, 165 nominal) agreement between measured and predicted frequencies is within 5%. For the near-stoichiometric case there is a 10% discrepancy, which is not unlikely considering the complexities of the actual combustor flowfield acoustics. Transverse mode pressure oscillations, which would occur at much higher frequencies, are not observed in the present study.

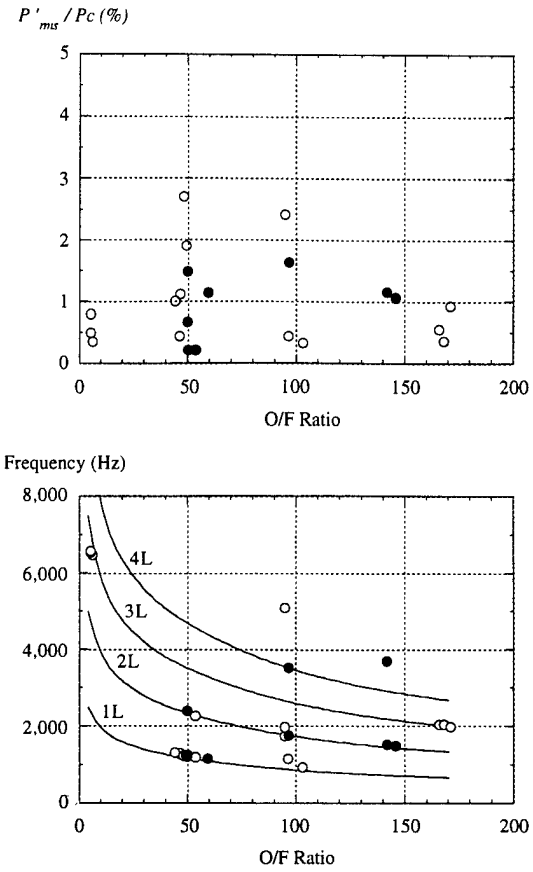

Figure 7. Root-mean-square of the high frequency pressure oscillations are shown normalized by chamber pressure for all the combustion runs (top graph), along with the associated frequency content (bottom graph): o -- 2.1 MPa combustion with small injector, and ● -- 4.8 MPa combustion with large injector. Predicted frequencies 1L, 2L, 3L, 4L, are indicated by the curves.

In one instance, O/F of 94.8, a number of unexpected frequencies are strongly excited. This combustion run was repeated several times with similar results. Even longitudinal modes of the chamber (2L, 4L, 6L, 8L) were excited to levels which resulted in the largest pressure oscillations observed in this study. Coupling with the injection and feedline characteristics is believed to be the source of the oscillations. It is noted that c*-efficiency dropped to 86.5% for this run as compared to 91.5% for a previous run at a very similar O/F ratio of 96.5

The present results are unique since they address the stability of a *single* injector element over a wide range of mixture ratios from 5 to 170. It is noteworthy that a previous stability characterization of swirl coaxial injectors with LOX/GH_2 propellants was performed by Hulka et al.[17] over a mixture ratio range of 3 to 9. In that study of dynamic stability of a multi-element, cylindrical chamber (32 to 114 kg/s total flowrate, or 70 to 250 lbm/s), Hulka et al. noted stable engine response to pressure perturbations (induced by non-directional bombs) without the use of stability aids for fuel-rich combustion. A comparison cannot be made, however, between the present oxidizer-rich, uni-element studies and the fuel-rich, multi-element studies of Hulka et al. owing to significant differences in hardware and experimental conditions.

Table 2. Results of High Frequency Pressure Studies

O/F Ratio	P'_{rms}/P_c (%)	Dominant Resonant Frequency Observed (Hz) for Various Positions in Chamber			
		x = 25 mm	x = 76 mm	x = 229 mm	x = 305 mm
6.1	0.35	6476			*
5.31	0.49		6534		
5.32	0.80			6580	
46.4	0.44	1279			1279
46.6	1.12		1291		
44.2	1.00			1309	
103	0.33	931			931
96.5	0.44		1154		
94.8	2.42			1740, 1975, 5081	
166	0.55	2032			2032
168	0.36		2029		
171	0.93			1987	
48.1	** 2.70			1224	1224
49.3	1.90			1245	1245
50.2	0.21			1251, 1236	1251, 1236
53.7	0.21			1196, 2258	1196, 2258
† **50**	0.67			1239	1239
59.3	1.14			1147	1147
49.9	1.48			1200, 2400	1200, 2400
96.6	1.63			1758, 3516	1758, 3516
146	1.07			1489	1489
142	1.16			1526	1526, 3693

* Data not available.

** Pressure data given for runs in bottom half of table are for the PCB gauge located at 305 mm.

† Larger injector used for run cases from this point on.

‡ Multiple frequencies are listed when the energy contained is those frequencies is comparable.

HEAT FLUX

Concurrent measurements of wall heat flux are obtained as described in an earlier section. The locations of both heat flux gauges (designated as Gauge A and Gauge B) are given in Table 1. For each of the combustion runs, thermocouple data from both gauges is obtained and reduced to obtain the wall heat flux level during the firing period. In this copper heat-sink chamber, heat flux to the wall varies with time during the firing. Initially, the heating level is high owing to the lower wall temperatures. As wall temperature rises, the wall heat flux decreases steadily during the firing. In most cases, the heat flux diminishes by a factor of two during the steady combustion period. Typical heat flux time-histories, from four combustion runs, for one of the heat flux gauges are shown in Figure 8.

The variation of heating with respect to O/F ratio and axial position within the chamber is determined by comparing time-average values of the transient heating profiles (cf. Figure 9). The results show that the highest heat fluxes are associated with the O/F ratio of 5 (nominal heating of 9.8 MW/m^2, or 6 Btu/in^2-s) with heating being insensitive to location in the chamber. Heating diminishes

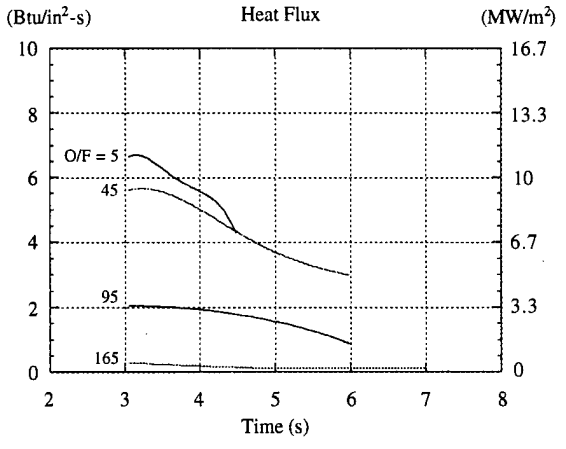

Figure 8. Typical time-history of heat flux for one of the gauges is shown for four combustion runs, each at a different O/F ratio. Gauge is located at x=25 mm for these runs.

for higher O/F ratios as may be expected since less fuel is available for combustion and less energy is released. This is seen in both the low and high pressure experiments. The heat flux levels at the O/F of 165 are lowest, ranging from 0.16 MW/m^2 to 0.65 MW/m^2 (0.1 to 0.4 Btu/in^2-s). The top graph in Figure 9 (low pressure study) includes one data point with the small injector at a higher pressure of 4.37 MPa, with gauges located at x=229 mm. No significant pressure effect is observed in this range.

This study reveals that the near-injector heating (x = 25 mm) at O/F of 50 and 100 is higher than at downstream positions. Local flame impingement/attachment to the wall is a likely explanation for this phenomenon. This trend is also borne out at the higher pressures. The photograph of Figure 5, which shows the injector flame rapidly expanding to the wall, supports this inference. It is possible to conclude from this that near-injector locations of a chamber experience larger heat fluxes owing to the spreading of the swirl coaxial flame.

The results for the O/F of 165 case (smaller injector) should be viewed as order-of-magnitude, however, because certain factors reduce the accuracy of this measurement. Initial heating due to the ignition torch is of the same order as the heating during the firing and preheats the chamber sidewalls non-uniformly to a temperature that is comparable to the adiabatic flame temperature of combustion temperature at O/F 165. In some firings, wall cooling occurs instead of heating. The heat gauge with the present thermocouples is not designed to work optimally at these low heat flux levels. More sensitive thermocouples might be able to resolve this problem. Finally, it is noted that heat transfer coefficient could not be estimated in this work since near-wall gas temperature measurements are not available.

A previous study of wall heat flux due to LOX/GH$_2$ swirl coaxial injectors was carried out by Petersen et al.[18] with a multi-element, cylindrical chamber operation at high pressures (11.8 to 16.3 MPa) and flowrates (~30 kg/s), and mixture ratios near 5.5. Wall heat fluxes of 40 MW/m^2 were observed for their baseline case, which is approximately four times the highest flux in the present study with the small injector. While a direct connection between the two studies is not immediately possible, further experiments using the present injector at higher pressures and element flowrates can be used to establish heat transfer scaling relationships. This is specifically recommended, particularly for the case of oxidizer-rich combustion where little heat transfer data is available.

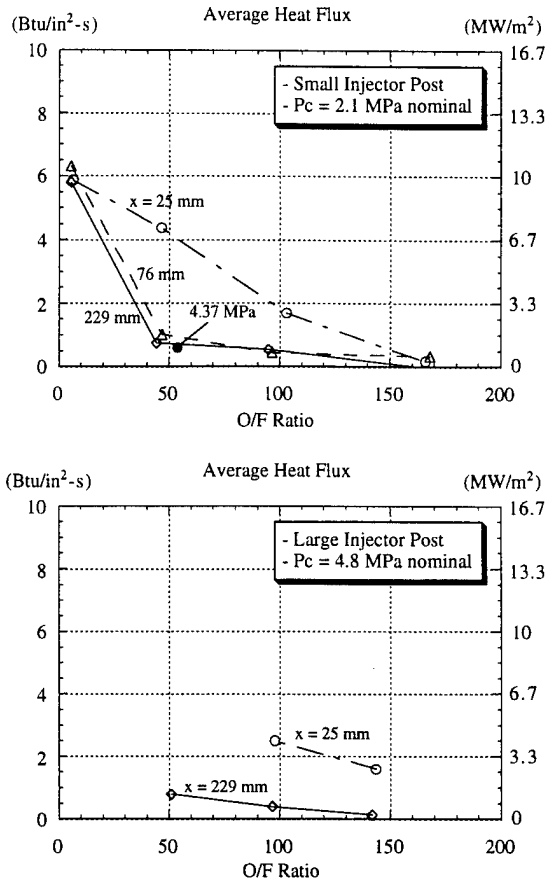

Figure 9. Results from the heat flux survey are summarized. Time-Averaged heat fluxes computed from the transient data are given for the entire matrix of combustion runs (both low and high pressure run conditions). Upper and lower graphs show measurements taken with the small injector and large injector respectively. Lower O/F ratio runs are avoided for the large injector to preclude damage to heat flux gauges.

CONCLUSIONS

The hot-fire results presented here demonstrate the viability of the present swirl coaxial injector for high mixture ratio rocket combustion. The present single-element studies at sub-critical and near-critical chamber pressures provide a characterization of this injector from the standpoints of performance, stability and heat transfer. In particular, the present injector provides for stable ignition, combustion, and flame holding over a wide range of oxidizer-to-fuel mixture ratio (by mass) from 5 to 170, and chamber pressures from 1.7 to 4.8 MPa (250 to 700 psia). Results from the combustion stability investigation demonstrate stable combustion with root-mean-square pressure fluctuations of 2% of chamber pressure or less, with weak acoustic coupling to longitudinal modes of the combustion chamber. Concurrent heat flux studies with this injector/chamber combination illustrate the thermal benefits of oxidizer-rich combustion conditions. An extension of the current work to higher chamber

pressures, flowrates, and multi-element injector configurations, is recommended in order to obtain scaling data for the design of a full-scale liquid oxygen preburner. There are currently plans to extend the chamber pressure range of the present work in a research facility being developed at the NASA Marshall Space Flight Center.

ACKNOWLEDGMENTS

Funding for this project is provided by NASA Marshall Space Flight Center under Grant No. NCC8-46, "Tripropellant Combustion and Oxygen-Rich Rocket Combustor Technologies." The development of one of the swirl coaxial injectors was funded by Dr. Mitat Birkan of the Air Force Office of Scientific Research, Air Force Systems Command, USAF, under grant number F49620-93-1-0365. M. Foust is acknowledged for contributions to the injector design, and H. Ryan III is acknowledged for developing the large injector. The authors also wish to thank L. Schaaf, M. Moser, and D. Escher (Penn State Propulsion Engineering Research Center) for their important contributions in conducting the hot-fire experiments.

References

[1]Knuth, W. K., and Crawford, R. C., "Oxygen-Rich Combustion Process Applications and Benefits," AIAA Paper 91-2042, AIAA/SAE/ASME 27th Joint Propulsion Conference, Sacramento, CA., June 24-26, 1991.

[2]Bailey, C. R., "A Preliminary Investigation of Oxidizer-Rich Hydrogen-Oxygen Combustion Characteristics," NASA TN D-3729, NASA Marshall Space Flight Center, December 1966.

[3]Farhangi, S., Hunt, K., Tuegel, L., Matthews, D., and Fisher, S., "Oxidizer-Rich Preburner for Advanced Rocket Engine Application," AIAA Paper 94-3260, AIAA/SAE/ASME/ASEE 30th Joint Propulsion Conference & Exhibit, Indianapolis, IN., June 27-29, 1994.

[4]Rahman, S. A., Pal, S., and Santoro, R. J., "Swirl Coaxial Atomization: Cold-Flow and Hot-Fire Experiments," AIAA Paper 95-0381, 33rd Aerospace Sciences Meeting and Exhibit, Reno, NV., January 9-12, 1995.

[5]Andreyev, A. V., Chepkin, V., and Fanciullo, T. J., "Investigation of Oxygen/Hydrogen Combustion Stability in Staged Combustion Liquid Rocket Engines," AIAA/SAE/ASME/ASEE 30th Joint Propulsion Conference, Indianapolis, IN., June 28-30, 1994.

[6]Atherton, R. R., "Air Force Reusable Rocket Engine Program - Final Report," AFRPL-TR-71-1 Vol. 1 (Air Force Contract F04611-68-C-0002), Pratt & Whitney Aircraft, Division of United Aircraft Corp., January 1971.

[7]Hulka, J., Schneider, J. A., and Davis, J., "Single Element Injector Testing for STME Injector Technology," AIAA/SAE/ASME/ASEE 28th Joint Propulsion Conference and Exhibit, Nashville, TN., July 6-8, 1992.

[8]Hautman, D. J., "Spray Characterization of Liquid/Gas and Liquid/Liquid Coaxial Injectors with the Center Liquid Swirled," Report No. UTRC89-31, United Technologies Research Center, East Hartford, CT., June 1990.

[9]Doumas, M., and Laster, R., "Liquid-Film Properties for Centrifugal Spray Nozzles," *Chemical Engineering Progress*, Vol. 49, No. 10, October 1953, pp. 518-526.

[10]Yule, A. J., and Chinn, J. J., "Swirl Atomizer Flow: Classical Inviscid Theory Revisited," International Conference on Liquid Atomization and Spray Systems (ICLASS-94), Rouen, France, July 1994.

[11]Private communications with: G. Cox and J. Clark of Pratt & Whitney Space and Government Engine Division, Florida.

[12] Moser, M. D., "Flowfield Characterization in a Uni-Element Rocket Chamber," PhD. Thesis in Mechanical Engineering, The Pennsylvania State University, May 1995.

[13] Pal, S., Moser, M. D., Ryan, H. M., Foust M. J., and Santoro, R. J., "Flowfield Characteristics in a Liquid Propellant Rocket," AIAA Paper 93-1882, AIAA/SAE/ASME/ASEE 29th Joint Propulsion Conference & Exhibit, Monterey, CA., June 28-30, 1993.

[14] Oppenheim, A. V., and Schafer, R. W., *Discrete-Time Signal Processing*, Prentice-Hall, NJ., 1989.

[15] Press, W. H., Teukolsky, S. A., Vetterling, W. T., and Flannery, B. P., *Numerical Recipes in Fortran: The Art of Scientific Computing*, Cambridge University Press, 1992.

[16] Liebert, C. H., "Measurement of Local High-Level Transient Surface Heat Flux," NASA Technical Paper 2840, 1988.

[17] Hulka, J., Schneider, J. A., and Dexter, C. E., "Performance and Stability of a Booster Class LOX/GH_2 Swirl Coaxial Element Injector," AIAA Paper 91-1877, AIAA/SAE/ASME 27th Joint Propulsion Conference, Sacramento, CA., June 24-26, 1991.

[18] Petersen, E. L., Rozelle, R., and Borgel, P. J., "Characterization and Wall Compatibility Testing of a 40K Pound Thrust Class Swirl-Coaxial Injector and Calorimeter Combustion Chamber," AIAA Paper No. 91-1873, 27th Joint Propulsion Conference, Sacramento, CA, June 24-26, 1991.

Attachment D

Similitude in pressure-swirl atomizer sprays

by

S. A. Rahman, S. Pal, and R. J. Santoro

Physics of Fluids
(manuscript in submission, August 1996)

Similitude in pressure-swirl atomizer sprays

S. A. Rahman, S. Pal, and R. J. Santoro

The Pennsylvania State University, University Park, Pennsylvania 16802

Two prefilming swirl atomizers, hydrodynamically similar in design but different in size, are used to investigate fluid dynamic similarity in pressure-swirl sprays. It is observed in water flow experiments that non-dimensionalized drop size and drop velocity fields resulting from the two atomizers are equivalent when flow conditions are chosen to match the injection Weber number. Injection film thickness and film velocity are identified as the relevant size and velocity scales controlling atomization. It is further observed that the fluid dynamic similarity between the sprays extends to drop distribution functions, diameter/velocity correlations, and velocity-rms. at every point locally within the spray where measurements were made. Freeze-motion images of the sprays support the findings by showing similarity in sheet breakup and atomization mechanisms for the two sprays.

I. INTRODUCTION

A pressure-swirl atomizer, also known as a simplex atomizer or centrifugal nozzle, is a liquid injection device used to produce a finely atomized, hollow-cone spray. Despite a large variety of atomizer designs and applications, all such atomizers operate by converting the pressure head of the flow into a swirling liquid film within the injector. The film subsequently emerges from the atomizer nozzle as a hollow-cone sheet, and then self-disintegrates into ligaments and drops (see FIG 1). Many aspects of this spray have been studied,[1] yet our fundamental understanding of swirl-induced atomization phenomena is far from complete. Basic knowledge on how injection conditions translate into drop size and drop velocity fields is still lacking, and much research needs to be done to elucidate the factors affecting sheet and ligament breakup into drops before a general predictive capability can be developed.

Studies of pressure-swirl sprays are generally divided into two areas: those that deal with the internal flow within the atomizer, and those that investigate atomization performance. The first area, internal flow, is amenable to analysis. A number of studies have focused on developing the detailed hydrodynamics relationships between atomizer geometry, discharge coefficients, spray cone angles, and exit conditions.[2,3,4,5] Algebraic equations have been derived to describe the Bernoulli relationship between pressure head and the swirl and axial velocity components of the vortex flow within the atomizer, under an inviscid flow assumption. Agreement with measurements is excellent, and hence atomizer internal flowfields for many geometries can be predicted *a priori* with confidence. This is useful for design purposes. The predictability of hydrodynamic performance has contributed to the wide use of pressure-swirl atomizers in industrial applications, as well as spurred more interest for research into atomization characteristics.

Studies on pressure-swirl atomization are abundant. However, unlike the previous case, most of the work is experimental. Generally, researchers examine characteristic drop size of a spray for different geometries and fluids of interest, where the information distilled from the work is ultimately summarized in empirical formulae.[6,7,8] Recent studies focus on obtaining detailed local information about the spray flowfield,[9,10,11] employing modern spatially-resolved sizing/velocimetry techniques, but this is only possible at the expense of few parameter variations. A few investigators have sought to model pressure-swirl atomization. One approach involves modeling the wave-like growth of disturbances on the conical liquid sheet and the ensuing sheet breakup (York et al.[12]), while another employs a control volume formulation utilizing the global conservation equations (Li and Tankin[13]). For the present, however, the analytical problem appears intractable so that the empiricisms are still the only guidelines

available for estimating atomization characteristics. Empiricisms offer some capability to estimate atomization, but there are limitations: (1) they cannot be relied upon to extrapolate beyond the boundaries (flow regimes) of the source experiments, (2) the correlation formulae are designed to give one overall characteristic drop size for a polydisperse spray, and hence do not give local information about drop size or drop velocity, (3) they offer little fundamental understanding about the phenomenology of the pressure-swirl spray.

In order to progress beyond the engineering pragmatism of correlations, the present study re-examines the fundamental breakup process of the pressure-swirl spray to deduce its basic phenomenology, and determine how the drop sizes and velocities are influenced by injection conditions. This is done by applying the current, spatially-resolved technique of choice for sprays (phase/Doppler interferometry), combined with careful experimental design, and complemented by flow visualization. Progress is made in identifying fundamental size and velocity scales for the spray flowfield in water flow experiments. This leads to conclusions on similitude of drop size and velocity statistics for such sprays at the conditions of the present experiments.

II. SIMILARITY HYPOTHESIS

Dimensional analysis[3] suggests that nine physical variables in this atomization problem can be recast into six dimensionless parameters to describe the flowfield:

$$\overline{D}/d = g\left(\rho_l/\rho_g,\ \mu_l/\mu_g,\ We_d,\ Re_d,\ \theta\right) \tag{1}$$

The globally-averaged spray drop size $\overline{D}$, non-dimensionalized by injector diameter d, thus depends upon the liquid-to-gas density ratio (ρ_l/ρ_g), viscosity ratio (μ_l/μ_g), Weber number ($We_d = \rho_l U_l^2 d/\sigma$), Reynolds number ($Re_d = \rho_l U_l d/\mu_l$), and swirl strength in terms of spray cone angle θ. The parameters on the right-hand-side refer to the injection conditions, except for ρ_g and μ_g which are properties of the ambient gas. Borodin et al.[2] put forth an equivalent relationship where the normalizing length scale in the drop size parameter $\overline{D}/\delta$ is the injection film thickness δ instead. They also conjecture that sheet breakup, defined by a breakup length parameter L_b/δ, is described by a relationship analogous to Eq. 1. Taking their viewpoint, one can modify Eq. 1 so that the functional model for pressure-swirl sprays incorporates the injection film thickness δ, and film injection velocity U_l, into the Weber and Reynolds parameters ($We_\delta = \rho_l U_l^2 \delta/\sigma$ and $Re_\delta = \rho_l U_l \delta/\mu_l$) so that we may write:

$$L_b/\delta = f\left(\rho_l/\rho_g, \mu_l/\mu_g, We_\delta, Re_\delta, \theta\right) \tag{2a}$$

$$\overline{D}/\delta = g\left(\rho_l/\rho_g, \mu_l/\mu_g, We_\delta, Re_\delta, \theta\right) \tag{2b}$$

Here, the improvement is that sheet breakup and atomization are tied to the physical process of liquid film injection at the atomizer exit. Even so, the functional model of Eq. 2 is deficient because it simplifies a polydisperse spray into a single characteristic drop-size $\overline{D}$, and hence does not describe how size (or velocity) statistics evolve spatially. From both a research standpoint, and a practical standpoint, it is necessary to know how the entire particle flowfield varies with injection parameters, particularly the Weber number. To date, studies have not delved into this area.

In order to address the spatially-varying nature of the flowfield, we propose to describe the spray instead in terms of the field variable $\overline{D}/\delta(z/\delta, r/\delta)$, which represents a local temporal average of a histogram of sizes sampled at a point $(z/\delta, r/\delta)$ in the spray, as opposed to the previous global average $\overline{D}$. Next, this variable $\overline{D}/\delta(z/\delta, r/\delta)$ may be substituted for the left-hand-side of Eq. 2b to extend the functional description of the spray. The substitution propounds a more comprehensive hypothesis and puts further importance upon the role of the film thickness δ. It implies that local information (drop size and velocity) from one spray flowfield can be scaled by δ, and also mapped by δ, to a corresponding location in the spray flowfield from a different size injector. In a complementary hypothesis, we propose that the drop velocity field should also be thought of as a dependent variable of the flowfield, but governed by a different scale, the injection velocity U_l. By defining the drop velocity vector $\bar{V}/U_l(z/\delta, r/\delta)$ to represent the cartesian component averages $\overline{u}/U_l, \overline{v}/U_l, \overline{w}/U_l$ for a sample of drops, we introduce an analogous relationship for average drop velocity to give the following equation set:

$$\frac{L_b}{\delta} = f\left(\frac{\rho_l}{\rho_g}, \frac{\mu_l}{\mu_g}, We_\delta, Re_\delta, \theta\right) \tag{3a}$$

$$\frac{\overline{D}}{\delta}\left(\frac{z}{\delta}, \frac{r}{\delta}\right) = g\left(\frac{\rho_l}{\rho_g}, \frac{\mu_l}{\mu_g}, We_\delta, Re_\delta, \theta\right) \tag{3b}$$

$$\frac{\bar{V}}{U_l}\left(\frac{z}{\delta}, \frac{r}{\delta}\right) = h\left(\frac{\rho_l}{\rho_g}, \frac{\mu_l}{\mu_g}, We_\delta, Re_\delta, \theta\right) \tag{3c}$$

The new functional model describes a spray in terms of a location L_b/δ where the hollow-cone sheet loses its contiguity, and subsequently transforms into a spatially-varying distribution of drops of characteristic size $\overline{D}/\delta(z/\delta, r/\delta)$, traveling at the average velocities given by a vector field $\vec{V}/U_l(z/\delta, r/\delta)$.

Owing to the advent of spatially-resolved drop sizing/velocimetry techniques, this hypothesis set may be tested by experiment. However, in order to begin, we confine our study to a specific case where an atomizer design is chosen (fixed swirl strength θ), and the fluids are given (e.g. water spray in air) — a study covering all variables would be a formidable task. From Eq. 3, the spray flowfield now varies only with Weber and Reynolds numbers according to the functional relationship $\overline{D}/\delta(z/\delta, r/\delta) = g(We_\delta, Re_\delta)$. We assume first that the effect of Reynolds number is not substantial, and focus instead on the Weber number as the key parameter governing atomization. The only physical variables which may be manipulated in an experiment to study this simpler relationship are the injection film thickness δ, and film injection velocity U_l. The first is varied by scaling the atomizer, while the second is varied by varying the flowrate of liquid through the atomizer. According to internal flow theory, both δ and U_l are independent of one another. Hence, it is possible to achieve the same Weber number with different combinations of the two. This is the approach taken here. In the present study, we employ two atomizers of different sizes with corresponding film thicknesses δ_1 and δ_2, and operate them at the required flowrates to achieve injection velocities U_{l_1} and U_{l_2} such that the Weber number is maintained. Thus, $We_{\delta_1} = We_{\delta_2} = \rho_l U_{l_1}^2 \delta_1/\sigma = \rho_l U_{l_2}^2 \delta_2/\sigma$. For instance, here we choose $\delta_2 = 2\delta_1$ and $U_{l_2} = U_{l_1}^{0.5}$ in order to equate the film injection Weber number. According to Eq. 3, this should result in equivalent values of the normalized spray parameters L_b/δ, $\overline{D}/\delta$, $\vec{V}/U_l$, from the two sprays for all equivalent positions $(z/\delta, r/\delta)$. We conduct flow visualization to examine the breakup phenomena, and perform spatially-resolved drop measurements in order to assess similarity of the field variables between flowfields. Based upon the results presented in this paper, we argue in favor of the underlying assumption that δ and U_l are the important scales describing the two flowfields.

III. EXPERIMENT

A. Atomizer Design

The geometry of the atomizers is illustrated in FIG. 2 where dimensions are given for the smaller unit. Swirl is imparted by means of three tangential-entry slots. Diameters and lengths of the flow passages are twice as big for

the large unit as compared to the smaller one. Despite the physical differences, the two atomizers are designed to be identical in terms of their hydrodynamic characteristics. Both atomizers deliver liquid at the same discharge coefficient C_d, feature the same spray cone angle θ, and result in equivalent values of the normalized injection film thickness δ/d. It is important to note that fluid dynamic similarity of the internal flow within the atomizers is a prerequisite for similarity in atomization characteristics. Thus, care is taken to ensure that the internal flowfields of the two atomizers are similar. Film thickness, discharge coefficient, and swirl cone angle are estimated from inviscid flow theory as presented by Yule and Chinn.[5] The values of C_d and θ are verified by experiment. While alternate and more widely-used descriptions of the theory are available,[1] Yule and Chinn[5] appear to be the first to give analytical closure to the atomizer design equations, while employing a completely general formulation. Their analysis yields the following parameters governing the prefilming process:

$$C_d = f(K, N) \tag{4}$$

$$\theta = g(K)$$

$$\delta/d = h(K, N)$$

where both K and N are dimensionless parameters describing the atomizer geometry. Similarities between the two injectors in terms of the variables C_d, θ, δ/d, stem from the fact that both units have the same atomizer constant K, and the same ratio of swirl-chamber diameter to exit-orifice diameter N. Unlike most pressure-swirl atomizers, however, the present design features a long exit-orifice tube, typical of rocket-injector applications. The effect of the tube is discussed later, but it is noted here that the L/d of the exit-orifices are also chosen to be identical so as to maintain similarity of internal flow in the exit-orifice tube as well. The effect of tube L/d is not yet incorporated into the internal flow theory, but to the extent that inviscid theory applies, the internal flowfields of the two atomizers should be similar. Therefore, our experiments focus strictly upon the effect of the difference in scale on the spray results.

B. Diagnostic Apparatus

Spray breakup characteristics for both atomizers are visualized using an imaging system, and drop measurements are made with a commercially available phase/Doppler interferometry instrument. Schematics of both are given in FIG 3. The visualization technique "freezes" the motion through the use of stroboscopic illumination of the spray (3 μs flash duration). A single image is acquired by a solid-state camera (CIDTEK Model 2250) employing 8-bit digitization of the light intensity corresponding to allow 256 levels of gray-scale.

Adequate resolution and contrast is achieved by imaging with a standard 50 mm lens onto a 512 $\times$ 480 pixel array detector in the camera. The near-injector region of the spray is visualized to capture the sheet and ligament breakup processes. Visualization of some of the larger drops is possible as well. The sprays are pointed both sideways and downwards in the imaging experiments. At the conditions of this study, gravity effects are found to be insignificant.

Spatially-resolved drop-sizing and velocimetry is performed using an Aerometrics phase/Doppler particle analyzer (PDPA). The instrument is operated in the manner of conventional laser-Doppler velocimeters, as a point measurement technique, with supplemental capabilities for drop-sizing. In its inception, this technique was described by Bachalo and Houser.[14] More recently, a good discussion of its operating principles is given by Wigley.[15] It's primary advantage over the widely-used line-of-sight technique[16,17] is the ability to measure velocity and size simultaneously within a spray to high spatial resolution. In the present work, a standard configuration of the PDPA is employed where refracted light from drops passing through a small probe volume is detected independently by three photo-multiplier tubes and subsequently analyzed to obtain the drop size and two components of its velocity simultaneously. The probe volume is formed at the intersection of two pairs of focused laser beams. In this set-up, scattering from the first pair at 514.5 nm is analyzed to determine the drop size and axial velocity component, while scattering from the second pair at 488 nm yields the radial velocity component. The detector system is focused onto a 600 μm $\times$ 100 μm slit at the center of the four intersecting beams, and oriented to receive 30° off-axis, forward-scattered light only from the slit. The water spray is pointed downward and traversed in order to interrogate multiple radial positions within the spray cone. Measurements are made for both atomizers by beginning at the spray centerline, and stepping radially to the outer periphery of the spray until the data rate becomes negligible. Further details of the implementation are provided in Table 1.

Table 1. Implementation details of the phase/Doppler technique

Transmitting Optics	
Light source	Argon-ion laser in multi-line mode
Wavelengths	514.5 nm green, 488 nm blue
Beam Power	30-35 mW beams
Focusing Lens f.l.	1000 mm
Beam crossing angle	0.57°
Probe Area	0.0148 cm^2
Detection Optics	
Light-scattering	30° refracted
Refractive Index (water)	1.33
Collimating Lens f.l.	500 mm
Focusing Lens f.l.	238 mm
Phase/Doppler options	
Sizing Range	39 to 1350 μm
Velocity Range	0 to 40 m/s
Sample Size	~15000 drops per position
Voltage to Photo-Multiplier Tube	350 Volts
Other Features	Intensity Validation of Drop Signals

Before presenting results, we note several issues regarding the application of the phase/Doppler sizing technique in a polydisperse spray. The following should be considered when obtaining results, and interpreting findings, from a spray experiment where a wide range of drop sizes is possible.

(1) First, the standard PDPA operates as a single-particle technique and presumes the presence of a single spherical scatterer in the measurement volume. Therefore, it must be employed downstream of the breakup zone in a dilute region of the spray such that the probability of multiple-drop scattering is low, [18] and where drops have had sufficient time to acquire a stable spherical shape. Here, we make use of flow visualization results to guide the choice of a suitable axial position. In addition, the acquired data are analyzed post-test to verify a low duty-cycle, i.e., particle crossing times are small relative to interparticle arrival times.

(2) Second, the PDPA measures the local radius of curvature in the plane of the intersecting beams (514.5 nm) to yield drop size information. For large drops, which may be deformed into spheroidal shapes by aerodynamic forces, the sizing results may not be perfectly representative of the drop as a whole. The sphericity constraint is not usually satisfied in polydisperse spray experiments where velocity gradients exist. Following Bachalo and Sankar,[19] we utilize an empirical expression to estimate possible deviations from sphericity for the largest drops in our experiments and present our conclusions in conjunction with the results. A related issue regarding the use of this technique in dense flowfields is that of secondary atomization. For the largest drops, the aerodynamic forces and/or collisions may result in fragmentation into smaller drops. Studies[3,20] have shown that this occurs at drop Weber numbers of 10 or higher ($We_{drop} = \rho_a U_d^2 D_d / \sigma$, for a liquid drop of diameter D_d moving at relative velocity U_d in an ambient gas with density ρ_a). In this work $We_{drop} < 3$, and the spray is expanding conically, thus aerodynamic breakup and collisions are not expected.

(3) Third, for a given instrument configuration, the sizing range of the PDPA is limited at the higher and lower extremes of a 35:1 dynamic range for sizing. Hence, the instrument effectively measures a truncated version of the "true" drop-size distribution, which is thought to extend from infinitesimal drop-sizes up to some (indeterminable) upper size limit. The sizing range, achieved through optical configuration, must therefore be chosen in a manner that fits the objectives of the experiment. We optimize the sizing range to get the best possible representation of the drop volume distribution in an effort to maximize the volume flux of the spray that is sampled by the PDPA. For our atomizers, this involved configuring to the maximum possible sizing range of the standard PDPA. In doing so, detection of the smallest drops is compromised in favor of sampling the largest ones.

(4) Fourth, the number of drops required to obtain a sufficiently representative sample of the drop distribution must be maximized, within the constraints of data storage and processing. In this work, 15000 drops are sampled at each location while obtaining a radial profile of measurements across the spray cone. Maximizing the number of samples per position improves the sample size for the mid-range, and large drop size bins, and helps to resolve the "tail" of

the drop distribution. As will be shown later, the mid-range and large drops, which are numerically a minor percentage of the total, contain a majority of the volume flux of the spray.

(5) Fifth, the phase/Doppler data acquisition system does not discriminate between refraction-scattering and reflection-scattering from the probe volume. While refraction-scattering at 30° off-axis is typically dominant over other scattering modes, the scattering intensity of first-reflection is comparable in magnitude for certain drop-sizes and drop trajectories glancing the edges of the probe volume. This leads to a small but significant percentage of erroneous drop size measurements creeping into the size histograms. Since it is important to correctly resolve the "tail" of the size distribution (large end of drop-size range), special effort is required to minimize the number of erroneous signals to an extent that it does not skew the statistics. According to Bachalo and Sankar,[19,21] these errors are largely removed by their intensity-checking algorithm. Since scattering intensity is proportional to the square of the particle diameter, by Mie theory, a size measurement is only accepted when the detected intensity is above a minimal threshold for that size bin, i.e., large drops cannot have low scattering intensity, and vice versa. User judgment is still required, however, to select thresholds for signal acceptance. We employ the following protocol to arrive at suitable thresholding criteria. Glass beads of three sizes (nominally 210 μm, 500 μm, and 840 μm) were sampled at the measurement volume to examine the light-scattering intensities for the particular laser and instrument configuration described in Table 1. Signal processing was performed with and without the intensity-checking algorithm for the glass beads. The intensity thresholds were then set to eliminate the erroneous signals without rejecting valid realizations. A final check is performed with a pump-spray bottle (generating a polydisperse spray up to 300 μm) to ensure that the intensity thresholds are appropriate for water as well as the silica beads.

In summary, this discussion addresses the challenge of maximizing the signal-to-noise ratio in making spray measurements. Here, "noise" is viewed as anything that detracts from the accuracy of the drop measurements — multiple-drop scattering, non-sphericity, relection-scattering, sample-size limitations, etc.. The degree to which these issues affect the conclusions of this study will be with dealt with in the results section.

IV. RESULTS AND DISCUSSION

A. Flow Visualization

Phenomenology of Pressure-Swirl Atomization

The essential features of pressure-swirl atomization are revealed in images obtained by the technique described in the previous section (see FIG. 4). Initially, a swirling liquid film of thickness δ emerges axially from the atomizer exit-orifice and turns away from the centerline owing to the azimuthal component of velocity. Small-scale structure is visible on the film, however, larger-scale structure quickly dominates the film as it expands into a the swirling hollow cone sheet. Downstream from the exit-orifice the sheet begins to "tear" and lose its contiguity. As the "tear" propagates completely around the azimuth, the conical sheet becomes a series of circular ligaments or distorted ligament-like structures. Ligaments disintegrate into drops which are on the scale of the ligaments widths. Drops of various sizes, smaller and larger, are produced by other processes as well. For instance, shear between the phases is responsible for the production of small droplets, while highly distorted ligaments yield many of the larger drops and globules. Further breakup of the larger drops into smaller ones can occur due to aerodynamic forces deforming the liquid spheres and also from collisions. The process described for this particular atomizer is identical to other observations.[22] In spite of the long L/d of the atomizer exit-orifice, the underlying mechanisms leading to atomization are equivalent to those for standard pressure-swirl atomizers.

The mechanism of atomization is shown in FIG. 4a-c for increasing values of Weber number, reproduced from Rahman et al..[23] In this case, higher We_δ is achieved by increasing the flowrate. A 51 mm region downstream of the injector exit is visualized. In normalized terms, the sprays are imaged up to the location z/δ = 150, or 15 exit-orifice diameters. At We_δ of 1060, a wavy and contiguous hollow-cone sheet is observed with breakup occurring downstream of the field of view. For a higher Weber number of 4250, the disintegration of the sheet into ligaments is visualized in the image, but the ligaments break up further downstream. At the highest Weber number of 9500, pictured in FIG. 4c, both sheet and ligament disintegration takes place within the 51 mm field of view of the image. Thus, increasing Weber number tends to accelerate the breakup process as surface tension forces give way to the aerodynamic and inertia forces disrupting the sheet. For increasing Weber number spray breakup and atomization occur earlier in terms of z/δ, and also occur earlier in time since a fluid parcel undergoes transformation from sheet to drop more rapidly for greater injection velocities. Spray cone angle, the total angle subtended by the diverging

sheet, is invariant with respect to Weber number in our experiments. This is consistent with the inviscid theory, which dictates that this angle depends only on the atomizer geometry, and not on the injection velocity or flowrate — a well-known feature of pressure-swirl sprays. At much lower Weber numbers (not shown), when the swirl momentum is insufficient for prefilming within the atomizer, the theory does not apply and experiments will show cone angle variations.

The effect of length-to-diameter ratio, L/d, of the exit-orifice is significant. The present atomizer, patterned after rocket-injector designs, features an exit-orifice L/d of 20. For more typical applications, exit-orifice L/d is less than 2. Wall friction effects for large L/d orifices will retard both components of film velocity, axial and azimuthal. Our experiments show that the spray cone angle diminishes with increasing L/d, suggesting that the azimuthal component is affected more than the axial (see FIG. 5). This has also been reported by Dombrowski and Hasson,[24] however, their experiments were limited to L/d up to 5. From the continuity relation applied across the exit-orifuce tube, we may deduce that a decrease in velocity is associated with an increase in film thickness. This is verified experimentally and analytically by Hutt et al.[25] employing a transparent Plexiglas atomizer of a similar rocket-type design. The phenomenology for long exit-orifice tubes is important for several reasons: (1) a reduction in spray cone angle with L/d implies a reduction in the spatial distribution of the spray, i.e. reduced "coverage," (2) the associated reduction in film velocity directly results in lower film injection velocity, and therefore lower drop velocity, and, (3) the increased film thickness at the injector exit manifests itself in larger drop sizes. This overview of the salient features of swirl atomization as evidenced with the atomizers applies to the range of conditions of this study and serves as the basis for interpreting the visualizations to be presented. Subsequent discussions now focus on atomizers with an L/d of 20, operating at flowrates corresponding to a fixed Weber number ($We_\delta = 4250$, unless noted otherwise).

Observations of Fluid Dynamic Similarity

Two pressure-swirl atomizers, different only in size by a factor of two, are compared in a series of visualizations at equivalent Weber number. From the internal flow theory, the liquid film is estimated to be twice as thick for the large atomizer. The large unit delivers four times more flowrate for the same supply pressure. In order to operate both atomizers flowing water at the same injection Weber number, the size difference is compensated by adjusting the injection velocity. The required flowrates are given in Table 2. The sprays are compared in FIG. 6. The first 51 mm downstream of the atomizer exit are imaged in the case of the small unit, and up to 100 mm

downstream of the exit for the large unit. In both cases, this corresponds to the region $z/\delta = 0-150$. When viewed in physical coordinates (z,r), the difference in scale is evidenced by the size of the sheet and ligament structures. However, if viewed in scaled coordinates $(z/\delta, r/\delta)$, the two sprays appear equivalent. In particlar, we note that breakup of the conical sheet occurs at the same dimensionless position for both, approximately $L_b/\delta = 110$ at an injection Weber number of 4250.

Table 2. Comparison of Atomizers and Flow Conditions

	Small	**Large**
δ	340 μm	680 μm
d	3.43 mm	6.9 mm
U_l	30 m/s	21 m/s
$\dot{m}_{H_2O}$	0.09 kg/s	0.26 kg/s
C_d	0.32	0.32
L/d	20	20
We_δ	4250	4250
θ	52°	52°

We find a correspondence in phenomenology of the two spray flowfields in downstream visualizations as well. When viewing corresponding positions in terms of scaled coordinates in FIG. 7, $z/\delta = 75-225$ and $z/\delta = 150-300$, we note that ligamentation and drop formation occur at approximately the same locations, and in the same manner for both atomizers. In both cases sheet breakup is followed by ligamentation, and then by disintegration of ligaments into rows of mostly spherical drops. Interestingly, the larger drops are visualized as well, and an upper size limit may be estimated from the images.

We compare the two atomizer sprays at different injection Weber numbers in FIG. 8. They are shown at Weber numbers of 1060 and 4250, where the images now cover a greater field-of-view of $z/\delta = 0-300$. Again, the Weber number is altered by varying the flowrates. Here we note two important points. First, as might be expected, we find that breakup characteristics are affected by the Weber number which reflects the balance of inertia and surface tension forces acting upon the hollow-cone sheet. Second, and more important, we observe equivalent

values of breakup length L_b/δ at a given Weber number for the two atomizer sprays. That is, in spite of the differences in atomizer scale and flowrate, the conical sheet disintegrates at approximately the same downstream position in terms of L_b/δ. This supports the hypothesis of Eq. 3a that the relative amounts of surface tension and inertia forces control sheet breakup through the Weber number, the result of which is measurable via the breakup length parameter L_b/δ. Overall, the sprays look visually similar at equivalent Weber numbers, either 1060 or 4250, even though the size of the atomizers, pressure drops, flowrates, and injection velocities are quite different for the two cases. The authors believe that this is the first presentation of similarity in hollow-cone sheet structure and breakup phenomena for pressure-swirl atomizer sprays. It is also important to mention that analogous conclusions were reached in a recent investigation of impinging jet injectors,[26] which in fact served to motivate the present study.

The remarkable correspondence in the visualizations of the two sprays alludes to a deterministic mechanism for pressure-swirl atomization for the present designs. Quantitative measurements of drop-size and velocity are made to see the extent to which this determinism is manifested in the atomization flowfield.

B. Drop-sizing and velocimetry

Complementary to the flow visualization findings, we now present a series of figures to illustrate similitude in measured drop-size and velocity statistics at $We_\delta = 4250$. As seen in FIG. 8, breakup of the ligaments into drops is complete at the downstream position of $z/\delta = 300$, therefore, this axial station was suitable for conducting drop measurements. Specifically, the location z/δ of 300 corresponds to a distance of 102 mm and 204 mm downstream of the atomizer exit for the small and large units, respectively. The two sprays are interrogated at corresponding locations in terms of the normalized coordinates $(z/\delta, r/\delta)$ by traversing radially in equal increments along r/δ. Flow conditions, chosen to equate the Weber number, were previously summarized in Table 2. Recalling the hypothesis presented in Eq. 3b, we examine the following two cases:

Case 1: $\overline{D}_1/\delta_1\,(300, r/\delta_1)$ = fcn.(850, 55, 4250, 10^5, 52°); $\delta_1 = 340$ μm, $U_{l_1} = 30$ m/s (small atomizer)

Case 2: $\overline{D}_2/\delta_2\,(300, r/\delta_2)$ = fcn.(850, 55, 4250, 1.4 x 10^5, 52°); $\delta_2 = 680$ μm, $U_{l_2} = 21$ m/s (large atomizer)

The fluid properties have been evaluated for water and air. Since all parameters on the right-hand-side are equivalent for the two cases, except for Re_δ which cannot be matched simultaneously here with We_δ, we expect to find that $\overline{D}_1/\delta_1 = \overline{D}_2/\delta_2$ at all positions interrogated. Analogously, we expect the velocity fields to be equivalent as well, that is $\vec{V}_1/U_{l_1} = \vec{V}_2/U_{l_2}$.

Results of the experiments comparing the two cases are presented in Fig. 9. Variation of mean drop velocity $\bar{u}(r)$ and $\bar{v}(r)$, Sauter mean diameter $D_{32}(r)$, and mass flux $\dot{m}''(r)$, with respect to radial position r is shown in both physical and normalized variables. Data points represent 15000 drop realizations each, except at the centerline and outer periphery where the spray is very dilute. For both atomizer sprays, size and velocity minima are at the centerline whereas the maximum values occur away from the spray axis. This is a distinguishing feature of pressure-swirl spray flowfields.[3] As indicated earlier, size and velocity measurements are normalized using theoretical estimates of film thickness δ, and liquid injection velocity U_l. Although actual values may be somewhat different, due to exit-orifice *L/d* effects, it is convenient to use the theory estimates as reference points. Flux is normalized by an "average" mass-flux, obtained by dividing the total atomizer flowrate by a circular cross-sectional area of radius $r/\delta = 300$. After normalization, we find that drop size, velocity, and mass flux profiles from the two atomizers are indeed similar in both trend and magnitude as expected. In particular, the velocity results exhibit good correspondence between the two sprays for the entire traverse. Drop size results show good trendwise correspondence, but a difference in the size parameter D_{32}/δ is observed for r/δ greater than 100. The disparity is believed to be artificial, arising in large part from sizing range limitations of the standard PDPA. The instrument does not measure drop diameters larger than 1350 μm, therefore an upper-end truncation of the drop distribution occurs for the large atomizer spray leading to lower than actual values of D_{32}. Flow visualizations of the large atomizer spray show the existence of drops which are larger than the upper limit for sizing.

The profiles of mass flux indicate that the spray distribution is equivalent for the two atomizers as well. Mass flux is a derived quantity based upon the size and velocity data, and estimates of the size of the measurement volume. We find that the bulk of the spray is distributed in a gaussian manner around the radial position r/δ of 140. Interestingly, this is also the location of size and velocity are maxima. The location is consistent with the divergence angle of the spray cone. We might expect that the mass flux to peak at a radius where the spray cone intersects the measurement plane. In this case, we estimate the location according to $r/\delta = z/\delta \, tan(\theta/2)$ $= 300 \, tan \, 26^\circ = 146$, which compares well with the measured value of 140. Upon radial integration, assuming

axisymmetry of the spray, the flux profiles yield values of flowrate that compare favorably to the metered flowrate of water, that is, 75% of the actual flow through the small atomizer, and 92% of the actual flow through the large atomizer. This serves as a consistency check for the mass flow extimates. Approximations incorporated into the flux calculations, in vendor-supplied software, allow for this level of disagreement, particularly in cases such as this where relatively high flowrate and large drop sizes are involved.

We find that the similarity in spray characteristics is a manifestation of similarity in the local drop size distributions between the two sprays. The 15000 drop measurements at each point of interrogation are binned according to size to obtain drop number distributions and drop volume distributions. The latter are presented in FIG. 10 for multiple radial locations (r/δ = 0, 75, 108, 140, 174) spanning the radial extent of the spray flowfield. The representation of polydispersity in terms of volume is preferred here instead of the more common number distribution approach because it illustrates how volume (mass) of the spray is distributed over the size range. As before, the figures show results in physical variables as well as normalized variables. We define a volume distribution function $g(D)$ based upon the bin volume fraction V_i/V_{tot} by the equation $g(D) = (V_i/V_{tot})/\Delta D$, where V_i ($= (\pi/6) n_i D_i^3$) is the volume of n_i drops accumulated in bin i (bin width ΔD), and V_{tot} is the summation over all size bins. In this manner, the distribution is made independent of sample size and binning method, and also integrates to unity since $\int g(D)\, dD \equiv 1$. Once again, the injection film thickness is used to arrive at a normalized drop volume distribution $\hat{g}(D) = (V_i/V_{tot})/(\Delta D/\delta)$. This is also shown in the figure plotted versus the normalized size parameter D/δ, where the normalized distribution also integrates to unity. The distribution $g(D)$ is significantly different for the two sprays, and indicates the reasonable result that the larger atomizer produces appreciably larger drops. On the other hand, the normalized results in terms of $\hat{g}(D)$ show the volume distributions to be equivalent at each r/δ. The shape of the function $\hat{g}(D)$ varies with radial position in exactly the same manner for both atomizers and magnitudes are comparable as well. This suggests that the mechanisms forming the drops must be the same for both atomizers at the same Weber number. With the small atomizer, the largest drop diameters approach four times the film thickness. For the large atomizer, the distribution is truncated at D/δ of 2.1 owing to the size-range limit of the instrument. This is the basis of the argument made earlier that Sauter mean diameter for the large spray is underestimated at some locations. The tails of the volume distributions could probably be better characterized in a future study with larger sample sizes, say, 60000 to 100000 drops per radial position. The associated increase in populations of large D/δ bins would reduce the data scatter which is seen at the upper end of

the size range, and thus clarify the truncation effects. Comparing results from different radial locations, we find that the width of the distributions is maximum at r/δ of 140, which is the position corresponding to the spray cone angle and peak mass flux. At the centerline, the spray is comprised of smaller drops as compared to the other parts of the flowfield. The overall agreement in the normalized volume distributions is compelling evidence of atomization similitude based upon injection Weber number. The authors believe this to be the first presentation of such findings.

In addition to the above, we also examine the correlation of drop size with mean velocity of drops. Size-discriminated velocity means were generated from the size-binned data which was the source of the drop volume distributions. Both axial and radial components of the bin-averaged velocities are shown as a function of drop diameter in FIG. 11 for multiple radial locations. The physical results are once again normalized by injection parameters δ and U_l. Data from the two cases collapse reasonably well at all radial positions shown. Similar trends and magnitudes are noted for both components of local drop velocity. Some disparity exists in the scaled axial velocity at positions r/δ of 75 and 108. The reason for this is unknown at this time. However, a variation on the order of 15% here is not inconsistent with azimuthal asymmetry of the spray cone, or exit-orifice tube effects. The measurements generally show that smaller drops are moving slower on average than the larger ones which travel in a ballistic manner. It should be noted that the large majority of the 15000 drop samples consist of relatively smaller drops ($D < 300\ \mu m$), and that there is considerable variation about the means in the motion of these small drops. The rms values of measured drop velocity illustrate this feature of the atomization field for four radial positions in FIG. 12. For each component of velocity, the rms variation for the drops in a given size bin is shown relative to the mean value for the bin. Thus, the parameters $u'(D)/\bar{u}(D)$ and $v'(D)/\bar{v}(D)$ are given versus D/δ for both atomizer sprays. The variability is greater at the spray centerline and less at the periphery. The favorable agreement of the results from the two atomizer sprays suggest that variance is also a feature of the spray that may be scaled from one atomizer to another.

Another view of the drop velocity results is afforded by correlating the two components. Size-discriminated data from FIG. 11, the bin-averaged axial component $\bar{u}(D)$ and bin-averaged radial component $\bar{v}(D)$, are cross-plotted in FIG. 13. A strong correlation between axial and radial drop velocity is noted in both atomizer sprays. For reference, radial lines are drawn from the origin which denote a locus of velocity vectors corresponding to hypothetical particles traveling radially outward in a straight line from the atomizer exit. Note that these lines are in rough agreement with the binned data, therefore, it is likely that this is the situation in the measurements as well. The issue of drop sphericity can now also be addressed. An empirical expression[19] to estimate the ratio of maximum

to minimum diameter of a spheroidal drop D_{max}/D_{min} as a function of drop Weber number, is evaluated for the largest drops and the highest drop velocity of the sprays (D=1350 μm and $\left(\bar{u}^2(D)+\bar{v}^2(D)\right)^{1/2}$=14 m/s). Hence, we get $D_{max}/D_{min}=\left\{1+0.07\left(We_{drop}\right)^{1/2}\right\}^3$ = 1.50. The same ratio for a drop of 300 μm size is 1.22, while that for a slower moving drops at 7 m/s is 1.11. Clearly, there can be aerodynamic deformation of the drops into spheroids, although, not enough to cause secondary breakup. While this cannot be avoided in such an investigation, it must be mentioned in giving proper interpretation to the results.

The detailed drop velocity results offer further evidence in favor of the similitude hypotheses. In fact, the results compel us to extend the discussion of similitude to include local size and velocity distributions as well. While dimensional analysis guides us to look for similarity of a general drop-size parameter D/δ, it appears that all global and local features of the atomization flowfield exhibit similarity characteristics. This includes the drop distributions, diameter/velocity correlations, drop velocity fluctuations, as well as any statistical quantities derived from them. Such similitude may be exploited for predicting an atomizer's drop size and velocity field. Since atomization characteristics are normalized by injection film thickness and injection film velocity, they are also scaleable via these parameters so long as the liquid injection Weber number is maintained. If an initial mapping of the atomization flowfield of a particular atomizer design is available for Weber numbers of interest, drop size and velocity distributions and statistics may be computed for other atomizer sizes by simple scaling of available data. This is true provided that the flow regime of the atomizer's internal flowfield is one where the inviscid theory applies and film injection Reynolds number is in the turbulent range as in the present experiments. Further research should focus determining whether the quantitative scaling is applicable for a variety of fluids.

V. CONCLUSIONS

In the present study, the fundamental nature of pressure-swirl atomization is investigated by examining the role of liquid injection parameters, Weber number in particular, in determining the resulting atomization flowfield. Unlike previously reported studies of swirl atomization, all of our results and interpretations are offered in terms of a new definition of injection Weber number based upon liquid properties, and the length and velocity scales of the swirling liquid film within the atomizer, thus ensuring a link to the physical phenomenon which is at the core of the swirl atomization process. Initial work on visualization of the near-injector region finds that this Weber number

correlates sheet breakup phenomena from very different pressure-swirl sprays produced by two atomizers which are similar in design but different in size. This confirms expectations that the breakup occurs in accordance with the balance of forces due to liquid inertia and liquid surface tension in the Weber and Reynolds number range of the present experiments. Further detailed measurements of atomization parameters, spatially-resolved simultaneous drop size and two components of velocity, yield the remarkable finding that the presently defined Weber number correlates drop diameter and drop velocity statistics from the two atomizer flowfields at every corresponding point interrogated in the two sprays. Specifically, comprehensive atomization similitude is observed in the radial profiles of Sauter mean diameter, mean axial and radial components of drop velocity, and mass flux, as well as the locally obtained temporal drop volume distributions, diameter-velocity correlations, and velocity-rms, upon normalizing the spray results with the atomizer film thickness and velocity.

For the present, the conclusion of Weber-based similitude should be restricted to the case of a single fluid where the film injection occurs at turbulent Reynolds as in the present study, however, some visualization studies of an ethanol spray produced by one of the atomizers lead us to conclude that breakup phenomena at least may be correlated through the Weber number also for different fluids with surface tension properties within the range of water and ethanol which differ by a factor of three. From above results it appears that Reynolds number, based upon the same length and velocity scale as the Weber number, does not play as significant a role here since atomization similarity exists in spite of a substantial difference in the Reynolds number value for the two atomizer sprays. Probably, the effect of viscosity is negligible in the present regime of spray injection and atomization.

In summary, we believe that our approach to the investigation of such sprays allows for the proper interpretation of all spray measurables in terms of the atomizer prefilming length and velocity scales and the associated liquid injection Weber number in a manner that is not unique to the present study. A similar interpretation can and should be applied to other pressure-swirl atomizer designs, and to different fluids, in order to more firmly establish the proposed similitude features for hollow-cone spray flowfields.

ACKNOWLEDGMENTS

Funding by Air Force Office of Scientific Research, Air Force Systems Command USAF (Grant No. F49620-93-1-0365), and by NASA MSFC (Cooperative Agreement No. NCC8-46), is acknowledged. H. Ryan III is acknowledged for providing one of the atomizers.

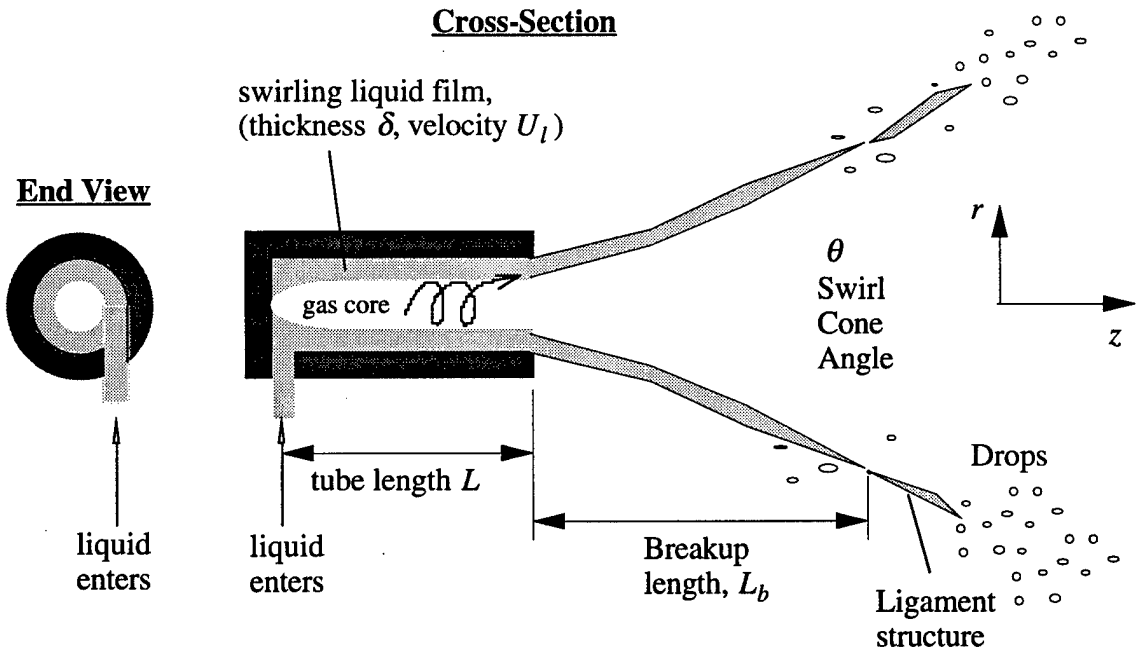

FIG 1. Schematic of a pressure-swirl atomizer spray.

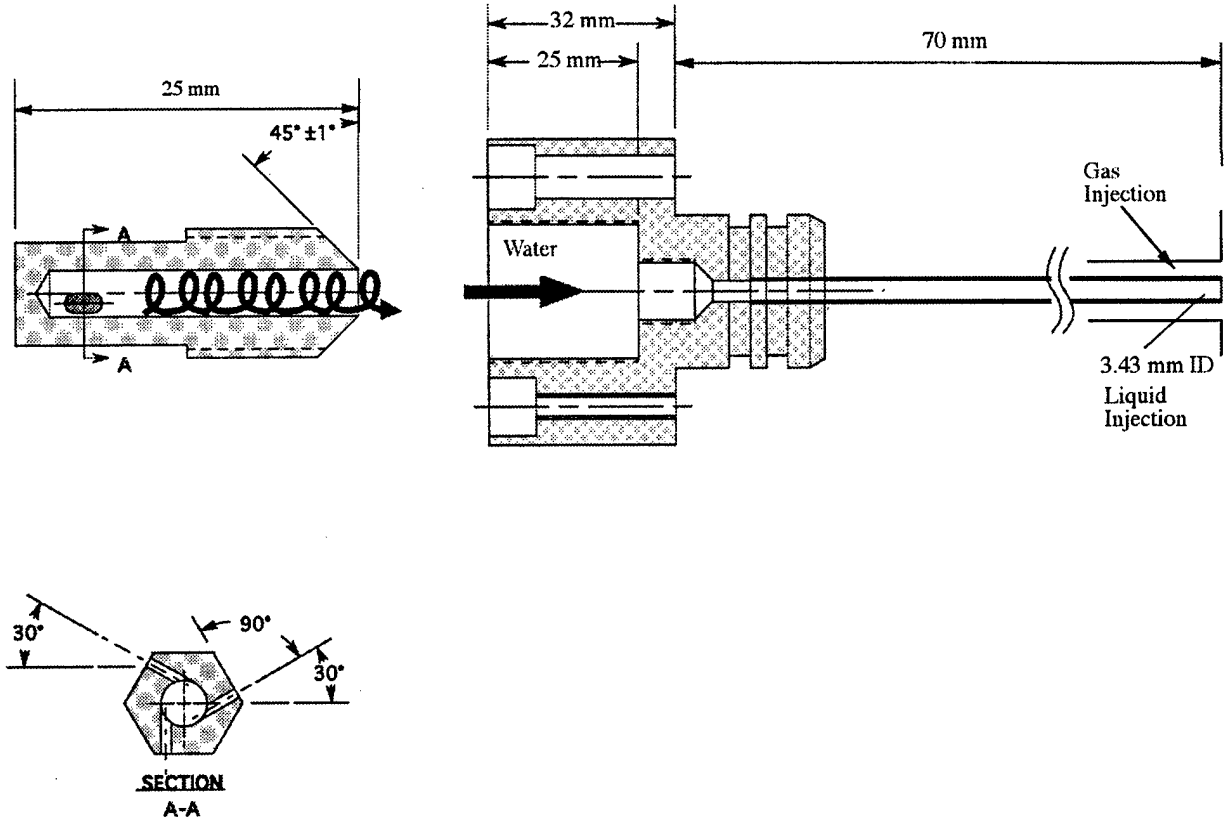

FIG. 2. Design of pressure-swirl atomizer.

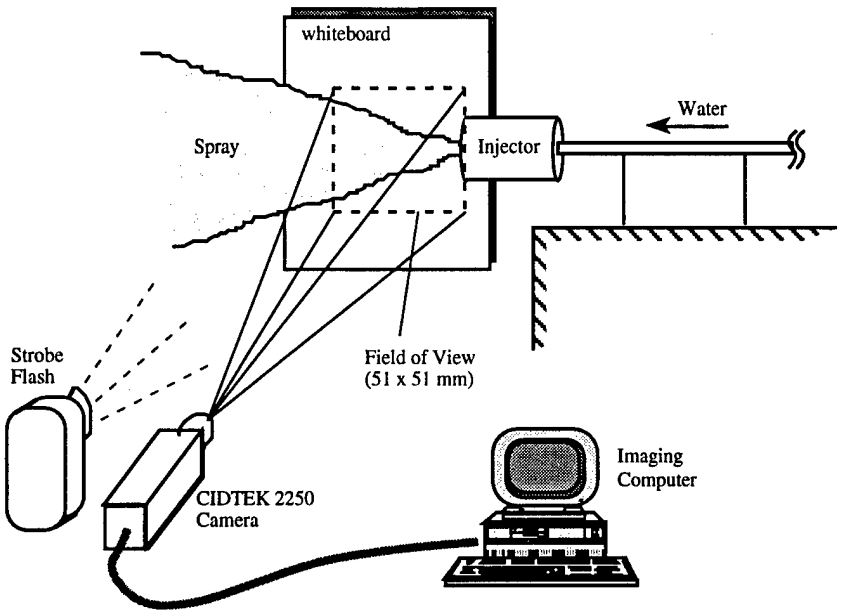

(a) a camera-based imaging system for flow visualization

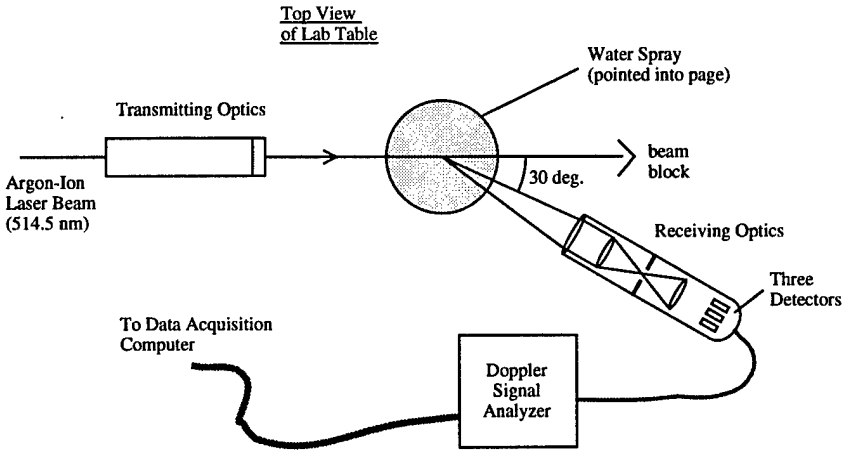

(b) set-up of the Phase/Doppler artical analyzer for drop-size and velocity measurements.

FIG 3. Schematics of spray diagnostic apparatus: (a) a camera-based imaging system for flow visualization, and (b) set-up of the Phase/Doppler artical analyzer for drop-size and velocity measurements.

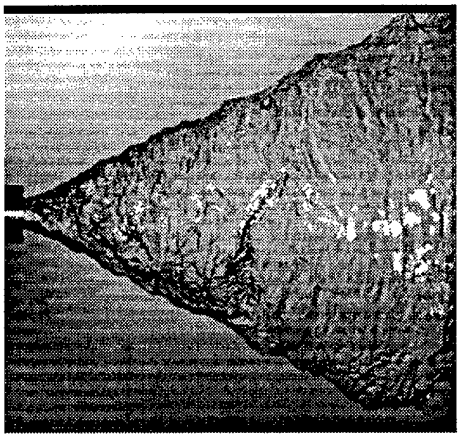

$We_\delta = 1060$ ($\dot{m}_{H_2O} = 0.045$ kg/s)

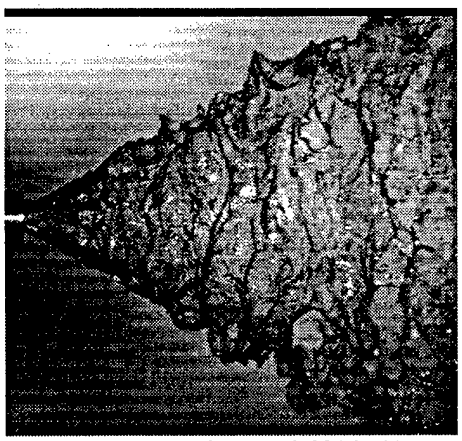

$We_\delta = 4250$ ($\dot{m}_{H_2O} = 0.091$ kg/s)

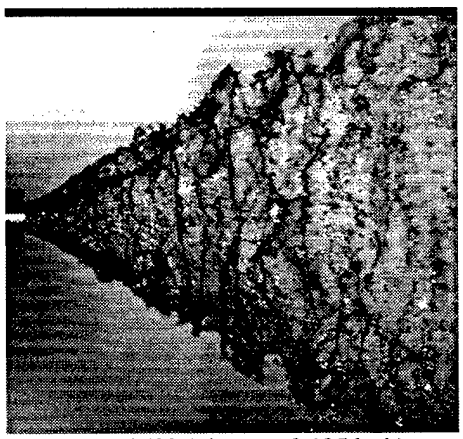

$We_\delta = 9500$ ($\dot{m}_{H_2O} = 0.135$ kg/s)

FIG. 4. Effect of increasing Weber number on the breakup of the hollow-cone sheet is shown. The small atomizer is used with an exit-orifce tube L/d of 20. Flow is from left to right.

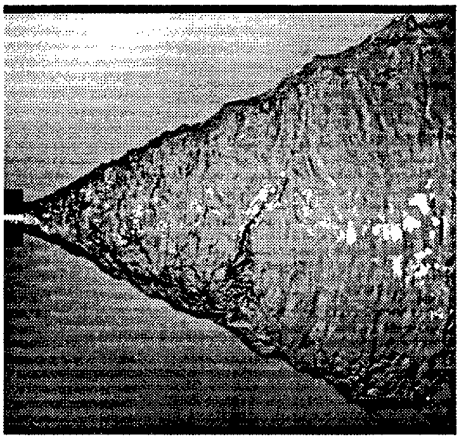

(a) $L/d = 20$

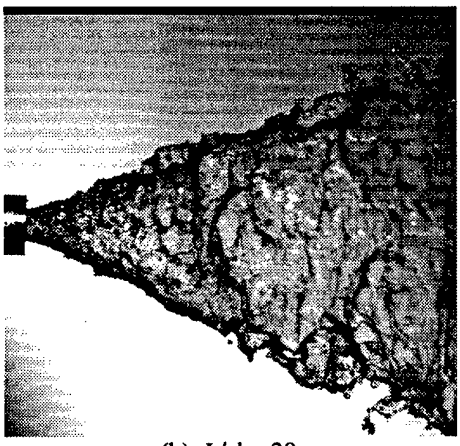

(b) $L/d = 30$

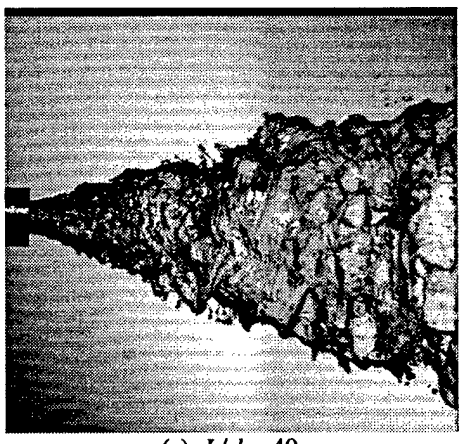

(c) $L/d = 40$

FIG. 5. Effect of length-to-diameter ratio on spray cone angle for pressure-swirl atomization is shown at $We_\delta = 4250$. The small atomizer is used with water flowrate of 0.045 kg/s. Flow is from left to right.

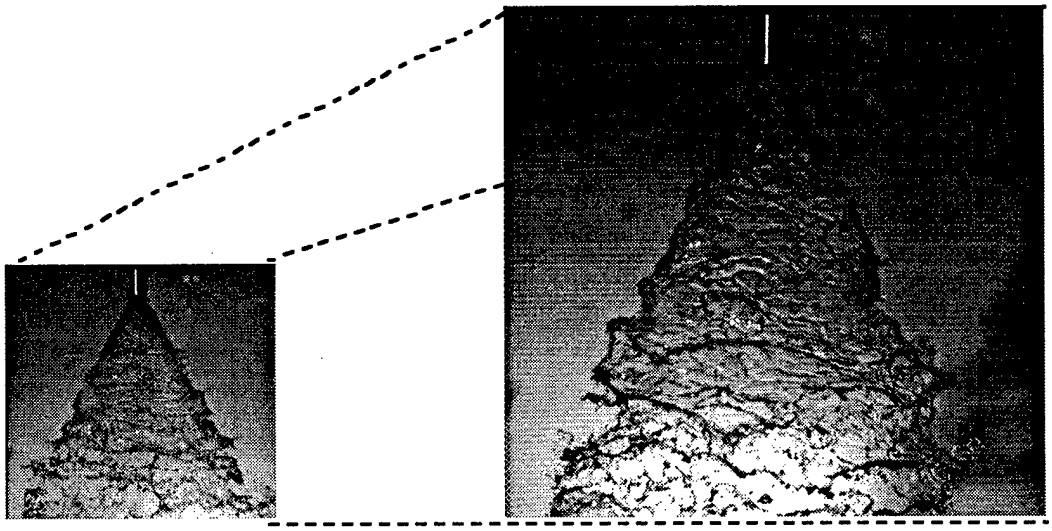

z = 0 -- 51 mm: Small Atomizer

z = 0 -- 102 mm: Large Atomizer

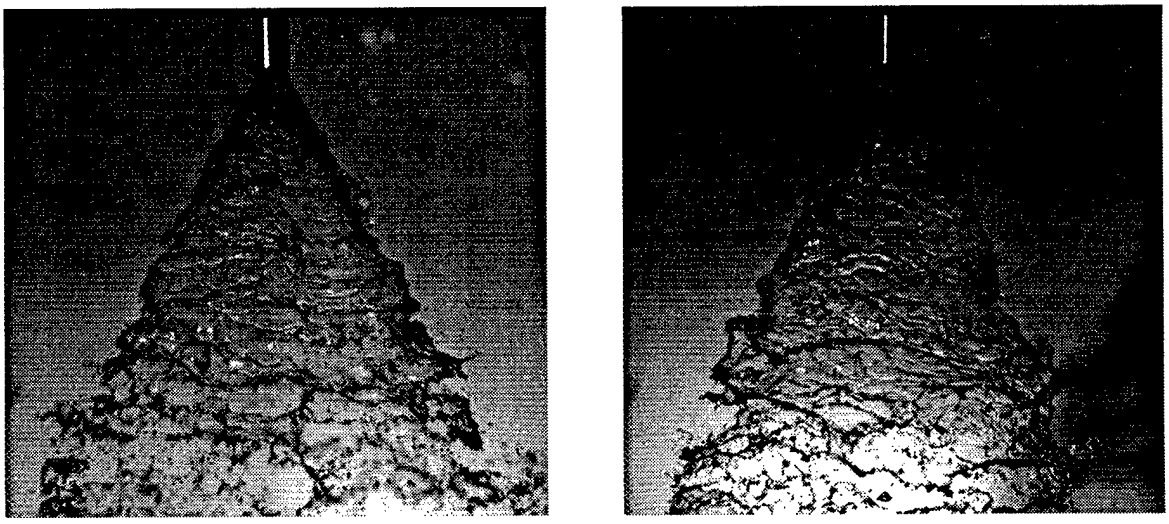

z/δ = 0 -- 150: Small Atomizer

Large Atomizer

FIG. 6. Visualizations of small and large atomizers sprays in physical coordinates (top) and normalized coordinates (bottom) show similarity of breakup phenomena for the hollow-cone sheet at Weber number of 4250. The images are taken under stroboscopic illumination. Water sprays are pointed downwards.

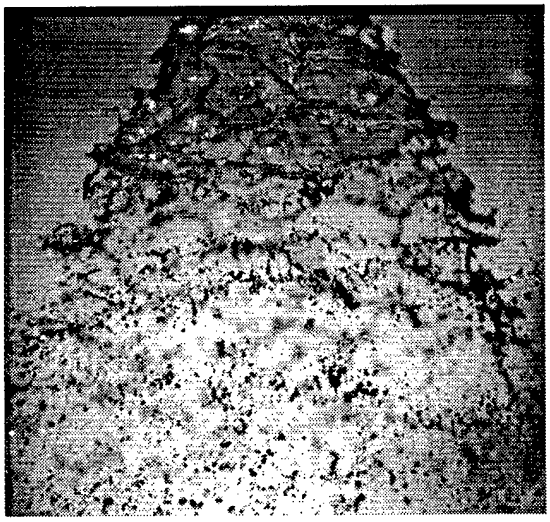

z/δ = 75 -- 225: Small Atomizer

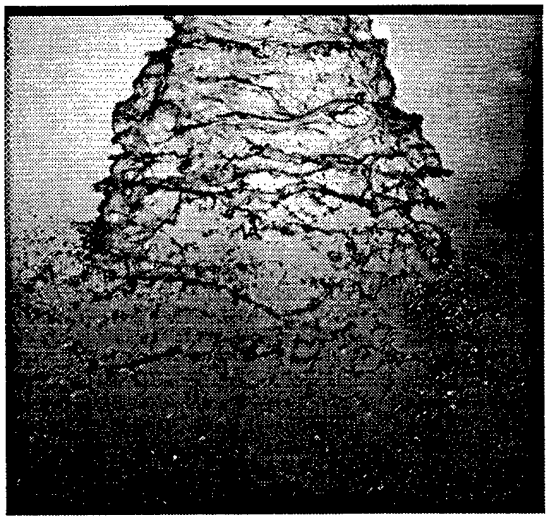

Large Atomizer

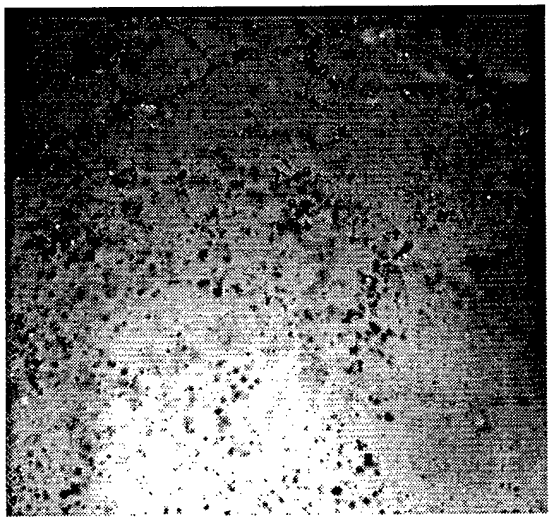

z/δ = 150 -- 300: Small Atomizer

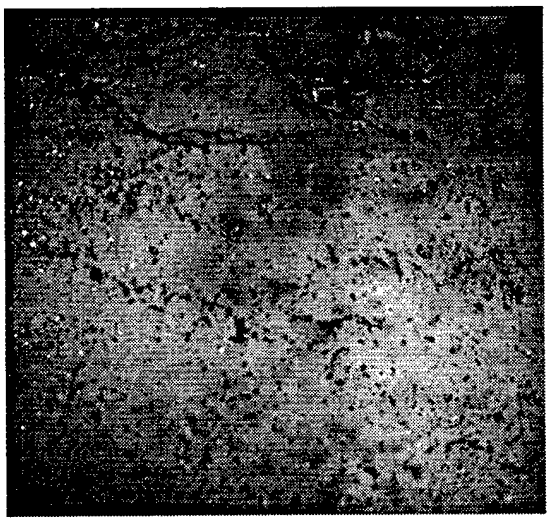

Large Atomizer

FIG. 7. Downstream visualizations of small and large atomizers sprays show breakup of hollow-cone sheet and drop formation processes at Weber number of 4250. The images, taken under stroboscopic illumination, are shown in normalized coordinates from z/δ = 75 -- 225 (top) and z/δ = 150 -- 300 (bottom). Water sprays are pointed downwards.

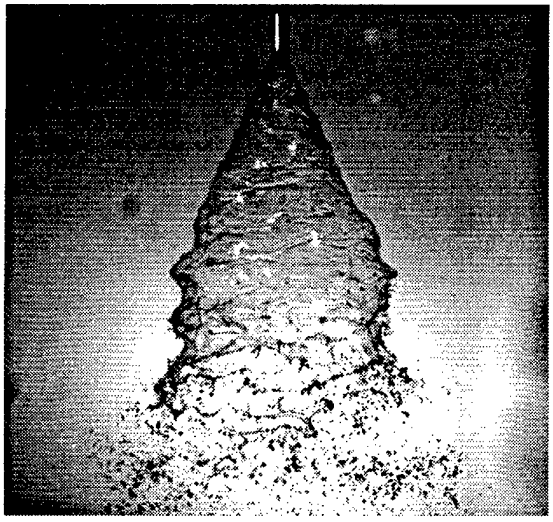

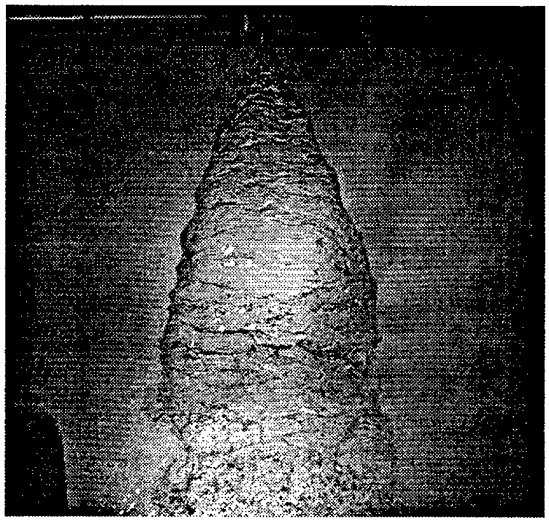

We_δ = **1060:** Small Atomizer

Large Atomizer

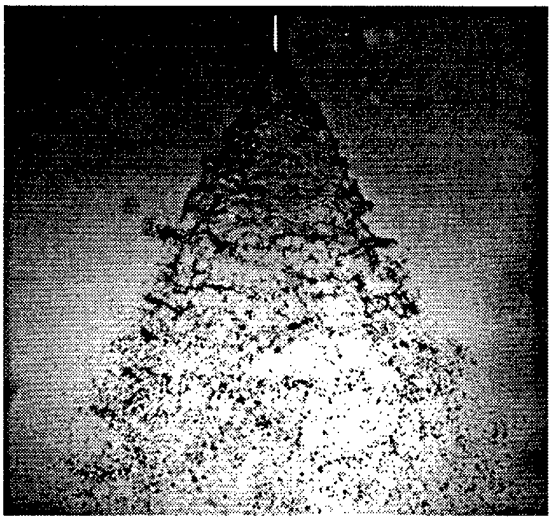

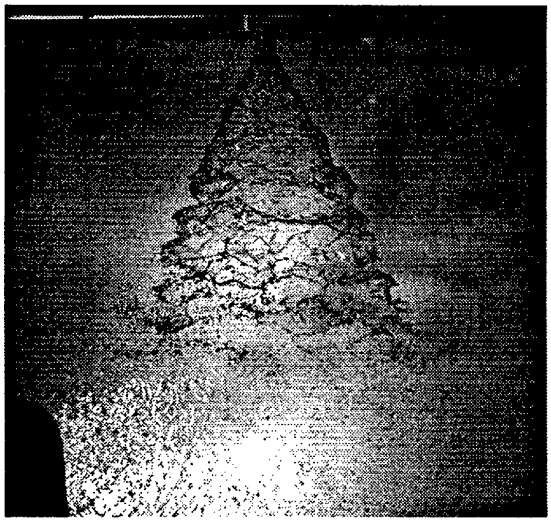

We_δ = **4250:** Small Atomizer

Large Atomizer

FIG. 8. Comparison of breakup and atomization flowfields for the small and large atomizers at two different Weber number. The near-injector region, extending to z/δ of 300, is imaged under stroboscopic illumination. Water sprays are pointed downwards.

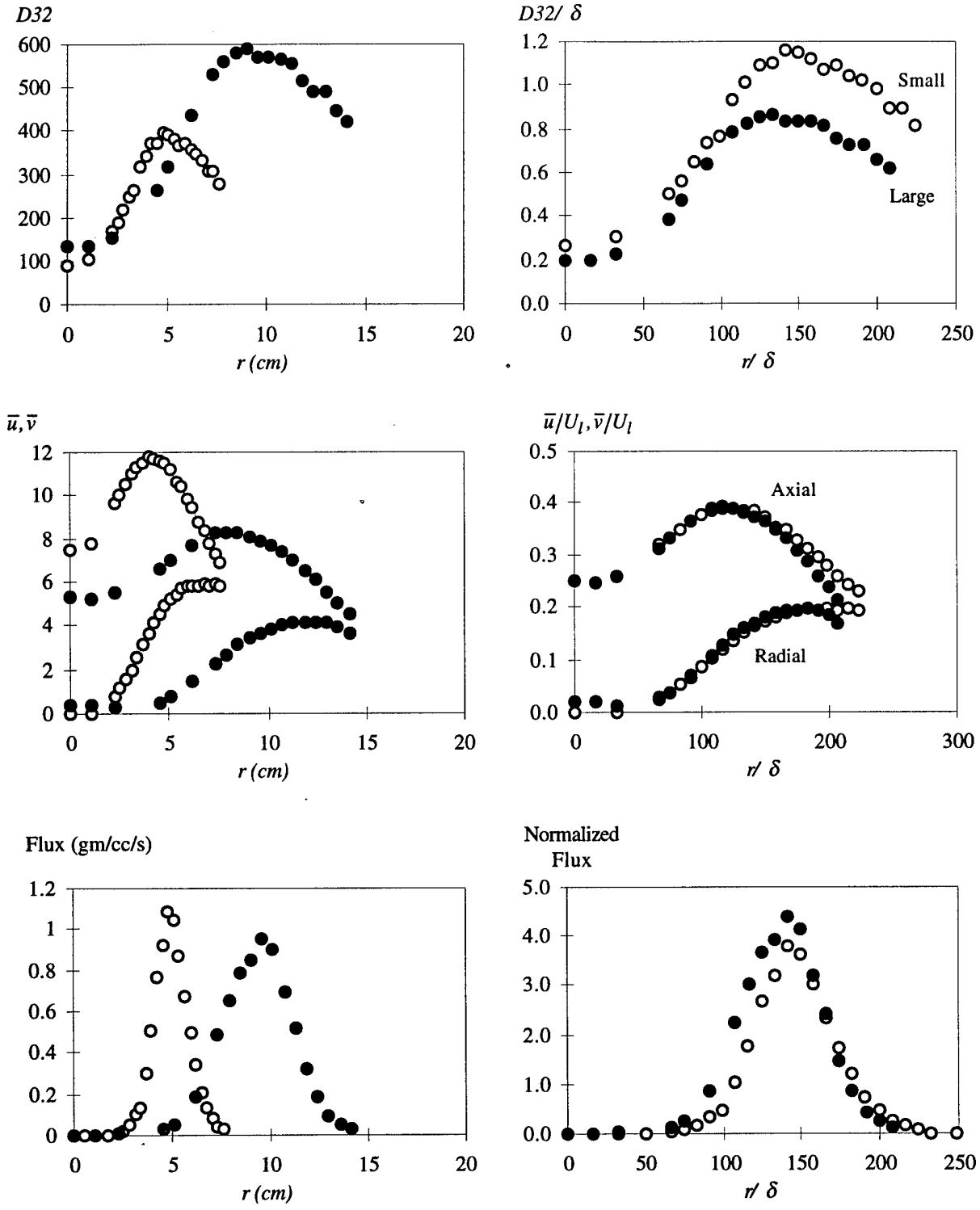

FIG. 9. Drop size, drop velocity, and mass flux results for the small and large atomizers are compared in physical variables (at left) and normalized variables (at right).

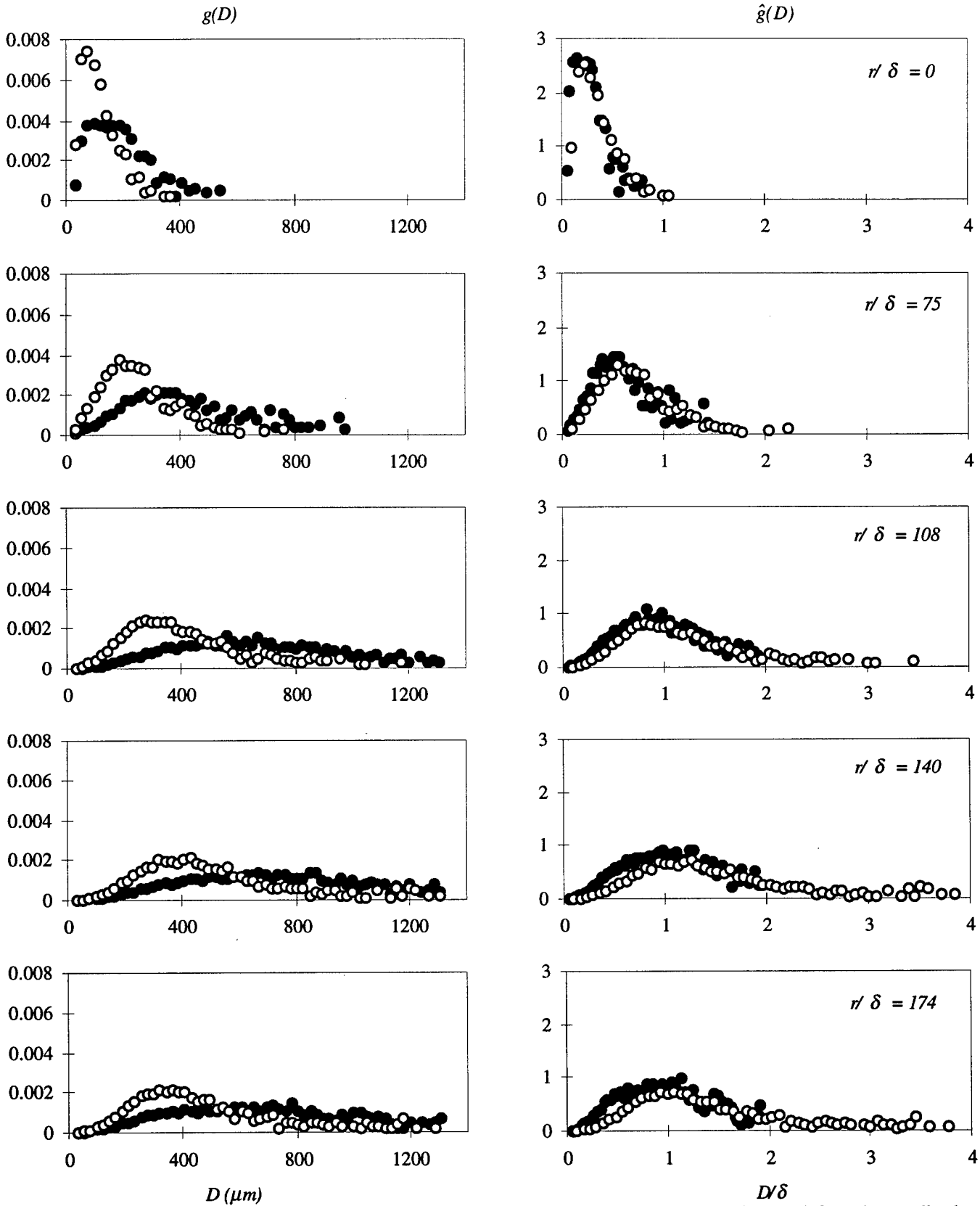

FIG. 10. Drop volume distributions for small and large atomizers are compared in physical variables (at left) and normalized variables (at right) for several radial positions at the axial station $z/\delta = 300$.

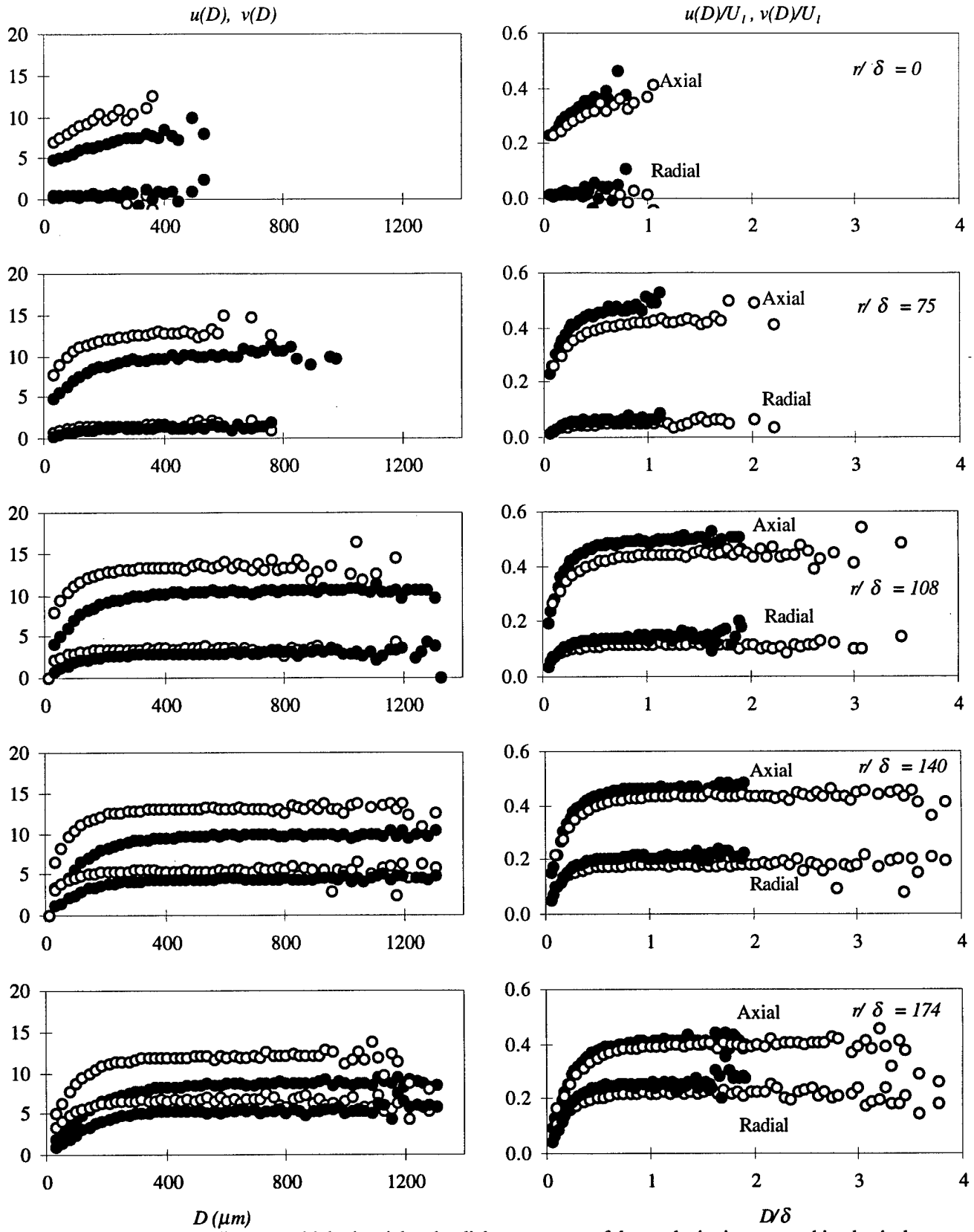

FIG. 11. Correlation of drop diameter with both axial and radial components of drop velocity is presented in physical variables (at left) and normalized variables (at right), for several radial positions at the axial station of $z/\delta = 300$.

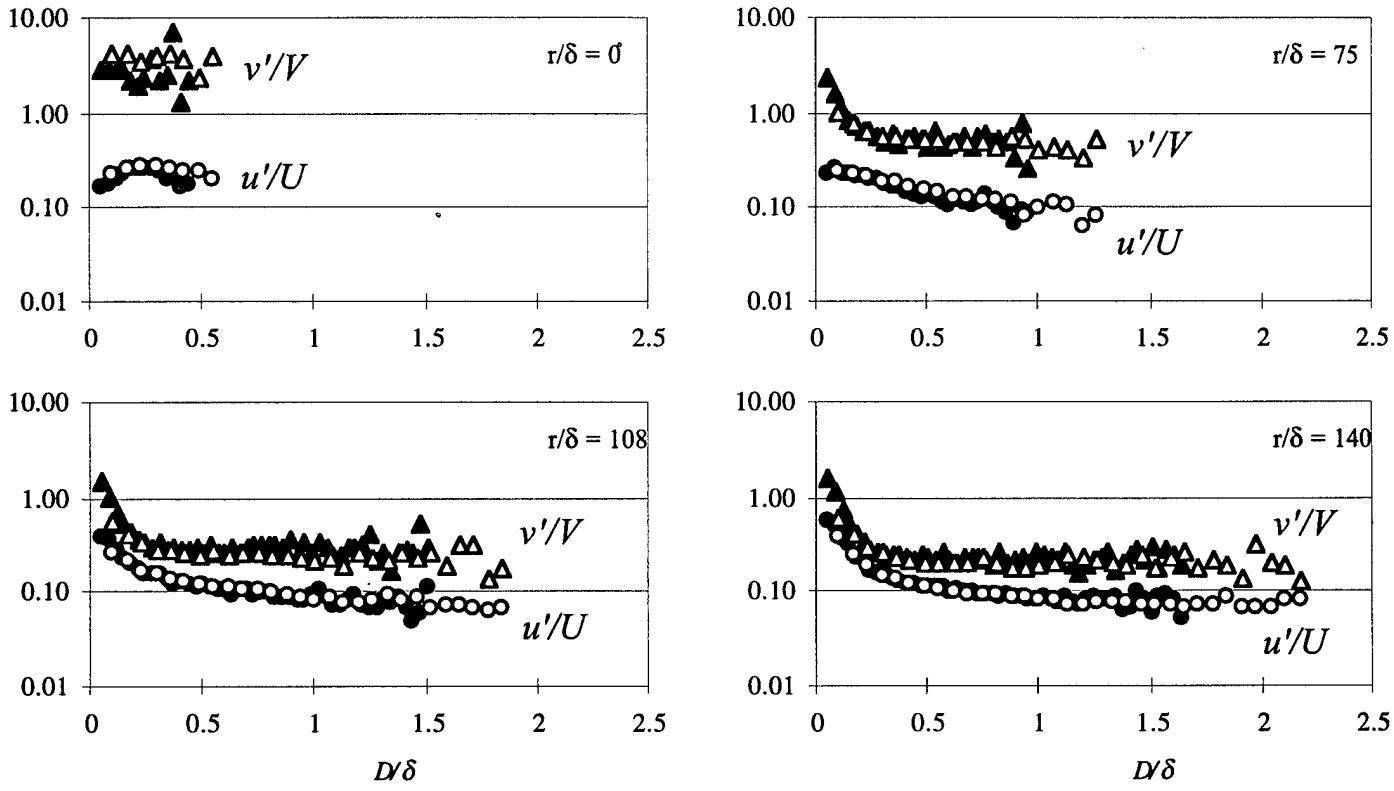

FIG. 12. Normalized drop velocity-rms for both axial and radial components are compared for the small and large atomizers at several radial positions in the two sprays.

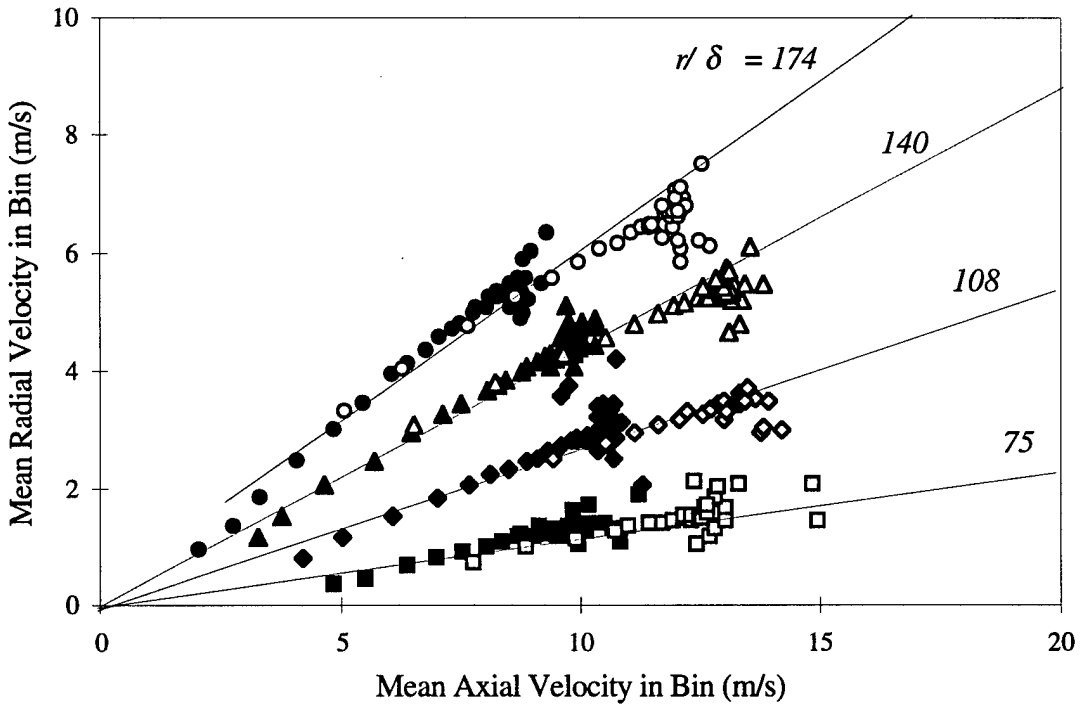

FIG. 13. Size-discriminated drop velocity data from previous figure shows a correlation of radial and axial velocity components at multiple radial positions in the sprays produced by the two atomizers. Each data point corresponds to a single size bin. For a given location and atomizer, lower velocity typically corresponds to size bins of smaller drops.

References

[1] Lefebvre, A. H., *Atomization and Sprays*, Hemisphere Publishing, New York, 1989.

[2] Borodin, V. A., Dityakin, Y. F., Klyachko, L. A., and Yagodkin, V. I., "Atomization of Liquids," *translation*, Report FTD-MT-24-97-68 (AD685151), Accession No. TM8501384, prepared by Foreign Technology Division, Wright-Patterson Air Force Base, 1967.

[3] Giffen, E., and Muraszew, A., *The Atomisation of Liquid Fuels*, Chapman & Hall, 1953.

[4] Doumas, M., and Laster, R., "Liquid-Film Properties for Centrifugal Spray Nozzles," *Chemical Engineering Progress*, Vol. 49, No. 10, Oct. 1953, pp. 518-526.

[5] Yule, A. J., and Chinn, J. J., "Swirl Atomizer Flow: Classical Inviscid Theory Revisited," *International Conference on Liquid Atomization and Spray Systems*, Rouen, France, July 1994.

[6] Tate, R. W., and Marshall, W. R., Jr. "Atomization by Centrifugal Pressure Nozzles - Parts I," *Chemical Engineering Progress*, Vol. 49, No. 4, April 1953, pp. 162-174.

[7] Tate, R. W., and Marshall, W. R., Jr. "Atomization by Centrifugal Pressure Nozzles - Parts II," *Chemical Engineering Progress*, Vol. 49, No. 5, pp. 518-526-5, May 1953, pp. 226-234.

[8] Simmons, H. C.., "The Correlation of Drop-Size Distributions in Fuel Nozzle Sprays," *ASME Journal of Engineering for Power*, Vol. 99, July 1977.

[9] Tokuoka, N., Yamaguchi, Y., Takada, M., and Zhang, F., "The Spray Structure from Swirl Atomizers: Part I and II," *Proc. of Int'l. Conf. on Liquid Atomization and Spray Systems*, Gaithersburg, MD, July 1991, pp. 233-248.

[10] Presser, C., Gupta, A. K., Semerjian, H. G., and Avedisian, C. T., "Droplet Transport in a Swirl-Stabilized Spray Flame," *Journal of Propulsion and Power*, Vol. 10, No. 5, Sept.-Oct. 1994, pp. 631-638.

[11] Lai, W. H., Yang, K. H., Hong, C. H., Wang, M. R., "Droplet Transport in Simplex and Air-Assisted Sprays," *Atomization and Sprays*, Vol. 6, pp. 27-49, 1996.

[12] York, J. L., Stubbs, H. E., and Tek, M. R., "The Mechanism of Disintegration of Liquid Sheets," *Trans. of the ASME*, Oct. 1953, pp. 1279-1286.

[13] Li, X., and Tankin, R. S., "Derivation of Droplet Size Distribution in Sprays By Using Information Theory," *Combust. Sci. and Tech.*, Vol. 60, 1988, pp. 345-357.

[14] Bachalo, W. D., and Houser, M. J., "Phase/Doppler Spray Analyzer for Simultaneous Measurements of Drop Size and Velocity Distribution," *Optical Engineering*, Vol. 23, 1984, pp. 583-590.

[15] Wigley, G., "Phase Doppler Anemometry and its Application to Liquid Fuel Spray Combustion," in *Optical Diagnostics for Flow Processes*, Eds. Lading, L., Wigley, G., and Buchhave, P., Plenum Press, New York, 1994.

[16] Dodge, L. G., Rhodes, D. J., and Reitz, R. D., " Drop-size measurement techniques for sprays: comparison of Malvern laser-diffraction and Aerometrics phase/Doppler," *Applied Optics*, Vol. 26, No. 11, June 1987.

[17] McDonnell, V. G., Wood, C. P., and Samuelsen, G. S., *Twenty-first Symposium (International) on Combustion, pp. 685, The Combustion Institute*, 1988.

[18] Edwards, C. F., and Marx, K. D., "Analysis of the Ideal Phase-Doppler System: Limitation Imposed by the Single-Particle Constraint," *Atomization and Sprays*, Vol. 2, pp. 319-366, 1992.

[19] Bachalo, W. D., and Sankar, S. V., "Factors Affecting the Measurement Resolution and Accuracy of the Phase Doppler Particle Analyzer," Second Int'l Conf. on Fluid Dynamic Measurements and Its Applications, Beijing, China, October, 1994.

[20] Hsiang, L.-P., and Faeth, G. M., "Near-limit Drop Deformation and Secondary Breakup," Int. J. Multiphase Flow, Vol. 18, 1992, pp.635-652.

[21] Sankar, S. V., Bachalo, W. D., and Robart, D. A., "An Adaptive Intensity Validation Technique for Minimizing Trajectory Dependent Scattering Errors in Phase Doppler Anemometry," *4th International Congress on Optical Particle Sizing*, Nuremberg, Germany, March 21-23, 1995.

[22] Van Dyke, M. *Album of Fluid Motion*, The Parabolic Press, Stanford, CA., 1992 ed., pp. 115.

[23] Rahman, S., Pal, S., and Santoro, R. J., "Swirl Coaxial Atomization: Cold-Flow and Hot-Fire Experiments," AIAA-95-0381, *33rd Aerospace Sciences Mtg.*, Reno, NV, January 9-12, 1995.

[24] Dombrowski, N., and Hasson, D., "The Flow Characteristics of Swirl (Centrifugal) Spray Pressure Nozzles with Low Viscosity Liquids," *AIChe Journal*, Vol. 15, No. 4, July 1969, pp. 604-611.

[25] Hutt, J. J., McDaniels, D. M., Smith, A. W., "Internal Flow Environment of Swirl Injectors," AIAA-94-3262, *30th AIAA/ASME/SAE/ASEE Joint Propulsion Conf.*, Indianapolis, IN, June 27-29, 1994.

[26] Ryan, H. M., Anderson, W. E., Pal, S. and Santoro, R. J., "Atomization Characteristics of Impinging Liquid Jets," *Journal of Propulsion and Power*, Vol. 11, No. 1, Jan.-Feb. 1995, pp. 135-145.